BEAM DYNAMICS FOR EXTREME ELECTRON BEAMS

Settore Scientifico disciplinare FIS/07

Tesi di Dottorato di:
Marcello Rossetti Conti

Coordinatore: Prof. Francesco Ragusa
Supervisore: Prof. Vittoria Petrillo

Contents

List of Figures

List of Tables

Abstract

The extreme electron beams are characterized by parameters that are comparable or superior to the state of the art. The parameters of the beams proposed in the more advanced machines under development or in operation demonstrate that extreme beam qualities are necessary to conceive experiments that meet the demands of cutting-edge research.

The optimization of parameters such as brightness, beam current or energy spread plays a major role in the design choices of new and competitive machines. A large amount of simulations of beam dynamics is required, accompanied later by a specific R&D of machine components and demonstration experiments.

In the field of beam dynamics, the development and improvement of tracking simulation programs and optimization tools is a main topic. For this reason, in the beam physics group of INFN & University of Milan the code GIOTTO [1], based on a genetic algorithm, is being developed for years specifically for this purpose.

During the work of PhD I developed new features in the GIOTTO code that allowed me to apply it to new type of problems: simulation of a beam based method for the increase of the brightness of linac beams, design from scratch of matching lines for plasma driven FELs (Free Electron Lasers), the study of new linear acceleration and compression techniques and a preliminary study on how to produce an ultracold beam for a quantum-FEL. All these works are united by being applied to linear machines dedicated to the production of high-brightness electron beams for various purposes. During the last year of PhD I had the opportunity to participate in the design of an FEL source, named MariX. MariX is based on a compact acceleration scheme where the electron beam propagates twice through a superconducting standing wave linac thanks to an arc compressor that reverses the direction of the beam and compresses it.

In the following is presented a brief description of the thesis outline.

In Chapter 1 I described some of the main applications that can benefit from the

use of electron beams with extreme characteristics.

After explaining why the choice of an electron linac is preferable for many of these experiments, I mentioned some techniques used worldwide to produce bunches with extreme characteristics of various kinds. For each of these cases I explained in which experiments these beams can prove to be advantageous and what values represent the state of the art.

In Chapter 2 I briefly presented the tools that I used during my PhD to study the dynamics of extreme beams and some optimization techniques with special attention to genetic algorithms and the code GIOTTO.

In Chapter 3 I described changes and improvements I made to GIOTTO during the various activities, showing the new features introduced. After that I presented the four major works on extreme beams that I did, using GIOTTO, and the various results achieved.

Finally, in Chapter 4 I introduced the MariX project and then I explained how the bubble arc that I studied works. I will therefore show the results of beam dynamics simulations optimized in the presence of CSR effects.

Overall, in this PhD work I have shown how the genetic algorithms can be used in combination with tracking codes to obtain working points for the simulated machines that allow to produce extreme beams, in presence of space charge and high chromatism conditions.

Finally, I have shown a possible way to compensate the effects of CSR in the MariX arc compressor.

The results of most of the works I presented in this PhD thesis have been published and presented in international conferences [2–5] We expect the MariX bubble arc to be the key to build a compact 1 MHz FEL capable of producing radiation up to 1.5 Å and we hope that the scheme can also be applied to other machines of this kind. The study of this scheme will be an integral part of the MariX Conceptual Design Report which will be presented soon. The transfer line for Eupraxia@SPARC_LAB designed with GIOTTO was presented in the Design study of the machine this year [6].

Introduction: extreme electron beams applications

Contents

1.1 Some machine applications

Many modern experiments based on electron accelerators ask for beams of ultrahigh quality. For example, high brightness electron beams are used to

enhance the performance of the radiation emitted in *Free Electron Lasers* (FELs) or *Inverse Compton Sources* (ICS). Even plasma based acceleration experiments can be performed only with high quality ultrashort beams.

First of all, I will introduce these phenomena and then I will proceed explaining more in details how electron beam parameters can increase the performances of these peculiar experiments.

Free Electron Lasers

The FEL is a tunable Laser classified as a 4th generation Synchrotron Radiation (SR) source [7–13]. These devices are linear machines that produce pulses of quasi-coherent radiation while a relativistic electron beam propagates in a special device called undulator. The undulator is an array of magnets that generates a periodic magnetic field that makes the electrons undulate transversally emitting SR along the longitudinal of the linac.

FELs have spread widely in the most advanced research centers since their first theorization by John Madey in 1971 at Stanford University [14]. This success is due to their tunability and to the possibility to use these machines as sources of coherent light in the UV frequencies and X-rays range (both hard and soft), where conventional lasers are not available [15–17].
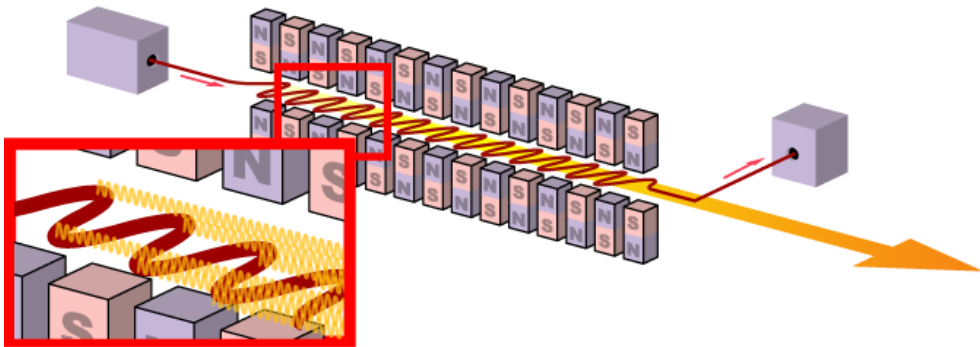
Figure 1.1. Production of coherent radiation starting from an high brightness electron beam propagating through a permanent magnets undulator.

FEL physics

I will follow the terminology and notations as in [18], where the main FEL scaling laws are obtained from the Newton-Lorentz and the Maxwell equations. The wavelength of the radiated electromagnetic waves is given by:

$$\lambda = \frac{\lambda_w}{2\gamma^2}(1 + a_w^2), \tag{1.1}$$

where λ_w is the undulator field period, $a_w = K_w/\sqrt{2} = eB\lambda_w/2\sqrt{2}\pi m_e c$ is the undulator parameter and γ is the Lorentz factor of the electron beam.

The tunability of the FEL radiation is mainly due to the possibility to vary the Lorentz factor, being for relativistic electron beams: $\gamma \simeq E_e/m_e$ with E the electrons average energy and $m_e \simeq 0.511$ MeV the electron rest mass. Another possibility is to vary the undulator parameter a_w intervening on the B value of the magnetic field by changing the gap between the arrays of magnets on the undulator [19].

The gain of the emission process is strictly connected to the Pierce parameter:

$$\rho = \frac{1}{2\gamma} \sqrt[3]{\frac{I}{I_A}\left(\frac{JJ\lambda_w a_w}{2\pi\sigma_x}\right)^2} \tag{1.2}$$

with $I = Q_b/(\sqrt{2\pi}\sigma_t)$ is the electron bunch current evaluated from the root mean square (rms) of the bunch duration in time, Q_b is the total bunch charge σ_x in the transverse dimension rms assuming cylindrical symmetry of the bunch (i.e $\sigma_x = \sigma_y$), $I_A \simeq 17.045$ kA represents the Alfvén current and $JJ = J_0(\xi) - J_1(\xi)$ is a correction factor needed in case of planar undulators where $\xi = \frac{1}{2}\frac{a_w^2}{1+a_w^2}$. We can now introduce the gain length, i.e. the growth rate of the FEL emission in Self Amplified Spontaneous Emission (SASE) regime:

$$L_g = \frac{\lambda_w}{4\pi\sqrt{3}\rho}. \tag{1.3}$$

So the power of the radiation increases exponentially:

$$P = P_0 e^{\frac{z}{L_g}}, \tag{1.4}$$

where P_0 is the power value at the beginning of the process.

The exponential gain process has an intrinsic limit, in fact at some point the electrons, which lose energy by irradiating, will no longer be able to give energy

to the wave. This limit is called saturation and occurs after a specific saturation length $L_{sat} \simeq 20L_g$.

The Pierce parameter described in eq. 1.2 is used to calculate the power at saturation:

$$P_{sat} \approx \sqrt{2}\rho P_{beam}, \tag{1.5}$$

where P_{beam} is the electron beam power, and to estimate the radiation bandwidth:

$$Bw = \frac{\Delta\lambda}{\lambda} \approx \rho. \tag{1.6}$$

The gain deterioration due to non ideal electron beam qualities (non negligible energy spread and emittance), can be described by introducing a three dimensional (3d) gain length:

$$L_{g,3d} = L_g(1+\eta) \tag{1.7}$$

where the factor η gives the degradation due to diffraction, energy spread and emittance and is defined in [18].

Conditions on the electron beam parameters for the growth of the signal are $\Delta E_e/E_e < \rho$ and $\varepsilon_n \lesssim \gamma\lambda/4\pi$, $\Delta E_e/E_e$ being the electron beam energy spread and ε_n the transverse normalized emittance.

The FEL radiation obtained from a planar undulator is linearly polarized in the plane of the electrons undulatory motion.

The FEL can work both in the *SASE* regime [20, 21], where the signal starts from the electron beam noise, or in the seeded mode [10, 22–26], where an initial laser pulse is superimposed to the electrons and amplified along the undulator. The quality of the radiation pulse can be upgraded also with techniques of self-seeding [27] or of *Echo Enhanced Harmonic Generation* [28]. The transverse coherence of the FEL SASE radiation is quite large [29]. In fact, although many transverse modes are excited at the beginning of the undulator, by the end of the exponential growth only the highest growth rate mode dominates.

As regards the longitudinal coherence, the SASE radiation exhibits a sequence of M uncorrelated temporal spikes, whose mutual distance is $2\pi L_c$ where the cooperation or coherence length is defined as $L_c = \lambda/(2\pi\rho)$ and $M = L_{beam} = (2\pi L_c)$. When the length of the electron beam L_{beam} is shorter than $2\pi L_c$, the FEL operates in the single spike regime [30, 31]. In this condition, the radiation presents a single spike structure both in the temporal and in the spectral domains with a substantial coherence during each single radiation shot, but, however, low

shot-to-shot stability. Due to the slippage, saturation is reached quite early. This can be compensated by chirping the electron beam and tapering the undulator [32] (and references therein). This regime permits the operation at low charge, with a control of emittance and energy spread at the maximum level.

The number of photons per pulse can be estimated as

$$N_{ph} = \frac{E_{sat}}{E_{ph}}$$
(1.8)

where E_{sat} is the emitted energy at saturation and E_{ph} the emitted photon energy.

Finally, the peak brilliance of the radiation [8] is

$$B_{peak} = \frac{N_{ph}}{(2\pi)^3 \sigma_x \sigma_y \sigma_x' \sigma_y' Bw}$$
(1.9)

and is usually expressed in $\frac{Photons}{s\ mm^2\ mrad^2\ Bw} (\%_0)$.

Some applications

The wide range of tunability of these advanced machines allows a wide range of applications in the field of imaging. A useful summary of the most interesting techniques and research fields now explorable with modern FELs is shown in Fig. 1.2.

For example, soft X-rays at 280 eV (4.4 nm) are used to perform carbon K-edge X-ray absorption spectroscopy, X-rays around 415 eV (3 nm) can be used for imaging in the water window, i.e. in the frequency range at which the water is transparent. Going toward higher energies, the oxygen ($\approx$ 500 eV) and the silicon (1.8 keV) K-edges follow. The access to energies above 5 keV allows the analysis of key earth-abundant chemical elements and provides atomic resolution. This last regime encompasses the K-edges of elements necessary for the large-scale development of photo-catalysts involved in the electricity and fuel production, as well as the biologically important selenium, used for protein crystallography. Studies of spin-orbit coupling which is at the basis of many aspects of material quantum mechanics can be also performed in this regime. The availability of wavelengths approaching or exceeding the Å range (~10 keV) provides novel fundamental capabilities for discovery science.

Another important advantage of this radiation source is the possibility to pro-duce short and ultrashort pulses of radiation simply decreasing the electron bunch length. The dynamics of molecular and atomic phenomena, i.e, fragmentation,
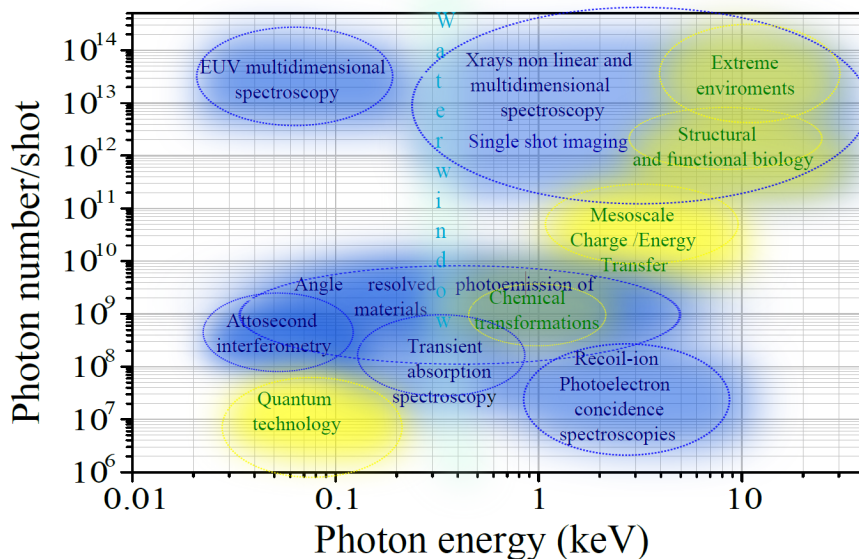
Figure 1.2. In blue techniques and in yellow research areas mapped vs photon energy and number of photons per shot. Re-elaborated from Ref. [33]

attachment/ detachment dynamics, solvation dynamics, intra and intermolecular charge transfer, can be detected by soft X-rays with pulse length of 10-100 fs, whereas the electronic processes involving outer and inner shells develop on atto-femto-second scale and need therefore of probes and methodologies in this duration range. Furthermore, since high intensity X-rays result in strong radiation damage of the samples, X-ray exposure shorter than the explosion time-scale of biological samples is needed (diffraction before destruction). Pulses of shorter or about a few tens of femtoseconds push back the traditional radiation damage limits of structural biology, while the resolution drop off for pulses longer than 70 fs. In Fig. 1.3 are summarized the various phenomena that will be accessible to detection and study with FELs considering the radiation pulse duration and the pulse energy. X-ray FELs are preparing to satisfy these demands.

The trend for newest and future set-ups is that of increasing by orders of magnitude the repetition rate with respect to the 10-100 Hz available in most present FELs. A continuous time distribution of the pulses should be moreover suitable. A high repetition rate of 1 MHz and an uniform time structure should provide the possibility to collect more than 10^8 scattering patterns (or spectra) per day with sample replacement between pulses, enabling methodologies as the serial crystallography and the multidimensional X-ray spectroscopy. The use of advanced data analysis methods, as for instance pattern recognition,
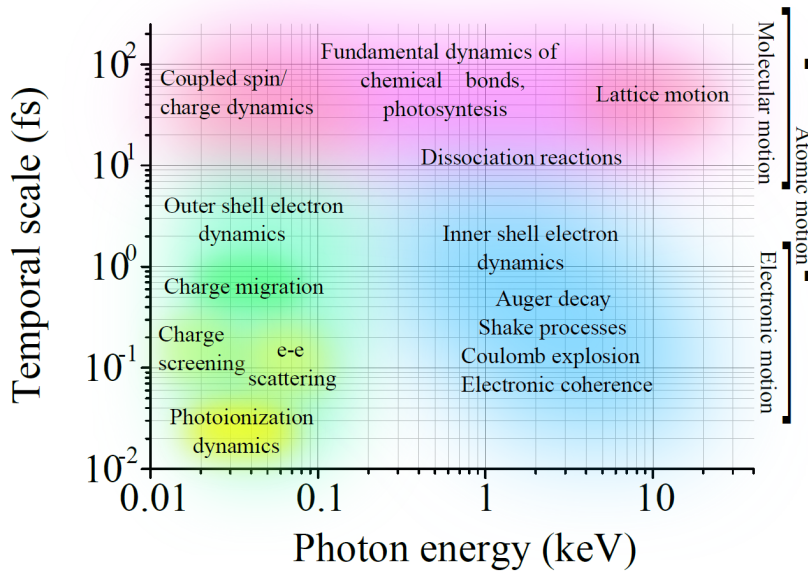
Figure 1.3. Molecular, atomic and electronic phenomena mapped vs their photon energies and temporal duration.

manifold maps, Bayesian analysis, genetic algorithms and deep learning will make possible the characterization of heterogeneous ensembles of particles. From the huge data set collected with such a repetition rate, moreover, the extraction of information about rare or novel transient events will be possible. The simultaneous measurements of the electronic structure and of subtle nuclear displacements at the atomic scale in environments requiring the penetrating capabilities of hard X-Rays and the sensitivity provided by high repetition rate will be accessible.

Regarding spatial coherence, the availability of a high average coherent power in the soft-hard X-ray range, combined with programmable pulses at high repetition rate, will enable studies of spontaneous ground-state fluctuations and heterogeneity at the atomic scale from micrometric and femtosecond scales using powerful time domain approaches such as the X-Ray photon correlation spectroscopy (XPCS). These capabilities will further provide a qualitative advance for understanding non-equilibrium dynamics and fluctuations via time-domain inelastic X-Ray scattering (FT-IXS) and X-Ray Fourier-transform spectroscopy approaches using Bragg crystal interferometers.

A strong difference between the synchrotron and the FEL radiation is the temporal degree of coherence and the monochromaticity of the signal. Control over the radiation bandwidth will be a major advance for high- resolution inelastic X-Ray scattering and spectroscopy in the hard X-ray range (RIXS and IXS). The

present scientific impact of RIXS and IXS suffers for the lack of large spectral flux from temporally incoherent synchrotron sources. New generation X-ray FELs will provide more than a 300-fold increase in average spectral flux compared to synchrotron sources, opening new areas of science and exploiting high energy resolution and dynamics near the Fourier transform limit. The possibility of seeded mode operations is in study in practically all X-ray FELs. Besides the direct laser seeding or the cascaded seeding, able to produce a statistically stable and totally coherent pulse, but limited toward the higher frequency due to the unavailability of the seed radiation, many other techniques have been proposed and developed. The use of monochromators for self seeding, the Echo-Enhanced radiation scheme or the operation in single spike regime are techniques that permit to select part of the pulse in the spectral or temporal regime, thus providing partially coherent radiation.

Inverse Compton Scattering

ICS are compact, high brilliance, mono-chromatic and tunable radiation sources. Thanks to these peculiarities, Thomson/Compton scattering sources are arising around the world in these years especially to deliver hard X-rays (with energies between few tens up to 200 keV). The radiation is emitted by a few tens up to few hundreds MeV electron beam colliding with a counter-propagating laser pulse. In particular, we call the phenomenon Thomson scattering when the interaction is classical, when the collision is elastic, and Compton scattering when there are an inelastic collisions, i. e. when the electrons recoil cannot be neglected [34]. For this reason in the literature sometimes Compton Sources are referred as Thomson Sources when the X-ray energies are lower than about 200 keV. In the following we'll use ICS for both regimes (Inverse Compton Source).

When an electron beam collides with a high power counter-propagating laser pulse the electrons are excited by the electro-magnetic field of the laser radiation and acquire vibrational energy of the frequency perceived. The relative motion between the two beams increases the frequency seen by the electrons due to the Doppler effect. The vibrational energy is then released emitting a boosted electromagnetic radiation that in the rest frame is revealed in the direction of motion of the electron beam. In practice, the electrons behave like a relativistic mirror and for a double relativistic Doppler effect the frequency of the electromagnetic radiation is increased of a factor γ^2 as shown in eq. 1.10.

The energy of the radiation produced goes from hard X-rays, for small sources,

up to γ rays for bigger machines [35].

$$E_\gamma = 2\gamma_e{}^2 \frac{1 + \cos\theta_L}{1 + (\gamma_e\theta_o)^2 + a_0^2 + \frac{4\gamma_e E_L}{mc^2}} E_L. \tag{1.10}$$

With:

$$\frac{4\gamma_e E_L}{mc^2} = \text{quantum recoil parameter}$$

$$a_L = \frac{eE}{m\omega_L c} = \text{vector potential of the laser field}$$

$$E = \text{laser electric field intensity}$$

$$E_L = \hbar\omega_L, \quad \theta_L = \text{collision angle}, \quad \theta_o = \text{observer angle}$$

As an example, with $E_L = 1.24$ eV (typical of a 1 μm wavelength laser) and $\gamma_e = 140$ (typical of a compact electron accelerator) we obtain an energy for the forward scattered photons (i.e. in the direction of the electron, when $\theta_o = 0$) of 91 keV.
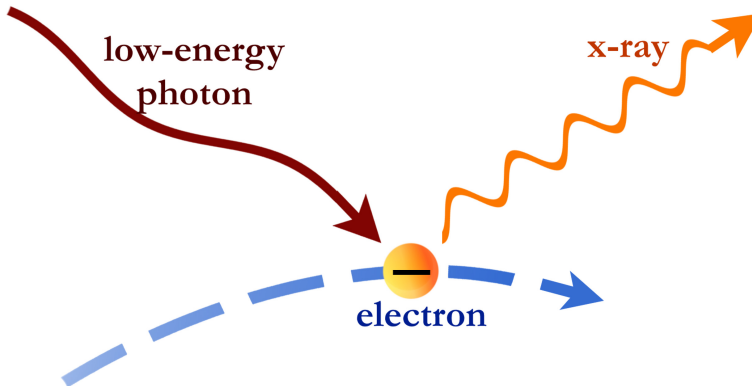
Figure 1.4. Simplified scheme of inverse Compton scattering. An X-ray photon is produced from the collision between a low energy laser photon and a relativistic electron.

The radiation obtained is incoherent because every charged particle emits photons in an uncorrelated way from the others but the energy of the photons produced are much higher, 20-500 keV.

The longitudinal dimensions of the electron beams use in this kind of experiments are limited by the laser diffraction that comes into play when the electron beam longitudinal size is comparable to the laser wavelength λ_L. Because of that in these experiments are used "short" electron beams ($\sigma_z \simeq 1\ ps$), to obtain shorter radiation pulses an FEL must be used.

The price to pay to such a nice "photon accelerator" scheme is a low efficiency in transforming the laser photons into X-ray photons via the back-scattering mechanism. The cross section of Thomson/Compton back-scattering is unfortunately very small (namely $6.65 \times 10^{-29}\ m^2$) , so we need to run a high luminosity collider in order to generate an intense X-ray beam: to achieve an operating regime so that almost each electron scatters at least one laser photon, the luminosity required must exceed that of large colliders like LHC! This, in turns, implies the need to collide extremely dense laser and electron beams, with the request for micron sized beams at the collision point, carried by pulses which are picoseconds long. However, the production of intense laser beams and high brightness electron beams meeting these tight requirements is nowadays state of the art. The real challenge of ICS is to make these electron-photon collisions to occur in a stable and controllable fashion, such to generate X-ray beams with the requested stability, reliability and tunability to the end users, as much as it is routinely achieved in the operation of synchrotron light sources.

The majority of the radiation obtained is contained in a cone with vertex in the interaction point, with axis on the electron propagation direction and angle $\theta = \frac{1}{\gamma}$ as an effect of the Lorentz boost. The scattered photons show a strong correlation between scattering angle and energy, with the most energetic particles traveling on the accelerator axis. Thanks to this peculiarity it is possible to choose an appropriate collimation angle in order to obtain the best trade off between low bandwidth and high flux. Moreover, with the correct collimation, it is possible to obtain a strongly monochromatic photon beam if the emittance and the energy spread of the electrons are very low.

Applications

The focus on enabled applications by a ICS in the at hard X-ray range is on medical oriented research/investigations, mainly in the radio-diagnostics and radio-therapy fields, exploiting the unique features of mono-chromatic X-rays,
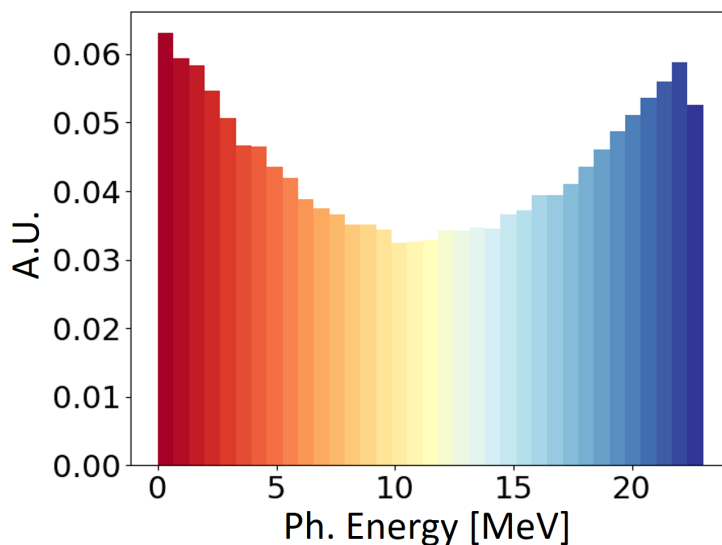
Figure 1.5. The figure shows the distribution in energy of the radiation produced by a Compton interaction designed for the production of photons γ to the energy $E_{ph} = 23$ MeV for kimberlite rocks scanning applications. The shape of the histogram is typical of the phenomenon, the maximum energy photons are those that propagate in the direction of the electrons, those with less energy propagate backwards, in the direction of the photons of the laser.

as well as in micro-biological studies, and, within this mainstream, material studies, crystallography and museology for cultural heritage investigations. Monochromatic bright X-ray beams have been already proven to be a unique tool for advanced imaging at the sub 100 μm resolution scale with huge reduction in the radiation dose to tissues, joined to an upgraded signal-to-noise and visibility enhancement via phase contrast imaging. The underlying enabling technology is on the strong rise over in the past decade, with an effective ongoing transition from R&D and demonstrative machines towards effective user facilities, based on ICS X/γ-ray Sources [36–44]. Experiments on the source characterization [45, 46], on imaging, K-edge techniques and computed microtomography on phantom [47], biological [39, 48], animal [49, 50] and human [40, 44] samples with keV range X-rays have been already successfully performed.

Plasma Acceleration

Plasma acceleration techniques are supposed to be a breakthrough in accelerators technology.

Actually the main obstacle for high energy machines are the dimensions and the costs of the whole apparatus that is needed to take particles to the TeV energy scale. The conventional accelerators are limited by the RF cavities breakdown limit, namely the value of the maximum electric field that can be borne by the cavity before it physically damages it. Therefore, if we consider a state of the art 12 GHz X-band cavity the accelerating gradient is limited to a value between 90–120 MV/m. This means that a 1 TeV electron linac requires at least 8 km only considering the RF cavities, taking into account also drifts, optics and diagnostics the dimensions will double easily.

Plasma acceleration technologies promise to be the solution to the problem of the cavity breakdown. The key idea is to generate a disturbance inside a capillary filled with neutral plasma by injecting and ultrashort electron beam, called *driver*, or an high power ultrashort laser pulse. The electrons of the plasma are expelled by the electric field of the driver/laser from its path while the plasma nuclei, the positive charges, move more slowly because of their bigger mass. The effect of this disturbance is the generation of a strong *wakefield* inside bubbles that travel behind the driver/laser pulse, see fig. 1.6.

In plasma, the accelerating gradient is not affected by the breakdown limit and can go up to 100 GeV/m that is three orders of magnitude higher than the state of the art gradients achievable in RF section [51]. It is possible to inject an ultrashort electron beam, called *witness*, inside of this strong wakefield with the correct timing in order to take energy from the perturbation and accelerate the witness.

At the moment, the most promising plasma wakefield acceleration techniques are *Laser Plasma Wakefield Acceleration* (LWFA) and the *Plasma Wakefield Acceleration* (PWFA).

LWFA

The *Laser Plasma Wakefield Acceleration* has been theorized for the first time by Tajima a Dawson in 1979 [52]. The plasma wakefield is generated by an extremely short, approximatively 10 fs, High intensity laser pulse. A decrease in the electron density that propagates in the medium like a wave is then generated. This is due to the ponderomotive force (eq. 1.11) associated with the pulse oscillating field
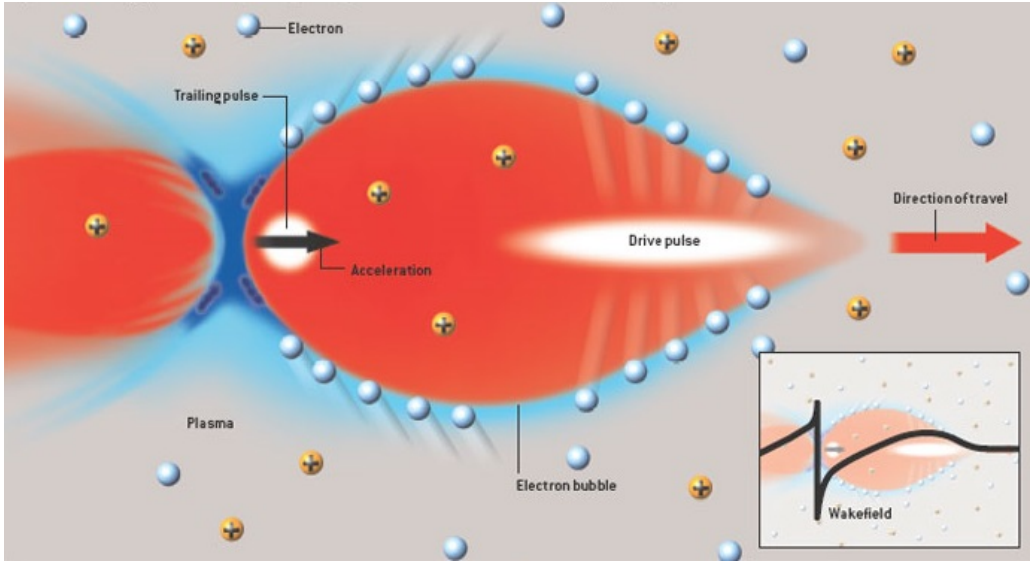
Figure 1.6. Wakefield generated inside a plasma capillary by the *driver*, a traveling high charge electron beam. A witness is being accelerated inside the first bubble in it's region of linearity

ω that moves the plasma electrons:

$$\overrightarrow{F}_p = -\frac{e^2}{4m\omega^2}\nabla(E_L^2). \tag{1.11}$$

Here e and m are the charge and the mass of the particle experiencing the force and E_L is the electric field amplitude of the laser.

If the laser pulse length is approximately half of the plasma wavelength, where $\lambda_p \simeq 1/\sqrt{n_e}$ (where n_e i the number of negative charges in the plasma) than an high amplitude wakefield is generated inside the capillary containing the plasma. The phase velocity of the wave is equal to the group velocity of the laser pulse that generated it, which is approximable to the speed of light in a vacuum. This is a necessary condition to accelerate electrons to ultrarelativistic energies.

If the witness is injected into the wave with the appropriate accelerating phase it can be accelerated significantly by the really intense fields present inside the bubble. This mechanism allows the electron beam to acquire a huge quantity of energy in a very short space (few millimeters).

It is important to inject the bunch with a as low as possible longitudinal dimension (σ_z) to fit well in the linear region of the wakefield (see fig. 1.6, bottom-right). Otherwise the accelerating field applied to the witness becomes

not linear and the acceleration process introduces longitudinal instabilities due to a strong energy spread increase.

PWFA

The *Plasma Wakefield Acceleration* technique consist in perturbing the medium with an ultrashort high charge electron beam (the *driver*). The mechanism that forms the wakefield is very similar to the one discussed for the LWFA case, except for the fact that the force responsible for the formation of the bubble is the Coulomb force. Therefore, the the plasma positive particles move (even if the amplitude of the oscillation is thousands of times smaller respect to the electrons motion) in the opposite direction respect to the LWFA case, indeed the ponderomotive force (eq. 1.11) does not depend on the charge sign.

The amplitude of the wakefield generated by the driver is proportional to Q_b/σ_z^2, where Q_b is the total charge of the bunch and σ_z is the rms length of the driver. Accordingly the driver must be as compressed as possible on the longitudinal dimension in order to maximize the wakefield strength but, at the same time, is important to transport a big charge.

The length of witness bunch in the linear acceleration regime (both in PWFA and in LWFA experiments) must respect $2\sigma_z \approx \lambda_p \propto 1/\sqrt{n_e}$ to maximize the wave-bunch energy transfer. In PWFA experiments are then required a couple of ultrashort bunches, very close each other and with significantly different total charge.

The Chromatic Length

The strength of the extreme electric field obtained inside the plasma bubble is the key for having a big accelerating gradient but introduces some important drawbacks. First of all, the injected beam must be compressed longitudinally to make the best possible use of the accelerating gradient, as mentioned before, but also must be transversally focused up to few micrometers to avoid bunch instabilities in the bubble. In fact, the bubble traverse dimensions are few tens of microns and the bunch's ones must be smaller to well fit in the safe region of the wakefield. Moreover, during acceleration, the electron bunch is subjected to extremely intense external forces that change very quickly away from the propagation axis. These forces couple with the internal repulsive forces that are ignited by the high charge density of the bunch and increase the beam energy spread and transverse momenta.

Designing a transport line for plasma accelerated bunches, able to preserve beam properties, requires particular care [53]. It has been shown that a relatively high amount of energy spread results in a consistent normalized emittance dilution even in drifts [54] (see fig. 1.7), whence the widespread conviction for the need of putting beam capturing optical elements as close as possible, compatibly with beam line constraints, to the plasma accelerator exit. However, an exact quantification of "how close" has never been given, so that beam line designers cannot decide if optics elements are close enough or if this requirement can eventually be relaxed in their specific situation. In the following chapters of this thesis, we will discuss this pressing question trying to provide an answer. Following [54] we write the normalized emittance as:
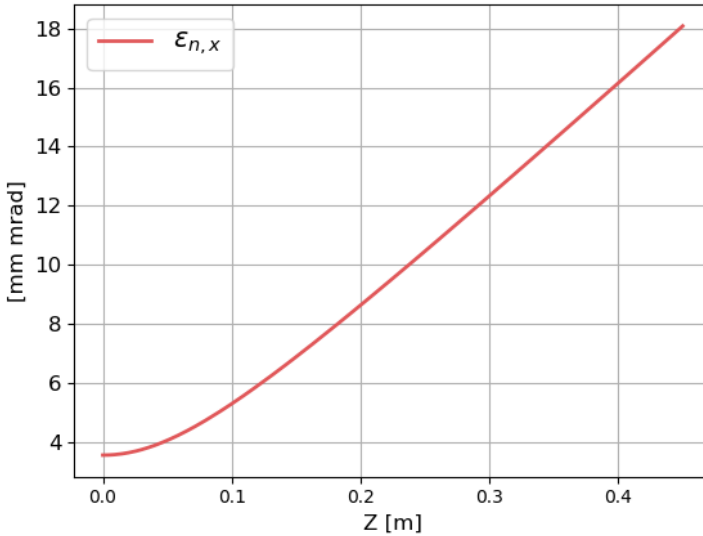
Figure 1.7. In the figure the simulated trend of the transverse normalized emittance (for a cylindrical beam) in the drift immediately following the capillary is shown.

$$\varepsilon_n^2 = \langle\gamma\rangle^2(\sigma_E^2\sigma_x^2\sigma_{x'}^2 + \varepsilon_0^2) \tag{1.12}$$

where $\langle\gamma\rangle$ is the average Lorentz factor, σ_E the relative energy spread, σ_x and $\sigma_{x'}$ respectively the values of bunch transverse size and divergence and ε_0 its initial geometric emittance $\varepsilon_0\sqrt{(\sigma_x^{(0)})^2(\sigma_{x'}^{(0)})^2 - (\sigma_{xx'}^{(0)})^2}$.

The beam transverse size evolution, assuming an emittance dominated beam, is $\sigma_x^2(s) = (\sigma_{x'}^{(0)}s)^2 + \sigma_{xx'}^{(0)}s + (\sigma_{x'}^{(0)})^2$, where s is the drift length. Inserting this result into eq. 1.12 and requiring the first term in parenthesis to be equal to the

second one (i.e. requiring a doubling of the initial squared normalize emittance), yield a drift length of

$$s = -\frac{\sigma_{xx'}^{(0)}}{(\sigma_{x'}^{(0)})^2} \pm \frac{\varepsilon_0 \sqrt{1 - \sigma_E^2}}{\sigma_E (\sigma_{x'}^{(0)})^2}. \tag{1.13}$$

Considering the positive solution, assuming the bunch initial condition is a waist (as is typical for a beam coming out from a plasma channel, disregarding ramps) and $\sigma_E^2 \ll 1$, allows to define the chromatic length as:

$$L_C \cong \frac{\varepsilon_0}{\sigma_E (\sigma_{x'}^{(0)})^2} = \frac{\sigma_x^{(0)}}{\sigma_E \sigma_{x'}^{(0)}} = \frac{(\sigma_x^{(0)})^2 \langle \gamma \rangle}{\sigma_E \, \varepsilon_0}. \tag{1.14}$$

By definition, L_C has a meaning equivalent to the Rayleigh length for a laser beam or the diffraction length for an emittance dominated particle beam, namely signals when the relevant quantity increases by a factor $\sqrt{2}$ with respect to its initial value or, equivalently, a range within which it can be considered approximately constant. It also explicitly shows how normalized emittance dilution is driven both by high energy spread and a small ratio between beam size and divergence. For a typical linac accelerated bunch with several hundreds of MeV energy and μm level normalized emittance, $\sigma_x^{(0)} \sim 10$ μm, $\sigma_{x'}^{(0)} \sim 100$ μrad and $\sigma_E \lesssim 10^{-3}$ gives $L_C \gtrsim 10^2$ m which is usually longer than the accelerator itself whereas, for a typical plasma accelerated beam of the same energy and emittance, $\sigma_x^{(0)} \sim 1$ μm, $\sigma_{x'}^{(0)} \sim 1$ μrad and $\sigma_E \gtrsim 10^{-2}$ the chromatic length is reduced to $L_C \lesssim 10^{-1}$ m, imposing the requirement of putting the first optical element as close as possible (i.e. within L_C) to the plasma channel end.

Ultrafast Electron Diffraction

Ultrafast Electron Diffraction (UED) or *Femtosecond Electron Diffraction* (FED) is an interesting recent application of high brightness electron beams in the field of ultrafast structural dynamics. The access to this new research field has been made possible by the advances of the beam compression technology and the growing interest in the study of atomic motions in real time.

UED is a pump-probe technique that exploits ultrashort electron bunches (with length, root mean square, between a few microns and a few tens of microns) diffraction through thin targets. It is possible to analyze transient structural dynamics with high spatial and temporal resolution by studying the diffraction pattern of the electrons [55–57].

The first results with UED were obtained in 2003 with a 30 keV linear electron accelerator based on a compact electron gun and showed a sequence of frames of an ultrafast solid-liquid transition of phase in polycrystalline aluminum [58]. In the latter case the target had a thickness of 20 nm, because electrons of such a low energy are not able to scatter efficiently through thicker samples.

Nowadays UED machines are divided in two categories:

- Table-top setups with energies of the beam in the 30–200 keV range, used to study materials like graphene that are considered mono dimensional [59]

- Linac driven by radio-frequency cavities in the 5–7 MeV range [60], used to access thick samples ($100\,\mathrm{nm} - 1\,\mathrm{\mu m}$) of protein crystals [61].

THz

High relativistic electron beams can also be used to produce *Transition Radiation* (TR) when passing through an inhomogeneous media, like boundaries between different media. This phenomenon have been theoretically demonstrated in [62] and suggested the use of transition surfaces rotated $45°$ with respect to the beam propagation axis. In this way the emitted radiation is perpendicular to the beam and easily detectable or reusable.

This emission of radiation can be interpreted intuitively as a mechanism of conservation of the total energy as the electric field associated to the beam has a sudden discontinuity located on the separation surface of the two media.

TR can be used as a valid way to measure the properties of ultrarelativistic electron beams, since the total energy of the emitted radiation is proportional with the beam Lorentz factor γ. Over the years, different methods have been developed to measure emittance and divergence of relativistic beams by exploiting the optical TR [63] [64].

In recent years the possibility of using sequences of ultrashort electron bunches to produce highly intense broadband THz radiation has been highlighted. The interest in the development of sources of this kind of radiation is due to the fact that the non-linear interaction between this light and matter can induce or even modify biological and chemical processes through the coherent control of quantum states [65, 66].

In particular, at the SPARC_LAB test facility [11] it is possible to use the laser comb technique to produce laser pulse trains of tunable temporal distance

impacting the photo-cathode [67]. It is thus possible to produce electron bunches in rapid succession that carry up to 100 pC of total charge. These bunches are then compressed in RF until they have longitudinal dimensions typical of ultrashort beams (sub-ps) thanks to the Velocity Bunching technique.

These extremely customizable pulse trains allow to obtain THz radiation of tunable frequency starting from 0.5 up to 5 THz [68, 69]. This kind of versatility is not attainable in alternative techniques for the production of radiation of this type, such as those based on undulators or dielectric waveguides [70, 71].

1.2   Extreme beams in linear accelerators

The applications described in the previous section will often take strong benefits from the characteristics of linear accelerators. Indeed, the enhancements of their performances are strictly related to ad hoc manipulations of the electron beams phase spaces. The more extreme are the properties that the beam will acquire, the more difficult is to preserve them during the tracking. For this reason the beam dynamics is often optimized in a special point of the line where the interactions take place, the *Interaction Point* (IP from now on).

These extreme gymnastics are hardly compatible with the periodicity of the beam parameters that is required in circular machines. It must also be taken into consideration that the electrons lose a lot of energy due to the emission of *Synchrotron Radiation* (SR) when they travel in the arcs and that this places a limit, depending on the ring radius, on the maximum energy reachable. Moreover, in high brightness linacs, the reduced presence of curvilinear paths decreases the impact on the beam quality of effects like the emission of *Coherent Synchrotron Radiation* (CSR) that leads to an increase of energy spread and the appearance of the *dispersion*, that is a measure of the difference in path that is traveled by particles with different energies.

Another important point in favor of linear machines is their tunability: the operating energy and the beam dynamics can be varied a lot. This is for example done in the test facilities like SPARC [11], where a single linac can drive different beamlines on which experiments are performed with very different beam requests. This operation would be extremely difficult in the rings as the tolerance on the beam parameters is very small two to the risk of introduction of resonances leading to losing the beam. The possibility to change the machine working point is a key feature for the radiation sources described as it takes the possibility to change the properties of the radiation produced (frequency, brilliance).

The cylindric symmetry of the bunch, or transverse symmetry, is another important quality that is preserved better in a linac. Once the beam is extracted from the cathode, each factor that can break the cylindrical symmetry ($\sigma_x = \sigma_y$ and $\sigma_{x'} = \sigma_{y'}$) has the effect of decreasing the beam brightness. This may occur, for example, due to unintended multipolar field components, misalignments of the line elements or image charges on asymmetric cavity walls. For this reason it is important to keep the cylindrical symmetry of the beam as much as possible.

At low energy the transverse beam shape is strongly influenced by the internal space charge forces that act radially in a symmetric way if the charge density is homogeneous. In this initial phase of life of the beam the transverse focusing is often performed by solenoids and RF focusing of accelerating cavities because both of them are cylindrically symmetric. Therefore, multipolar magnetic fields induced by specific magnets or by misalignments and inhomogeneity of the beamline elements must be compensated during the tracking to reduce the effect of this symmetry breaking.

1.3   Extreme beams worldwide

The techniques described in this chapter may take advantage beam dynamics manipulations to increase their performances. For *extreme beams* I mean the situation in which manipulation techniques bring you close or beyond the state of the art beams parameters.

I will now describe briefly some important beam parameters and peculiarities that can be enhanced performing extreme manipulations and the key mechanisms that can lead to this.

Ultrashort length

Electron beams are considered *ultrashort* when their rms longitudinal dimensions are few femtoseconds (that corresponds to a range that goes from few microns up to few tens of microns).

Ultrashort electron beams are very popular today because of the experiments in which they can be used. In Section 1.1 we saw how those beams are fundamental for plasma acceleration experiments and how they enhance the temporal resolution of UED diffraction patterns. Therefore, they can be used in FELs to work in *single spike* mode, when $\sigma_z \leqslant L_c$ (where L_c stays for the cooperation

length), to generate extremely intense coherent ultrashort radiation pulses used in *diffraction before destruction* experiments [72].

There are few strategies to compress electron bunches up to these longitudinal dimensions:

Magnetic compressors or *chicane bunchers*, are dispersive paths that allow the compression of appropriately chirped bunches thanks to their high R_{56}. In practice, the particles inside the bunch have a specific linear correlation in the longitudinal phase space (called *energy chirp*) that force head particles (which are the least energetic ones) to travel a longer distance respect to the tail electrons as shown in fig. 1.8. After the buncher, when the dispersion is closed again, the resulting bunch will be compressed. This machine works very well at high energy but, on the other hand, suffers from emittance degradation due to the emission of CSR when the bunch current reaches high values.

Magnetic compressor are the main device used to enhance the peak current by compressing the bunch in modern FELs.

Ballistic compression is another technique that make use of longitudinal energy chirp in the bunch, but works, for electrons, only under few MeV when $\beta \ll 1$. Therfore, different energy means also significantly different linear velocity between head and tail of the bunch and traveling a simple drift will lead to a longitudinal compression.

This technique is especially suited to FED experiments, where the energy is low and the reduced σ_z is crucial.

Velocity Bunching (VB) is a recent acceleration technique that permits to compress the bunch during its acceleration in RF Traveling Wave (TW) cavities [73]. To achieve this effect it is necessary to inject a low energy electron beam at zero phase (i.e. when the acceleration is zero), $\phi = 0°$, in this conditions the bunch experience a compressing forse due to the electric field gradient between head and tail. Since the beam velocity is lower than the traveling wave velocity (c) the bunch will slip back on the wave, in this way an accelerating force will add to the compressing one. The bunch is extracted when the slippage take it on crest $\phi = 90°$ and the introduced longitudinal energy spread is compensated by the space charge force that is turned on again by the compression.

The VB in an interesting tool that can be used in TW linacs to obtain high quality compressed beams at few tens up to few hundreds of MeV it have been used in many experiments like FEL, ICS, plasma acceleration.
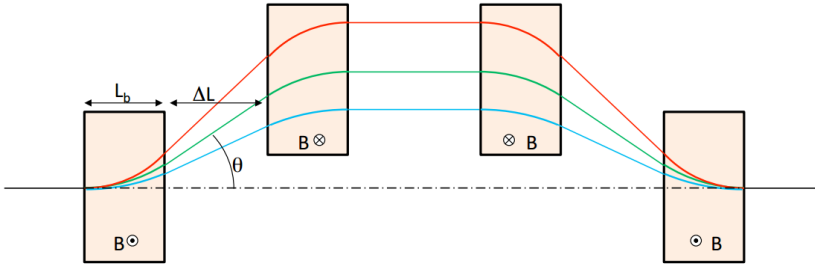
Figure 1.8. A particular configuration of the dipole magnets that make up the chicane, one can clearly see the effect of the dispersion of the particles with different energy and the different lengths of the trajectories they travel. In blue the trajectories of the most energetic particles are shown, in red those of the less energetic ones.

Beam with dimensions of few micrometers are usually obtained in FEL facilities working in *single spike* regime like LCLS [74] ($0.4-1.7\,\mu$m for 20 pC bunches), XFEL [75] ($\sigma_z \simeq 0.4\,\mu$m at 20 pC and $\sigma_z \simeq 1.9\,\mu$m at 100 pC) and in plasma acceleration experiments working with external injection [76].

High peak current

The concept of peak current (I_{peak}) is very helpful when working with Free Electron Lasers. Indeed, the FEL is a machine able to force electrons to cooperate in a process of stimulated emission, but this coherent mechanism works well for neighboring electrons that are inside the same cooperation length. For this reason, it is important to perform a beam slice analysis rather than one of the whole beam and the peak current, i.e. the current carried by a beam slice, is the most correct figure of merit to evaluate the Pierce parameter in eq. 1.2 instead of the beam total current. Therefore, considering slices of length $\Delta z \sim L_c = \lambda_r/(2\pi\rho)$, where λ_r stays for the radiation wavelength, the peak current of the beam is the maximum slice current:

$$I_{pk} = \max_{\Delta z \sim L_c} I_{slice} = \max_{\Delta z \sim L_c} \frac{N\,e\,c}{\Delta z}. \tag{1.15}$$

where N is the number of particles in the slice, e the elementary charge and c the light speed in vacuum.

The very high values of beam peak current are nowadays reached in important FEL facilities like:

LCLS [8] $I_{pk} = 3$ kA with 250 pC bunches of length $\sigma_z = 22$ µm for production of hard X-rays, and $I_{pk} = 4$ kA with 20 pC bunches of length $\sigma_z = 0.9$ µm for production of ultrashort pulses of hard X-rays in *single spike* mode [77] [74].

European XFEL [13] $I_{pk} = 5$ kA for four of the five declared working points of the machine, at $0.1, 0.25, 0.5, 1$ nC with pulse durations $\sigma_t = 6.4, 16.6, 30.6, 76.6$ fs [78][75].

SACLA [9] (recently) $I_{pk} = 10$ kA on both of its operative beamlines in the hard X-ray range ($\lambda \sim 1$ Å, with a 10 fs ~ 3 µm long beam). [79]

These results are reached with several magnetic compressors.

High brightness

Brightness is an figure of merit of the quality of an electron beam that binds the beam current with its transverse normalized emittance ($\varepsilon_{n,x-y}$, for this reason often it is referred as normalized brightness):

$$B_n \propto \frac{2I}{\varepsilon_{n,x}\varepsilon_{n,y}} \tag{1.16}$$

with:

$$\varepsilon_{n,x} = \beta\gamma\varepsilon_x \,, \quad \varepsilon_x = \sqrt{\langle x^2 \rangle \langle x'^2 \rangle - \langle xx' \rangle^2} \,, \text{ where } x'_i = \frac{Px_i}{Pz_i} \tag{1.17}$$

This important parameter can be considered equivalent to the particle density in phase space and it is essential to optimize the performance of the most common sources of radiation, such as FEL and Compton sources.

Maximizing this quantity require a careful study of the machine working points as it is necessary to obtain beams with low transverse normalized emittance but at the same time with reduced longitudinal dimensions and high charge. During transport in the first few meters of the beamline, these parameters strongly correlate in a non linear way due to the space charge. This makes it difficult to identify the correct optimal setting.

The VB, especially in its variant that preserves the longitudinal laminarity of the beam (whose mechanism will be explained later), has proven over time to be a technique that excels in the preparation of high-brightness beams in a few meters of linac thanks to its emittance compensation mechanism [73].

Ultralow energy spread

Low energy spread beams are very useful in many applications, including electron diffraction and electron microscopy, to increase the signal to noise ratio and in radiation sources. In fact, the energy of the emitted photons is always linked to the energy of the emitting electron, consequently the bandwidth of the radiation yield is limited by the energy spread of the bunch. The energy spread of a beam can be divided into two components:

uncorrelated energy spread: it can be seen as the thickness of the electronic cloud in the longitudinal phase space and represents the thermal noise of the particles inherited from the phase of extraction of the bunch from the cathode

correlated energy spread: often the largest component of the bunch energy spread, it is clearly visible in the longitudinal phase space as a correlation (or sum of these) between the position and energy of the particles in the bunch. There are different causes of these correlations, the most frequent are the difference in electrical field perceived by the particles in the RF cavities (first order correlation, or *chirp*, and second-order correlation) and the effects of the space charge field (correlation of the third order) of the bunch which decelerates the tail and accelerates the head.

Once the beam is extracted from the photo-cathode, it is really difficult to reduce the uncorrelated energy spread of a beam. Beam cooling system, requiring expensive and cumbersome devices such as laser coolers and storage rings should be used in order to reduce this component. On the other hand, with appropriate beam dynamics and the use of higher harmonic cavities it is possible to minimize the growth of the correlated energy spread and remove its first and second order components that are collected during beam acceleration. For example, in [80] a simulated beam, considering space charge, with absolute energy spread $\sigma_{E_k} = 15$ eV and relative energy spread $\sigma_{E_k}/E_k = 4 \times 10^{-6}$ obtained in this way is shown.

Electron beams with this order of magnitude of relative energy spread are also called *ultracold beams*, because their kinetic energy spread is considered mainly thermal.

An interesting and exotic application of those ultracold beams is the *Quantum Free Electron Lasers* [81]; this FEL machines are meant to be compact and almost completely monochromatic but, as explained, they need extremely low energy spread to decrease consistently the radiation bandwidth. Further in this thesis, I

will show the results of a beam dynamics optimization done to obtain an ultracold beam for a QFEL simulation in collaboration with professor Rodolfo Bonifacio.

Exotic pulse shaping

The increasing demand for research on wakefield acceleration techniques (in plasma and in dielectrics) has highlighted the need to control the shape of the electron bunches to optimize the energy exchange between the medium and the beam. This quantity is related to the important figure of merit, defined for particle driven experiments, called *Transformer Ratio* (T_r). The Transformer Ratio depends on the *driver* bunch distribution and it is defined as the ratio between the maximum accelerating field located behind the driver E_z^+ and the peak of the decelerating field inside the *driver* bunch E_z^-:

$$T_r = \left| \frac{E_z^+}{E_z^-} \right| \tag{1.18}$$

For symmetric beams it have been demonstrated in [82] that the transformer ratio is limited to $T_r \leqslant 2$, but asymmetric current profiles can overcome this limit. Considering the possibility of further increasing the energy exchange of the driver and the discovery that a correct modeling of the *witness* would reduce its final energy spread, the precise control of the current profile of the bunches has become an important research objective.

Some methods have been developed to control the form of these bunches, including correlation based methods [83] and fine pulse shaping of the laser pulse on the photo-cathode [84].

I will talk about a promising technique, based on a complex beamline setup, called *emittance exchange* (EEX from now on) that is used to exchange the longitudinal phase space distribution with one of the transverse phase spaces, generally the horizontal. In reality there are different kinds of EEX beamlines but, for compactness I will consider the layout used at Argonne Wakefield Accelerator (AWA) that was recently used to reach a measured record transformer ratio of $T_r \simeq 5$ [85]. The advantage introduced by this approach is linked to the easiness with which one can model the transverse current profile via a masks and than exchange this transverse profile with the longitudinal one with the EEX beamline [86]. It is also possible to produce combed bunches with the same mask by applying more cuts, with the drawback being a greater charge loss.

The EEX beamline is substantially composed by two identical doglegs, each one made with 2 bending magnets with bending angle α separated by a drift long L, and a deflecting cavity working at 3.9 GHz in mode TM_{110} put between the twin doglegs; a schematic is show in Fig. 1.9. It is important to setup the
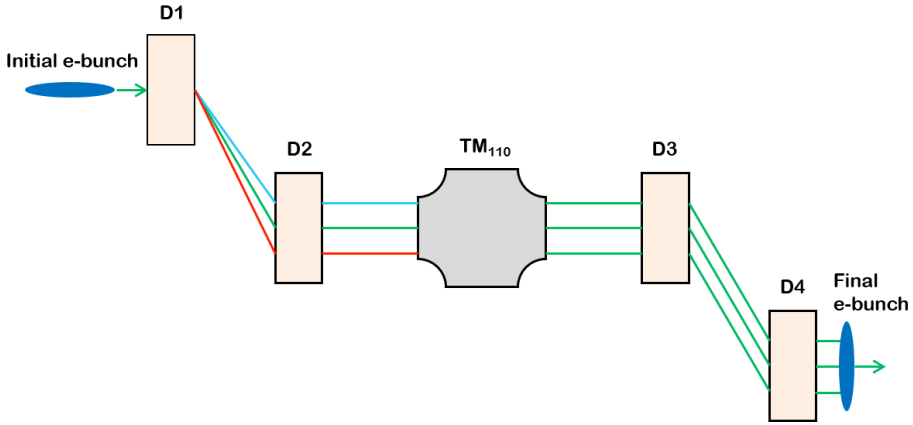
Figure 1.9. The EEX beamline layout used at AWA (not in scale). The beam is moving from left to right.

deflecting cavity strength $\kappa = 2\pi eV/\lambda_{RF}E_b$ in order to compensate the horizontal dispersion η, where V is the cavity voltage, λ_{RF} the RF wavelength and E_b the electrons energy. This in guaranteed if the following condition is respected:

$$\kappa = \frac{-1}{\eta} \tag{1.19}$$

The resulting transfer matrix of the whole EEX beamline would work only on the horizontal and the longitudinal emittance parameters without changing the vertical ones:

$$\begin{pmatrix} x \\ x' \\ z \\ \frac{\Delta_p}{p} \end{pmatrix}_{out} = \begin{pmatrix} \mathbf{A} & \mathbf{B} \\ \mathbf{C} & \mathbf{D} \end{pmatrix} \begin{pmatrix} x \\ x' \\ z \\ \frac{\Delta_p}{p} \end{pmatrix}_{in} \tag{1.20}$$

The matrix elements in bold are 2×2 sub-matrices of the whole M_{EEX}. The terms **A** and **D** should be equal to zero to have a perfect emittance exchange, but this is not possible due to the finite length of the cavity and effects of higher order like coherent synchrotron radiation and space charge. However, in an ideal case, considering thin lens approximation for the bending magnets and the condition

in eq. 1.22, the EEX beamline transfer matrix become:

$$
M_{EEX} = \begin{pmatrix} 0 & 0 & -\frac{1}{\alpha} - \frac{L}{\eta} & -\alpha L \\ 0 & 0 & -\frac{1}{\eta} & -\alpha \\ -\alpha & -\alpha L & 0 & 0 \\ -\frac{1}{\eta} & -\frac{1}{\alpha} - \frac{L}{\eta} & 0 & 0 \end{pmatrix} \tag{1.21}
$$

High average current

The average current takes into account all the charge that a bunch of N particles is transporting and the temporal spacing of the bunches t_b and represents how much charge is transported in a second. For example, for bunched beams in an electron linac the average current is:

$$
\langle I \rangle = \frac{Ne}{t_b} = NeR_r \tag{1.22}
$$

where e is the elementary charge and R_r the repetition rate of the linac.

In Compton light sources the average current is proportional to the radiation flux. Depending on the experiment you want to perform with an ICS or FEL source, one may need high repetition rates. In an FEL, once the correct peak current is guaranteed to trigger the phenomenon, a high repetition rate can be obtained by increasing the average current transported in the linac. For this reasons, $\langle I \rangle$ plays a fundamental role in experiments that require a high level of measurement statistics or repetition rate. Unfortunately, to increase a lot the average current, it is necessary to adopt precise strategies during the machine design phase. It will be necessary to adopt a gun capable of extracting a large amount of charge per second, which is very stressful for the photo-cathode, maintaining a high beam quality. For this reason it is necessary to opt for guns that work in *continuous wave* (CW). Nowadays the the state of the art gun for high $\langle I \rangle$ is represented by the Cornell ERL injector prototype [87]. Table 1.1 lists the main injector parameters.

Even the acceleration phase becomes very delicate, in fact it requires a much greater power to be transferred to the beam and the need to operate in CW. These requests go against the use of standard hot RF cavities in favor of the adoption of cryogenic cavities that can withstand higher powers.

Another important feature that can be assessed in the design phase is the use of a *Energy Recovery Linac* (ERL). This special linac makes use of cavities that

Table 1.1. Cornell ERL Injector design parameters

Parameter	Value
Beam Energy	5–15 MeV
Charge per bunch	77 pC
Max $\langle I \rangle$	100 mA
Bunch length (rms)	2 ps
Normalized emittance (rms)	1 μm
Operating frequency (CW)	1.3 GHz

can recover energy from bunches directed to the beam dump to transfer this recovered energy to new bunches during acceleration. In this way the bunches that have already interacted are slowed down and the beam dump will have to dissipate less power, reducing the dangers and costs associated with radiation protection, and less electricity will be required on tap.

A machine of this kind is being studied at the University of Milan for the future University campus [88]. It will be composed of two main blocks:

Brixs a double ERL to a high repetition rate (100 MHz) dedicated to the inverse Compton scattering scattering to produce hard x-rays.

MariX a high repetition rate FEL (1 MHz) for the production of soft x-rays that will use a special arc compressor to double the energy that the beam buys from the same booster. The results of the single bunch simulations I have conducted are presented in this Ph.D. thesis in chapter 4.

Computational tools

Contents

2.1   Simulation tools

The simulation of the motion of N electrons inside a single bunch in the particle accelerator is not absolutely simple and immediate even for a computer of the latest generation. Suffice it to say that only the coulomb interactions between charges in each instant of time will be $N(N-1) \sim N^2$ if N is large, then we must perform the equations of motion and get the new positions. If we then add the high quantity of elements that can compose a beamline with all their different fields and the fields generated by the beam itself, we obtain a huge amount of data that is really difficult to manage in terms of consumption of system resources.

For these reasons, the adoption of already known and tested programs, developed in the most advanced research centers or even by individual researchers

who are experts in the field, is often preferable rather than the development of your own simulation code from scratch.

Nowadays, the most established programs are few and with their peculiarities, each one makes use of different approximations and takes into account only some phenomena. So it is often good to choose the program to be used based on the problem you want to deal with.

As we will see, in the course of this thesis work I have mainly used two different tracking codes:

Astra [89]: was chosen to simulate the beam tracking in the presence of space charge effects or for beams characterized by a low chromatic length (see Chapter 3.2), ie in all the works presented in the Chapter 3.

Elegant [90]: have been chosen to simulate high energy beams in dispersive paths taking into account the emission of Coherent Synchrotron Radiation and its secondary interaction with the same bunch that generated (see Chapter 4). The goal is to compensate for the effects on the beam and maximize its peak current.

Astra

ASTRA (*A Space Charge Tracking Algorithm*) is a suite of programs (*Generator*, *Astra*, *Fieldplot*, *Postpro*, *Lineplot*) that respectively allow the generation and transport of beams, the diagnostics of fields produced by the beamline elements and the beam data analysis [89]. This detailed introduction of the Astra code is important because this tracking code plays a major role in the GIOTTO's optimizations [1], as explained below in the dedicated paragraph.

It is written in *Fortran 90* and, like Elegant, is a multi-platform code. The main development platforms are LINUX and Windows. Executables for other platforms are made available even if they are less frequently updated.

Graphic programs controlled via the menu are based on the *PGPLOT* libraries.

Astra performs particle tracking through external fields defined directly by the user, also taking into account the space charge fields generated by the same cloud of particles. Tracking is based on non-adaptive integration with the 4th order Runge-Kutta method.

One of the greatest merits of this program is to take into account, during the tracking, the effects of the space charge, this makes it preferable in situations where the particles still have low energy and therefore the effects of relativistic

freezing are not observable. In particular, it can take into account the space charge, with a cylindrical symmetry model, then a 2D model that makes it very fast, or even in "full 3D" with a Cartesian mesh.

The beamline elements are defined by adopting the coordinate system normally used in accelerator physics. The axis of the motion of the package is taken as the z axis (longitudinal axis), the x axis is the horizontal axis and the y axis the vertical axis.

All Astra calculations are performed in double precision while the output can be, at the discretion of the user, either in single or double precision.

In the Astra suite of programs there is *Generator*, a code used to simulate the extraction of electrons from the photo cathode of *Gun* and generate the distribution of starting electrons. This particle set is then saved to a file that Astra reads at the beginning of the tracking. This strategy for saving and reading the particle file allows the user to read or process the distribution with his own programs.

The same Astra can save at the end of a tracking the final distribution that can be reused to simulate a subsequent section of the line. The broken simulation has significant advantages in terms of computational time and order, especially in the case of long beamlines.

The distribution of the beam is therefore described in a file which assigns to each particle the data line described in Table 2.1:

	1	2	3	4	5	6	7	8	9	10
Parameter	x	y	z	px	py	pz	clock	macro charge	particle index	status flag
Unit	m	m	m	$\frac{eV}{c}$	$\frac{eV}{c}$	$\frac{eV}{c}$	ns	ns	-	-

Table 2.1. Structure of each line of a file that contains the distribution of beam particles.

The first line of these files defines the coordinates of the reference particle in absolute coordinates, generally referring to the center of the bunch. The longitudinal coordinates of the particles, i.e., z, pz and t are given as a value relative to that of the reference particle.

As already seen, Astra is a fundamental tool when the space charge is dominant in transport, which is why I decided to go into more detail in the way the code simulates its effects. This is very important for my work, in fact the ultra short beams I studied are obtained with the *Laminar Bunching*, described in Chapter 3.2, where the effects of space charges are very important.

The two techniques used by Astra to simulate the spatial charge are strongly optimized and are very similar in terms of computational time, however the full-3D calculation requires a much higher amount of macro-particles to avoid statistical problems (due to the larger number of cells in the simulated grid). In the case of using the 3D algorithm, a linear interpolation is applied between the cells of the grid, while a spline-like cubic interpolation is performed in the cylindrical grid algorithm.

Space charge effects with Astra

If the energy of the bunch is sufficiently high, the fields generated by its spatial charge distribution can be considered a slowly variable time function. Precisely for this reason, instead of calculating the new fields generated by particles at each instant, it makes sense to scale the field coefficients in this way:

$$E_r \propto \frac{Q}{Q_0} \left(\frac{\sigma_{r_0}}{\sigma_r} \right)^{nr(r)} \left(\frac{\sigma_{z_0}}{\sigma_z} \right)^{nr(z)} \left(\frac{\gamma}{\gamma_0} \right)^{nr(\gamma)} \tag{2.1}$$

$$E_z \propto \frac{Q}{Q_0} \left(\frac{\sigma_{r_0}}{\sigma_r} \right)^{nz(r)} \left(\frac{\sigma_{z_0} \gamma_0}{\sigma_z \gamma} \right)^{nz(z\gamma)} \tag{2.2}$$

$$B\varphi \propto E_r \frac{\beta}{\beta_0} \tag{2.3}$$

where $\frac{Q}{Q_0}$, $\frac{\sigma_r}{\sigma_{r_0}}$, $\frac{\sigma_z}{\sigma_{z_0}}$, $\frac{\gamma}{\gamma_0}$ and $\frac{\beta}{\beta_0}$ are the relative variations of the charge, of the radius, of the longitudinal length, of the energy and of the speed respectively of the bunch.

At the same time, however, the grid must be rescaled with the variation of the radial dimension and the length of the bunch. $nr(r)$, $nr(z)$, $nr(\gamma)$, $nz(r)$ e $nz(z\gamma)$ they are functions that depend on the aspect ratio, defined as $A \equiv \frac{\sigma_z}{\sigma_r} \gamma$, of the bunch in the resting reference system. These quantities are constant if $A \gg 1$. In the case of *pancake* shaped bunches the fields will be proportional to:

$$E_r \propto \frac{Q}{Q_0} \left(\frac{\sigma_{r_0}}{\sigma_r} \right)^2 \frac{\gamma}{\gamma_0} \tag{2.4}$$

$$E_z \propto \frac{Q}{Q_0} \left(\frac{\sigma_{r_0}}{\sigma_r} \right)^2 \frac{\sigma_{z_0} \gamma_0}{\sigma_z \gamma} \tag{2.5}$$

while for a *cigar* shaped one we will have:

$$E_r \propto \frac{Q}{Q_0} \frac{\sigma_{r_0}}{\sigma_r} \frac{\sigma_{z_0}}{\sigma_z} \tag{2.6}$$

$$E_z \propto \frac{Q}{Q_0} \left(\frac{\sigma_{z_0} \gamma_0}{\sigma_z \gamma} \right)^2 \tag{2.7}$$

the user can define the maximum value of rescaling that can be achieved, if this value is exceeded the calculation of the fields generated is reinitialized.

The maximum duration of each step is recalculated hand in hand, so that you can deal accurately with any situations in which the fields vary faster. In these situations, in fact, the values of the fields are updated more frequently.

A situation to be kept under control is that in which no significant variations in the size of the bunch occur but the distribution of the particles varies considerably. In this case the scaling routine should update the field values too frequently, slowing down the computation considerably. A situation of this type occurs during processes of compensation of the effects of the space charge, in this case the beam emittance starts to grow again after reaching its minimum and, physically, the particles inside the bunch propagate outwards while those external still move towards the center of it. To cope with such a situation it is sufficient to set a maximum number of updates that can be carried out.

The rescaling procedure is deactivated as long as new particles are emitted by the photo cathode in order to maximize the accuracy of the calculations.

These scaling parameters can be represented in graph at the end of the tracking or saved in a log file.

Elegant

`Elegant` (ELEctron Generation ANd Tracking) is a code written in *C++* and developed entirely at the *Advanced Photon Source* (APS) at the *Argonne National Laboratory* (ANL) [90]. It was designed to respond to specific requests that the simulation codes currently available could not address.

This is a constantly evolving multi-platform code, even if a UNIX shell is required, which is still used to simulate and optimize both the closed orbits of the ring accelerators and the linear accelerator trajectories present at the ANL.

The program has no graphical user interface (GUI) to offer greater flexibility and better performance.

Once a tracking has been performed, a considerable amount of useful data on the beam is made available to the user, including α and β functions, centroid trajectories, ground coordinates of beamline elements, dispersion, amplification factors and many more.

All `elegant` input and output files are in a format specially designed for APS called *Self Describing Data Sets* (SDDS), a standardized protocol adopted by all the programs developed there. The advantages of using this format are many, among the most important is the easy communicability between different programs that is so permissible and the possibility to use a flexible set of programs (currently more than 80) specially developed for the phase post processing, the so-called *SDDS Toolkit*. These factors have convinced many simulator code programmers for particle accelerators to adopt the SDDS format, in some cases conversion tools have been produced, in others, as in the case of *MAD* and *MAD-X* developed and used at *CERN*, in Geneva, the code has been adapted to the new standard.

The lattice definition and the `elegant` operation options are assigned to two text files containing *namelist* of *Fortran 90* inherited from *MAD* (even if improvements have been made that made them less rigid than the original ones).
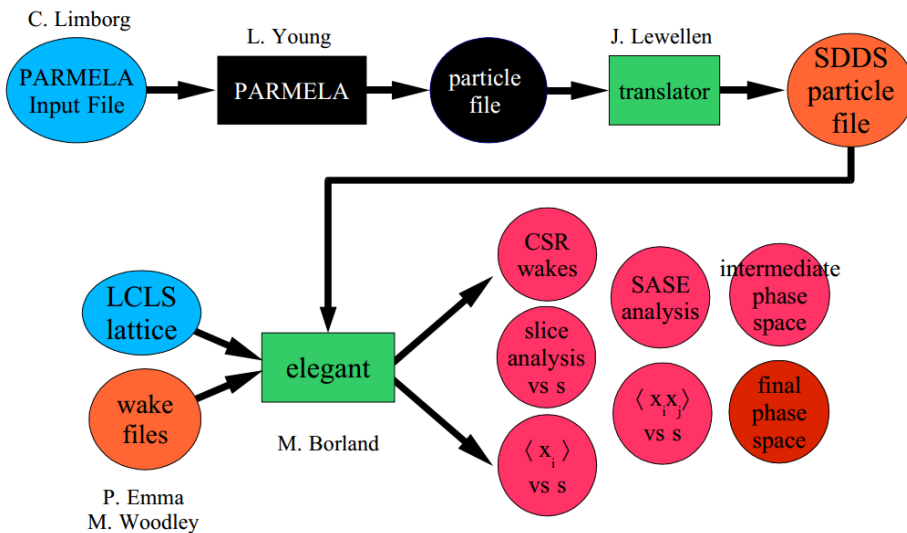

Figure 2.1. Multi-code simulation performed at LCLS, we can observe how `Elegant` can be used in sequence with other codes easily, the final results obtained were then used as input for *Genesis* to simulate the FEL.

elegant simulates the propagation of the beam using the transport matrices, practically every element of the beamline is translated into the corresponding

matrix that acts on the parameters of each single particle $[x, x', y, y', s, \delta]^\mathsf{T}$, where x and y are the horizontal and vertical transverse coordinates, the primed quantities are the divergences defined as $x' = \frac{p_x}{P}$ and $y' = \frac{p_y}{P}$, s the distance traveled on the orbit and δ is the momentum deviation.

Thanks to its remarkable computing capability and the flexibility of SDDS files, `elegant` has been successfully used in many facilities and international laboratories, including *LCLS*, in chain with other important simulation codes such as *PARMELA* and *Genesis*, to simulate the accelerating beam from 150 MeV to 14.35 GeV by simulating the effects of *Wakefield* and *CSR* [91].

2.2   Optimization tools

The particle beam tracking simulation is an essential step for studying beam dynamics in complex machines. However, in the absence of tools dedicated to advanced optimizations the setting of beamlines dedicated to the production of beams of that extreme quality can not be carried out. This is primarily due to the need to set the machine injector behavior with high precision, a situation in which the non-linear forces of space charge play a major role in the dynamics of the beam.

To deal with problems of this kind I used a code, called GIOTTO [1], based on a genetic algorithm. As we will see, this code is able to use Astra directly to test a large number of machine settings and gradually converge towards a solution that satisfies the user's requests.

I will now introduce the GIOTTO code which will then be further extended in Chapter 3 . Later, I will briefly explain how to optimize with `elegant` since I did some optimizations with this tool (as reported in Chapter 4).

GIOTTO

The code *GIOTTO* (*Genetic Interface for OpTimising Tracking with Optics*) was born from the desire to entrust to a genetic algorithm (Appendix A) the solution of specific beamline optimization problems. This choice was made given the ability of these algorithms to solve problems where the variables involved are strongly correlated in a non-linear way, as often happens in problems of electromagnetism [92].

The control parameters of a linac dedicated to the production of high quality beams are strongly correlated with each other, in particular when the effects of space charge are preponderant. Certainly in the case of ultra short beams this correlation, strongly non-linear, is even stronger, in fact the increase in the beam current keeps the space charge on even for relatively high energies.

The definition of a beamline that allows to obtain high-brightness beams, like all those that I deal with in this PhD thesis, involves an extremely high number of parameters. In this case, determining the value of these parameters is so critical that it is not possible to optimize them manually by finding an optimal solution. This limitation is particularly true for the Laminar Bunching (LB) compression technique (Chapter 3.2) which is based on a balance of internal forces (the space charge) and external forces (accelerating cavities and beam optics) to bring the beam to the maximum compression values.

GIOTTO is a genetic code, developed in *Fortran 90*, and has been parallelized with *MPI* libraries, which allows to directly control and vary beamline parameters treating them as *genes*. The code is able to launch tracking programs, extrapolate the results to evaluate the *fitness function* that the user defines and create the next set of *chromosomes* based on the best solutions of the previous generation.

In most cases, GIOTTO begins its operations by driving the Astra tracking code and its particle distribution generator, freeing it to use all their parameters as possible knobs for optimizations. GIOTTO, in fact, is able to interact natively with the input files used by Astra and the generator, which are written in the form of Fortran Namelist. Once a simulation is complete, the output files are analyzed in search of the results of the tracking and it is evaluated whether to perform a different subsequent simulation or if the requests have been satisfied.

One quality that should be highlighted is the user's ability to define constraints through analytical equations evaluated by the beam parameters during transport. This characteristic gives the possibility to define the parameter of longitudinal laminarity fundamental for the LB.

This tool can also be used to perform statistical analysis by changing some line parameters and collecting the results of the simulations. This can be done to perform analysis of the machine's jitters, in the Chapter 3.2 we will see how this ability of the code has been exploited to test a new experimental methodology that I propose in this thesis.

The development of this program has been carried out in the last decade but during my thesis work a lot has been improved. For this reason I will introduce here some features of the program and I will show in the Chapter 3.1 how it was improved during the PhD.

Elegant optimiation capability

`elegant` is designed to be started in sequence also altering various parameters so as to easily find the variations on the beam, this process can also be guided by the program itself to perform a targeted optimization of the parameters of the elements that make up the beamline. This is carried out in an extremely flexible manner, in fact the following characteristics of the optimization process can be set by the user:

- You can set any number of parameters that we want to change, each of it can be referred to a given element of the beamline, for example you can vary the intensity of the magnetic fields inside the quadrupoles and / or change the position altering the length of the drift between them.

- The range within which every single parameter can be changed and the step variation that can be applied every time.

- Numerous types of optimization algorithms (random-walk, simplex, genetic optimization, ...) that can be more or less effective depending on the space of the possibilities that you want to explore.

- The number of steps that the process can do in the space of possibilities before stopping, this prevents loops within relative minima of space.

- An expression that is a function of any parameter that `elegant` can calculate (Twiss functions, beam envelopes, dispersion, ...) more or less complex to maximize or minimize at the desired point.

- The value that the objective function must reach and its range of acceptability.

- The number of interactions with which the optimization process can be performed, the result of each iteration is retained only if better than the previous one and serves as the basis for the following process.

As we will see in the course of my work, this ability to `elegant` has proved extremely useful to compensate for the effects induced by CSR on the beam itself.

Application and development of GIOTTO

Contents

3.1 GIOTTO development

GIOTTO and, more generally, *Genetic Algorithms* (GA) have proved to be extremely effective tools in the optimization of working points for high-brightness accelerating machines even in presence of space charge. For this reason, GIOTTO has been employed in numerous works on which I worked in the last three years and has been updated and improved. Indeed, I had the opportunity to work

directly on the program code to improve its performance, add features that made it more user friendly and that allowed it to tackle more complex problems from the point of view of the exploration of the space of the solutions.

In this chapter, I describe the main changes that I made to GIOTTO over the years and I show the works done with the new versions of this tool with the results.

Objective functions

The first feature added to the code was to allow the user to define the *Fitness Function* (FF) as the sum of different *Objective Functions* (OFs) that individually try to optimize a single beam parameter.

Gaussian functions were normally used as an OF. These functions are centered in the target value (T_x) of the parameter x that is to be optimized so that, trying to maximize its value, the beam parameter object of the optimization is naturally approached to the target value. The Fitness (F) value, that is none other than the score assigned by the FF, is the sum of all the N OFs defined:

$$F = \sum_{i=1}^{n} H_i \cdot e^{-\frac{1}{2} \frac{(x_i - T_{x_i})^2}{w_i^2}} \tag{3.1}$$

Every single Gaussian is defined by three terms:

Objective Target (T_x) is the target value of the parameter that is optimized in this OF, it can be a fixed value or even another beam parameter. For example, one can set a value of the transverse dimension of the envelope required in a beam focal point by setting $T = 5$ µm (obtaining as target $\sigma_x = 5$ µm) or decide to request the cylindrical symmetry of the envelope by imposing $T = \sigma_y$ (imposing $\sigma_x = \sigma_y$ and $\sigma_x' = \sigma_y'$ with a second Gaussian). By setting both the T parameters in two different OF, one can request that both situations occur, ie a symmetric beam of fixed size.

Heigth (H) represents the height of the Gaussian function, in practice it is the maximum value that this can assume (ie when the objective condition is satisfied).

Modifying this parameter allows you to change the gradient of the function and increase the optimization priority on this function. In practice, raising or lowering the value of this parameter is a way to set the preferred direction of exploration of the algorithm in the solution space.

Width (*W*) is the standard deviation of the distribution (since $\sigma = W$) and, therefore, governs its width.

It is generally used to ensure that the optimization of the parameter is fast, so you try to position the current value of the parameter in a point of the Gaussian in which its derivative has a high absolute value, so that small parameter variations result in large changes in the fitness value F.

It can also be used to position the current value of the beam parameter in the Gaussian "plateau", the region closest to the center of the distribution. At this point the absolute value of the derivative of the function drastically decreases and therefore the parameter remains "locked" on the current value. The result is a change of direction of the optimization, the algorithm maintains the current value of the OF and automatically proceeds to the maximization of the other of those.
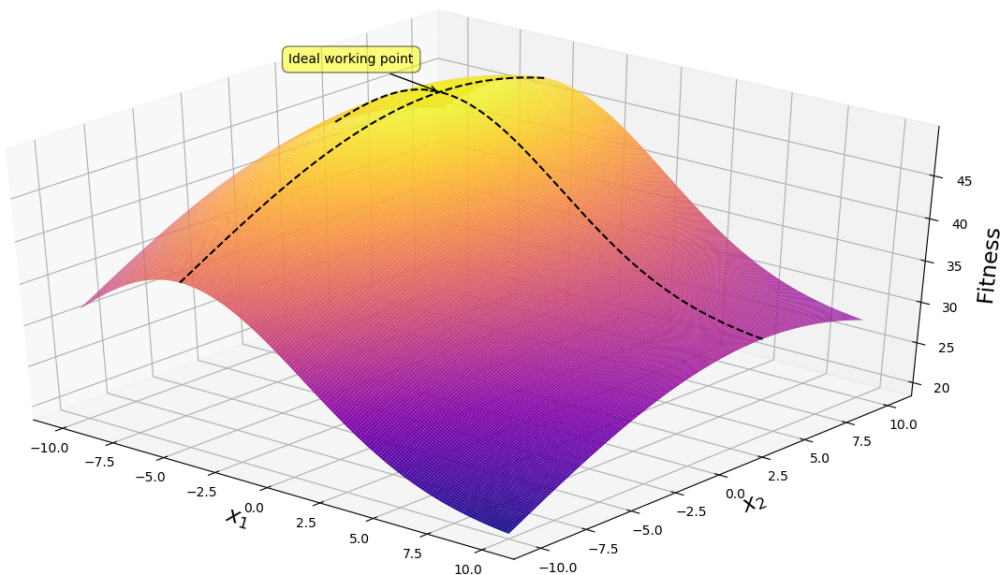
Figure 3.1. in this figure a portion *fitness function* that optimizes on two parameters: $20 \cdot e^{-\frac{(x_1+5)^2}{8^2}} + 30 \cdot e^{-\frac{(x_2-4)^2}{20^2}}$ is shown.
The absolute maximum point of this two-dimensional surface represents the point that verifies both the $x_1 = -5$ and $x_2 = 4$ conditions and therefore represents the ideal working point. The dotted lines represented the maximum points for each of the OFs. In the ideal working point shown the value of the FF is $F = 50$ that is the sum of the maximum values of both the Gaussian functions.

This approach allows to modify the height and width of a Gaussian OF to force the algorithm to give greater priority to the approach of the corresponding

parameter to its target, once observed the convergence rates of the different parameters.

The definition of the FF through single OFs makes it possible to distinguish much better which parameters are more easily optimized and which are far from the optimized value.

GIOTTO post-processors

In the following months I programmed some Python [93] scripts that are still used as post processors of the current optimization data. The first program, which is based on a *Graphical User Interface* (GUI) was written in order to better visualize the characteristics of the defined OFs and assist the user in modifying them to intervene on the exploration of the space of the solutions.
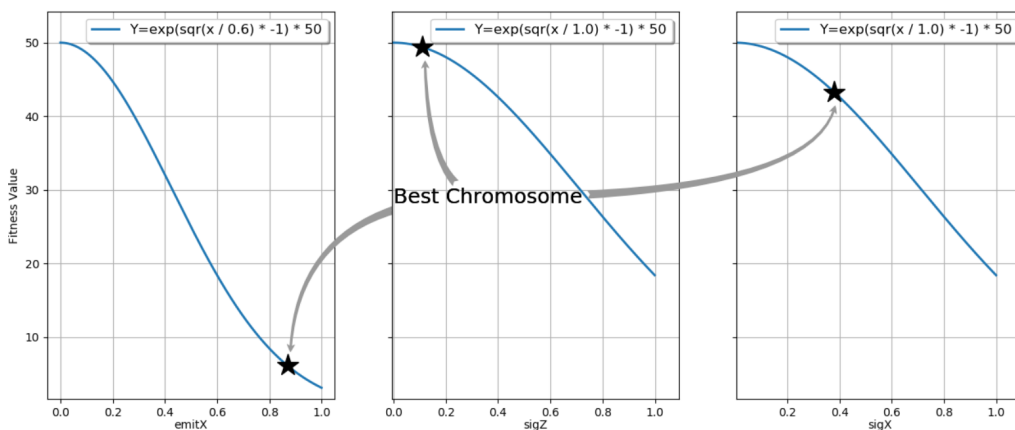
Figure 3.2. A GIOTTO post-processor that shows position of the parameters values on their relative objective functions. For example, here one can notice that the emittance $\varepsilon_{n,x}$ value is far away from its target, increasing the width W of the Gaussian would speed up the optimization.

The GUI is a script that reads from the GIOTTO input files the OFs that make up the FF and draws the graphs showing in which position the parameter optimized by each of them is located on the curve (a typical output of the script is shown in Fig. 3.2). In this way it is possible to understand how much each OF contributes to the fitness score and choose how to modify the functions.

A second script reads the logs that are constantly updated by GIOTTO to recreate the trend of the optimization. A typical output is shown in fig. 3.3, the bottom plot shows the trend of the fitness score of the best solution as the

optimization proceeds and the populations of the genetic algorithm are tested, the top picture shows the absolute deviation of each parameter from its target value.

It is thus possible to keep track of the different solutions identified during the evolution of the GA and, if necessary, easily identify the machine parameters that generated the interesting solutions in the logs.
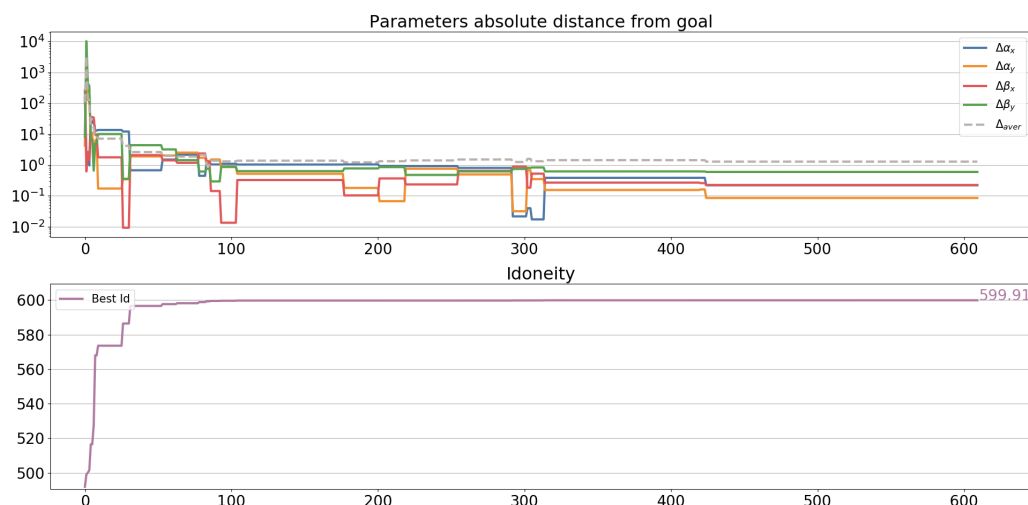
Figure 3.3. A GIOTTO post-processor that shows the evolution of the best chromosomes during genetic optimization.
Bottom plot shows (in semilogarithmic scale) the trend of the fitness score of the best solution as the optimization proceeds and the populations are tested, top picture shows the absolute deviation of each parameter from its target value.

Twiss parameters support

GIOTTO can natively read the beam parameters directly from ASTRA-generated files. However, these outputs do not contain information on the Twiss functions associated with the electron beam.

On the occasion of the work done for EuPRAXIA@SPARC_LAB to design its matching line [6](see Chapter 3.2) we have introduced in GIOTTO the possibility to define parameters customized by the user. This allows us to define parameters of merit useful for the purposes of optimizations, but has also allowed us to define the Twiss parameters within the program code that can be used directly in the FF.

Now, being able to optimize directly on the values of the Twiss functions, you can use GIOTTO to set and, as we shall see shortly, even design matching lines from scratch.

Tackle wide-ranging research problems

GIOTTO, as already explained, was born to perform genetic optimization of beamlines and statistical analysis [1]. It is able to communicate with ASTRA, a tracking code which takes into account the full-3D space charge effects.

GAs are a class of stochastic optimizers with a great ability to address problems in which the parameters are strongly correlated in a non-linear way (more details in Appendix A). The beam dynamics in particle accelerators can be a problem with these characteristics. For example, when the energy of the beam is low, the effects of the space charge on the particles induce strong nonlinear correlations in the beam parameters that make machine tuning very complicated. These effects can also occur in relatively high-energy beams, as in the case of a transverse focusing point (such as an *interaction point*) or in case of a high longitudinal compression, nowadays required in many advanced applications.

All these features make GIOTTO ideal for the research of working points of linear accelerators in the early stages of acceleration and have allowed it to excel, for example, in the optimization of the Velocity Bunching technique at SPARC [94] [95]. However, the speed at which a GA can explore large-scale solution spaces looking for regions with optimal solutions suggests that these algorithms can be applied to more general problems.

In those years I found myself having to draw a matching line that could contain a highly energetic and divergent plasma-accelerated electron beam and transport it to the undulators of an FEL. This transport must be done both by preserving the initial normalized emittance of the beam which tends to grow spontaneously due to the low chromatic length (see Chapter 1.1, eq. 1.14) of the beam coming from the plasma stage and taking care to match the correct Twiss parameters for the injection in the undulators.

To solve this problem we could not begin to simulate the line from a known work point, but we had to simulate the matching line from scratch looking for a correct positioning and setting of quadrupoles that fit the available beam.

A problem of this type is characterized by a much wider research domain than the optimization of a known working point. From now on I will refer to similar situations by calling them *Wide-Ranging Research Problems* (WRRP) because the

name well describes the different approach to the problem from the GA point of view.

As the name of the WRRP suggests, to find an appropriate solution to the problem it is necessary to efficiently explore a larger solution space. This, in the case of GAs, translates into a greater variation range of gene values when populations are randomly generated or mutations occur (if necessary, an explanation of the meaning of these terms is presented in the Appendix A). These measures have the effect of greatly increasing the genetic variability and pushing the proposed solutions to move in an increased radius in the space of the solutions.
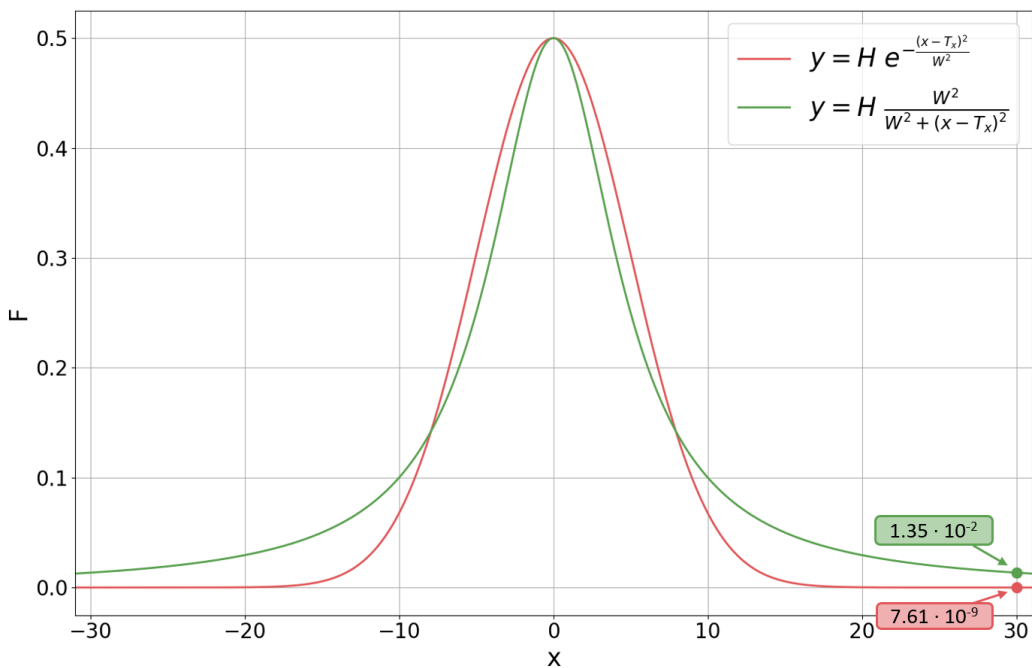
Figure 3.4. The figure shows the comparison between a Gaussian and a Lorenzian. The height, width and target value parameters are the same in both the functions ($H = 0.5$, $W = 5$, $T_x = 0$). Both functions are evaluated in the point $x = 30 = 6W$.

The simulation must start from an arbitrary point of the space of the solutions (in our case we have chosen the origin of the space [3]) that is generally located at very distant points from the region we want to identify. If the distance is too high, the objective functions are likely to return fitness scores too low to be distinguished from zero and this results in blocking the process of population evolution. This block of evolution occurs because the mutations and crossings cause variations that are no longer distinguishable from the FF and it is no longer possible to rank the proposed solutions, therefore the reproduction of

the chromosomes becomes totally random and the exploration ineffective.

To solve this problem it was necessary to change the way in which the chromosomes are selected for reproduction and, above all, to change the shape of the objective functions. The Gaussian functions, in fact, drop in value very quickly when they are evaluated far from their average value. It was therefore decided to move from Gaussians to Lorentzians as an objective function the fitness score is assigned as follows:

$$F = \sum_{i=1}^{n} H_i \cdot \frac{W_i^2}{W_i^2 + (x_i - T_{x_i})^2} \tag{3.2}$$

where the terms H, W and T_x have the same meaning and function that they assume in the previous case with Gaussian functions.

What may seem like a marginal modification has actually changed the way in which the fitness score is assigned to relatively distant points. Just think that a point that is evaluated in $x = 10$ $W = 10$ $\sigma = 1$ has a score of $F_L \simeq 1 \cdot 10^{-2}$ if evaluated with a Lorentzian-like function or $F_G \simeq 2 \cdot 10^{-22}$ with a Gaussian-like one (in fig. 3.4 a comparison at $x = 6$ $W = 6$ σ is shown).

3.2   Improved-GIOTTO applications

Over the last three years I have been able to apply GIOTTO in the optimization of lines for the production of extreme beams and to study particular methodologies that would allow to increase the brightness of the beams. In this way I was able to test the new features of GIOTTO described above, in some cases even I could not reach satisfactory results without having applied these important improvements.

Beam-based method for elements alignment

In 2015 I began to study the misalignments of the solenoids that are mounted in the SPARC_LAB linac [11], at the national laboratories of Frascati (LNF) [2]. This machine is a test facility dedicated to the production of high brightness beams using the technique in *Velocity Bunching* (VB) [73].

The VB allows the electron bunches to be compressed longitudinally as they are accelerated. This particular technique is carried out during the first cavity acceleration phase and requires an external focusing force in the transverse plane

to contain the beam envelope because the radio frequency focusing is not strong enough. For this reason, the accelerating cavities dedicated to acceleration in VB are equipped with numerous solenoids that surround the cavity.

In the SPARC_LAB case, the first two cavities (*AC1* and *AC2*) are surrounded with 7 solenoids each disposed in a configuration similar to the Helmholtz one. The presence of these elements considerably complicates the dynamics of the beam when the beam trajectory is not coaxial with the coils [96], for these reasons, the positioning of the coils is a very delicate problem.

In the test facilities that work on different experiments, it may be necessary to use beams with various operating energies, this means that the introduction of a small misalignment or angle of inclination of an element in the linac produces different trajectories in different energy beams. Having more trajectories of the beams is a big problem that prevents the solenoid re-alignment process and must be resolved before trying to estimate the correction to be applied in the solenoid positions. For this reason, we have developed a new beam based method that allows to determine the trajectory closest to the *Electro-Magnetic Axis* (EMA) of an accelerating cavity.

This special trajectory that we can call *Golden Orbit* is the orbit less sensitive to the energy variation of the beam. This method was tested using simulations and a virtual experiment explained later.

The second method that we want to introduce here, is applied in sequence to the first one and is necessary to estimate the exact misalignments between the solenoids axis and the reference beam trajectory. This method is based on real measures made on the machine (beam centroids on a Yag target) and beam simulations in the machine itself.

The method is based on the variation of the beam centroid position, on a target, caused by varying magnetic field produced by each single solenoid. These beam positions on the target data are taken in laboratory by real beam measures and then interpolated, by using a homemade tool, with beam dynamics simulations. This method has been verified on the real machine and was able to estimate a displacement manually applied to the solenoid.

The use of the both methods gives us access to the data needed to set an ideal trajectory, stable for different energies of the beam and the values of the corrections to apply, on both the transverse axis, to the position of the solenoids.

A method to find the golden orbit

The ability to find an optimal orbit for a beam passing through an active beamline element is a critical problem. For example, a focusing coil wrapping around an accelerating cavity must be centered as close as possible to the orbit of the beam, which must be as near to the cavity EMA as possible. Vice versa, if a different axial position is chosen, the transverse kick on the bunches is usually not negligible and moreover, for the different beam energies it changes.

First of all we started to study how to reduce this phenomenon of separation of trajectories as a function of the accelerator gradient. This is proportional to the distance between the position of the particle and the EMA of the cavity. We can define the EMA of the entire linac as the place of the points (which defines a curve) in which the undesirable transverse contributions to the motion of the particles are reduced to a minimum. These contributions are introduced by the positioning and geometry of the linac elements, but also by geometric imperfections or inhomogeneities of the materials that make up the elements. As a consequence, the EMA is not exactly known a priori and therefore, the problem of finding the orbit closest to the EMA, already defined as golden orbit, is not trivial.

The *steering magnets* are used to correct the beam's trajectory and to force it as close as possible to the EMA. If we apply a set of currents to the steering magnets, we can measure the beam centroids positions on a target and see their displacement by varying the accelerating gradient. The amplitude of these displacements is proportional, in average, to the integral distances between the points on any trajectory and the points of the EMA (in a mathematical approach). A trajectory very close to the EMA will show much stable centroids (in position) versus different accelerating gradients of the cavity.

Our idea is to map randomly the possible trajectories at different energies and to observe where centroids gather on a target. To demonstrate the efficiency of the orbit correction method we did a virtual experiment with the aim to find the golden orbit in a short linac. The virtual experiment is structured in two phases: a series of simulations and an analysis of the trajectories.

The tracking had been performed with the ASTRA [89] code in order to consider the effects of the space charge forces that dominates the beam dynamics in the initial part of the linac.

We made use of GIOTTO to drive ASTRA performing statistical analysis. Then we have chosen randomly a collection of sets of currents (one for each steering) and 6 different operative energies of the linac. The sets of currents were chosen in order to avoid collisions of the beam on the walls of the cavity and

the propagation of the bunches was simulated for each set of currents applied to the steering magnets and for each of the 6 working energies.

In the end we analyzed 640 different families of trajectories and saved the centroids arrival positions on the target. To test the method, we simulated the following beamline:

1. A SW S-band photoinjector Gun.

2. The Gun's solenoid.

3. A TW S-band accelerating cavity SLAC type.

4. Two couples of steering magnets. The first one is just after the exit of the Gun's solenoid, the second one is about 50 cm after the beam entrance in the accelerating cavity.

These elements are placed with the following misalignments and rotations (Z as the propagation axis, X as the horizontal one and Y as the vertical one):

- Gun and Gun's solenoid: same misalignment $(X, Y) = (-500.0 \ \mu m, \ 0.0 \ \mu m)$

- Accelerating cavity: tilted on XZ-plane, 0.17 mrad (referred to the Y axis at the cavity center)

- Steering magnets: centered in $(0, \ 0)$

Our goal was to demonstrate that the method is able to identify the closest possible trajectory to the EMA in all its points, ie the golden orbit without knowing any information about the misalignments and tilts of the elements. This goal is achieved by doing a bi-dimensional histogram of the centroids positions on the target and finding were they gather, as shown in Fig 3.5, where upper part shows the entire target with the Cartesian axes (X, Y) are in black. The red cross represents the prosecution of the cavity's EMA. In the lower part of the Fig 3.5 is shown a zoom of the most populated area and the centroids. The circled centroid families refer to the same steering magnets settings, but with different accelerating gradients.

To better judge the quality of the trajectories we introduce the parameter I that evaluates the instability of the trajectory:

$$I = \text{Var(x)} + \text{Var(y)} \tag{3.3}$$

where the function Var() evaluates the variance of the Cartesian coordinates that identify the position of the centroids on the plate plane.
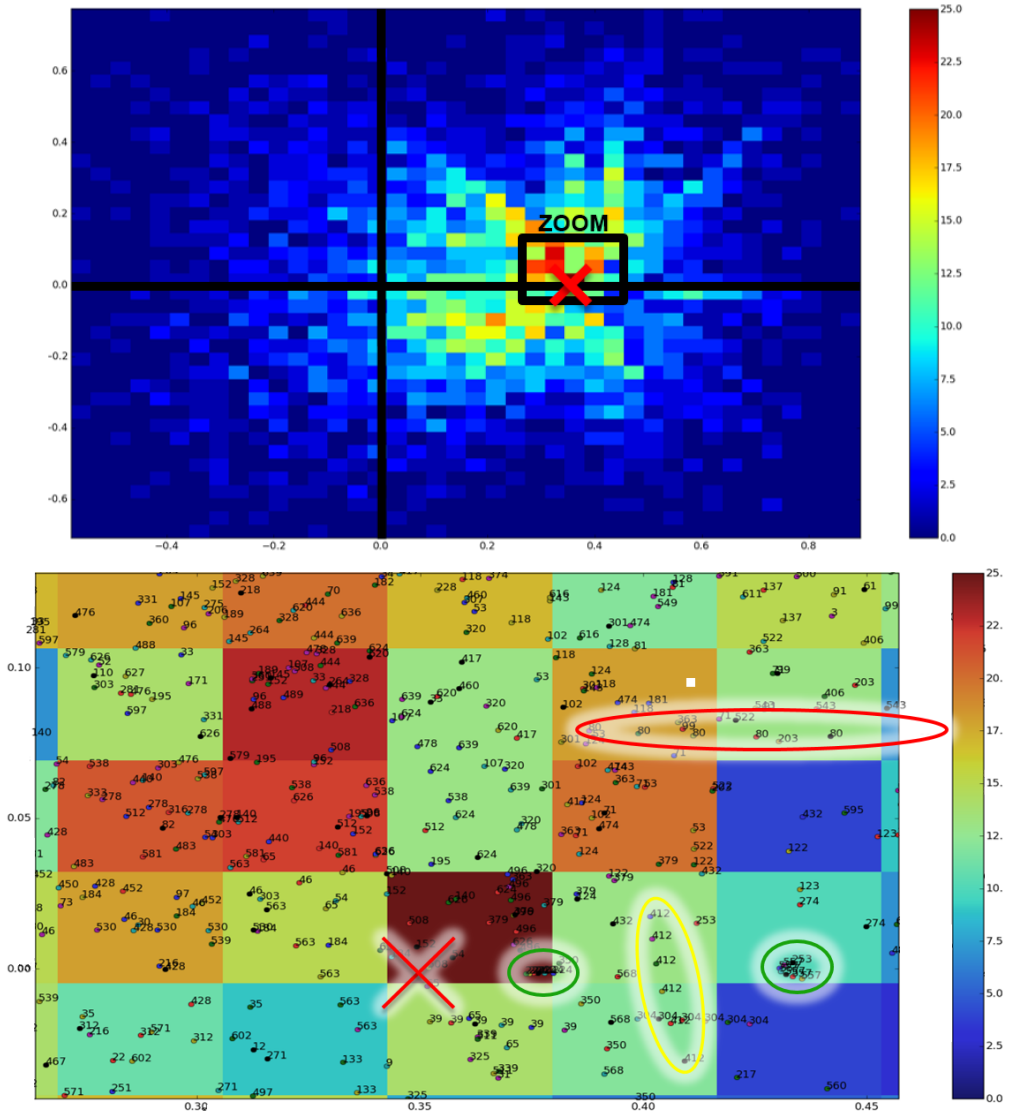
Figure 3.5. 2D histogram of the positions of the centroids on the plate plane. The figure below shows an enlargement of the area most populated by centroids. As you can see in this area are the most stable trajectories (families of green circled centroids) near the point where the EMA of the cavity intercepts the plane of the plate (red cross). Centroids identified by the same number belong to the same family (same setting of steering magnets but different average energy of the beam).

In the lower part of Fig 3.5, the two families of centroids that are circled in green are the most stable in the whole simulated set (with the value of the lowest parameter I). The best of these two, the one that we consider the golden orbit, is the one on the left and is very close to the point where the continuation of the

EMA of the cavity intercepts the plane of the plate, about 25 μm.

In Fig 3.6 are compared two trajectories: a bad orbit, in violet, and the golden orbit found with this method, in green. It is easy to see that the golden orbit found with this method is very close to the EMA of the cavity, shown in blue, in every point. If needed, the method can be iterated (scanning more trajectories or a smaller area of the target near the supposed EMA position) in order to find a better final trajectory.

We accepted the best steering magnets currents set found with this method corresponding to the green trajectory in Fig 3.6 and pursued with the analysis of the solenoid misalignment.
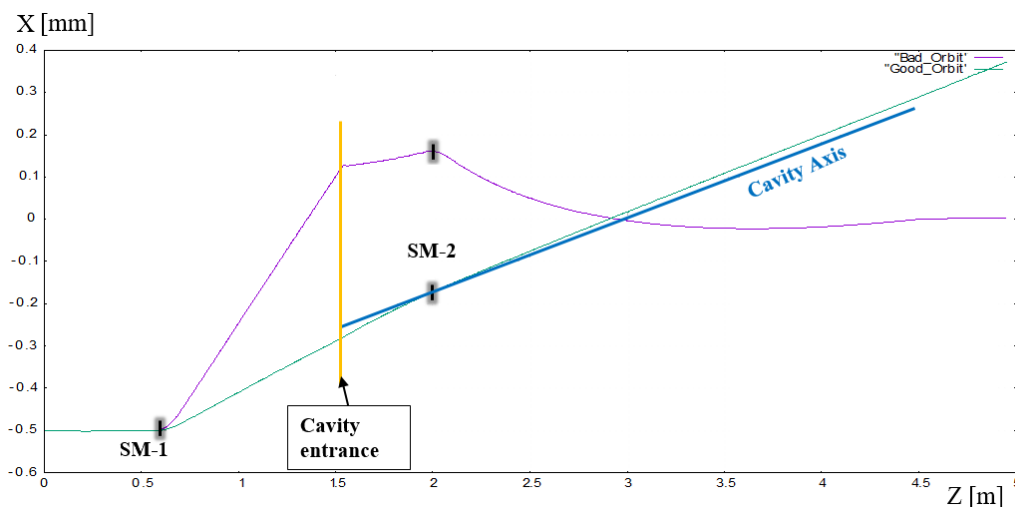
Figure 3.6. Two trajectories, represented in the horizontal plane. The best trajectory found is colored green, while the purple one is an example of a non-optimal orbit (with high instability). The EMA of the cavity is represented in blue (it is the geometric axis). As you can see the most stable trajectory found with this method is very close to the EMA of the cavity in every point.

At this point we can assume to have set an orbit as stable as possible in the linac and we can proceed to estimate the correction to be applied to the position of the solenoids.

We hypothesized that the angle of incidence of the beam on the input face in the solenoid is very small once the golden orbit has been set. This is because the solenoids that wound $AC1$ are mounted orthogonally to its geometric axis. In this case, the effects of inclination of the solenoid on the dynamics of the beam are minimized and can be ignored in the analysis of positioning errors.

We have investigated a method to compare the simulated effects of beam propagation in a misaligned solenoid with the real dynamics measured on the

machine.

The following measurement procedure has been applied in the laboratory to gather information on beam dynamics: only one coil is ignited at a time and ten different current values are applied (0 A, 20 A, 40 A, ..., 180 A). For each current a fixed energy beam (we have repeated the experiment at 114 MeV and 165 MeV) is propagated in $AC1$ and hits the downstream target. The data on the positions of centroids on the target are therefore acquired.

The obtained laboratory data are compared with other simulated data with ASTRA reproducing the procedure with which the measurement is performed. A misaligned coil is simulated using its field map, so that field interactions with the metal shell around the coils can be taken into account. In Fig. 3.7 I compare the simulated data of the positions of the beam centroids on the target obtained varying the the coils currents with 8 different field maps of misaligned coils. The misalignments are purely on the horizontal axis only (-2 mm, -1 mm, $+1$ mm and $+2$ mm) or on the vertical axis (-2 mm, -1 mm, $+1$ mm and $+2$ mm).
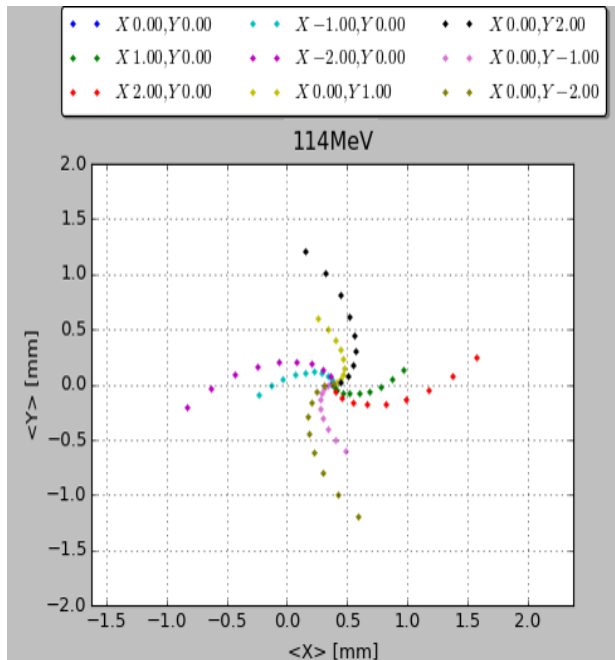
Figure 3.7. The simulated data of the positions of the beam centroids on the target obtained varying the the coils currents for 8 different misaligned coils are shown. Each of these misaligned coils is simulated using a calculated field map. In the the legend the misalignment magnitude (in mm) on the horizontal (X) and vertical (Y) axis are shown.

Looking at the Fig. 3.7 we note that the union of these patterns has radial symmetry, we have therefore verified that it was possible to reconstruct the other

patterns starting from the one obtained with a single field map. This can indeed be done with the use of two operators:

Rotation operator rotating the points of the patter obtained around the origin of the plate (the point that crosses the EMA) to simulate the effect of a coil misaligned from the magnetic axis of the cavity of the same quantity.

Stretch operator multiplying the X and Y components that identify each point on the target by a factor of $k > 0$ to simulate the effect of a minor or major misalignment, in this case the k factor is the proportionality factor between the misalignment of the field map whose effect is to be rebuilt and the simulated one.

We have shown that, in the absence of effects introduced by the coil tilt, it is possible to use a single field map for each coil to simulate the effects of many other misalignments of the same coil. We can make use of this expedient thanks to the cylindrical symmetry of the simulated system, this approximation holds until the influence of the shell walls in the field is negligible (it has been verified for misalignments below 4 mm).

We have created a Python script to display on the screen the positions of the measured centroids superimposed on those simulated for a single coil, at a given operating energy. The data sets consist of 10 points, one for each current value, arranged on a curve. The script allows you to rotate and stretch the set of simulated points to go to superimpose them to the best pattern measured in the laboratory, the result of a fit done with this tool is shown in Fig. 3.8. At this point the misalignment of the coil generating the simulated data set can be deducted from the rotation angle and the applied stretching coefficient and is taken as the true misalignment of the reel.

Conclusion

The two methods previously explained need to be used together in order to correct the positions of the solenoids on a machine that runs at different energies. We performed a more complex virtual experiment, compared to the one described here, to show that the second method leads to incorrect conclusions when used on an orbit with high instability value.

On the other hand, these can also be used properly as standalone methods. The first method can be used separately to find an orbit very close to the real EMA of the machine and so to rise the beam quality. This method can also be used to realign cavities, in fact the trajectory found has slope similar to that of the
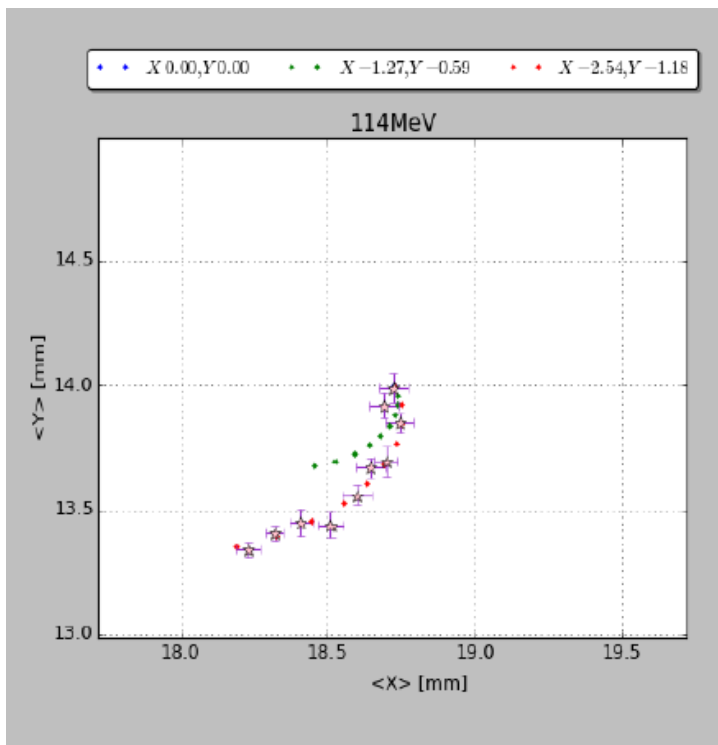
Figure 3.8. This figure shows the results of a fit made on 10 measured points, represented with purple stars, and simulated point sets with only one field map, 10 red points. Once satisfied by the fit, it is possible to read in legend the misalignment corresponding to the rotation and the stretch applied, in this case ($X = −2.54$ mm, $Y = −1.18$ mm).

EMA (with this golden orbit the rotation estimation is about 0.19 mrad, the real value is 0.17 mrad). In the case of a machine that operates with a single operative energy, i.e. with always the same trajectory, the second method predicts the correction to apply to the alignment of the solenoids.

The choice to fit manually the distribution of centroids may at first sight appear approximate but the intent, at first, was to demonstrate the validity of the method in predicting the misalignments manually introduced on purpose. In a future, an automatic fitting system of the measured pattern could be developed. A study of a "tilt" operator have still to be completed so the latter method, at the moment, is not accurate in case of incident angles $\alpha > 0.1°$.

The methods are ready to be tested on a real machine, and a test on *SPARC* will be performed in the future when the beam time is available.

Matching of low chromatic length beams

In the Chapter 1 we saw how the *Free Electron Lasers* (FEL) [14] work.

In the Chapter 1.1, dedicated to the *Plasma Acceleration* (PA) techniques, we discussed how their performances are pushing forward, thanks to the high interest of the whole scientific community. This situation suggests the possibility of exploiting the PA to obtain more compact and less expensive FEL machines. A compact layout can be achieved using a very short plasma stage as main accelerator and building a compact transfer line able to control and match the beam coming from the plasma acceleration stage in the undulator section.

We studied the possibility of application of a *Genetic Algorithm* to the matching problem of a machine like the Eupraxia@SPARC_LAB Free Electron Laser. We used GIOTTO and ASTRA to perform a wide-ranging research for the correct parameters of the *Transfer Line* (TL). The goal of optimization is to obtain transfer lines with many features:

- they must be compact in order to fulfill the compactness objective that leads to choose a plasma stage as an accelerator

- they must be able to carry the beam up to the undulators, preserving the emittance from the deterioration due to the reduced chromatic length of the beam

- they need to have the proper values of the Twiss transverse functions of the beam (α_x, α_y, β_x, β_y) at the injection point in first undulator required by the FEL operation.

In this work are presented 4 different TLs lattices found using GIOTTO. These lines differ in terms of lengths, number of quads and type of quads (permanent or electromagnetic). We did not enter in merit of the different advantages or disadvantages between the different lines (as jitters or misalignments), because the aim of the work is to present a new methodology to cope with this kind of problems.

The beam on which I worked was simulated by transporting it in a conventional accelerator with the *Laminar Bunching* technique (described in Section 3.2), in order to preserve its cylindrical symmetry and the low emittance. Then, the bunch is immediately injected as witness in a plasma channel and strongly accelerated to its final energy and is ready to be transported and matched to the undulator.

In this section I will briefly show the concept of matching the beam in the undulator modules and how it fixes the beam characteristics that we have to

obtain with our transfer line. I will then present four alternative transfer lines obtained with this methodology that are able to match the given bunch. A small focus on the most interesting line will be shown in conclusion.

The matching in the undulator

The trajectory of an electron bunch in a long undulator is unstable because this element develops quadrupolar components of its magnetic field. In fact, this element is characterized by a strong vertical focusing effect and a weak horizontal defocusing effect on the electron beam. For this reason, the undulators are divided in modular portions separated by magnetic quadrupoles that compensate the undulator quadrupole effect.

The matching in the undulator is performed imposing the periodicity of the Twiss functions ($\alpha(z)$ and $\beta(z)$) all over the periodic module of the lattice (see Fig 3.9). Once the undulator is chosen, the existence of the solution of this problem depends on beam parameters, such as average beam energy (and normalized transverse emittance), and on the emitted radiation wavelength [97].

It is also very important to crosscheck the quadrupole strength needed to compensate the undulator unwanted effects and the spot size of the beam in the quadrupole bore, the values of these parameters must be in agreement with the state of the art of the technology of the quadrupoles. Once this condition is granted, the exact values of the Twiss functions of the bunch at the entrance of the first undulator module are known and the design of the transfer line, i.e. the set of quadrupoles upstream the undulator that are responsible of matching these initial parameters (used below as target parameters of our genetic code), can start.

Transfer line design

The beamline portion dedicated to match the beam at the entrance of the first undulator is called Transfer Line (TL) and the magnetic elements used in this portion are quadrupoles. In fact, as said before, at the entrance of the first undulator module it is needed to obtain values of the Twiss functions as close as possible to the ones that grants the periodicity of these functions in the modules.

The TL lattice is often studied analytically. The quadrupoles and the drifts are described by their associated transfer matrix, like lenses in optics. The product between the 6D vector associated with the beam $X = (x, \, p_x, \, y, \, p_y, \, \Delta z, \, \delta)^\mathsf{T}$ and these matrices give the transferred beam vector after the propagation through
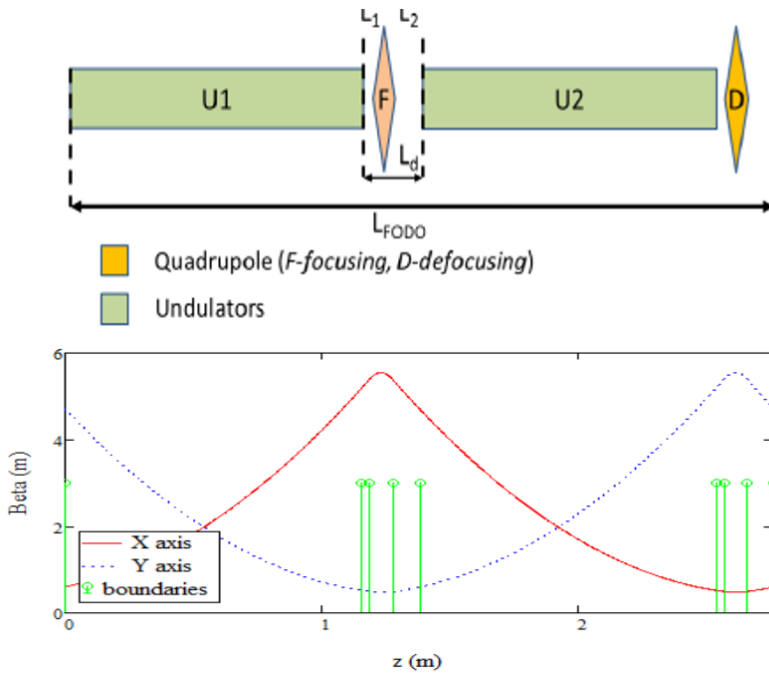
Figure 3.9. Top. The periodic block of the undulator of Eupraxia@SPARC_LAB, composed by 2 undulators and 2 quadrupoles. The quadrupoles are in FODO configuration. **Bottom.** The values of the transverse β functions in the periodic block. This setting of the line grant the periodicity of the solution all over the undulator if the beam is matched.

the element. From the transfer line equivalent matrix, obtained multiplying all the matrices associated with the optic elements, one can obtain the transfer matrix for the Twiss parameters [98] and figure out how to design the TL.

Considering the layout of the machine, the starting point of the TL will coincide with the output of the plasma channel, here the bunch suddenly passes from a region characterized by an extremely strong electric field to a drift space. The beam inherits from the plasma acceleration stage a big energy spread and transverse momenta. In these special conditions most of the approximations done to obtain the transfer matrices are lost and is necessary to consider the quadrupole transfer matrices approximated up to the second order [99]. The analytical approach becomes more complex and the solutions have to be carefully checked by simulation. Considering these problematics, we have chosen a different approach which is based directly on the particle tracking able to give a full phenomenon description.

As said before, the propagation inside the plasma channel is responsible

of the high values of the beam energy spread and transverse momenta, the combination of these features with the small transverse dimensions of the bunch at the beginning of the TL causes big issues due to the high chromaticity of the beam.

Let us look again at the Chromatic Length defined before for a transversally symmetric beam $(\sigma_x^{(0)} \simeq \sigma_y^{(0)})$, equation 1.14.

For the bunch, described in the following section "Beam Preparation" and shown in Fig 3.10, with transverse rms dimensions $\sigma_x \simeq \sigma_y \simeq 1.8 \cdot 10^{-5}$ m, energy spread $\sigma_E \simeq 2.7 \cdot 10^{-2}$ and divergence $\sigma_{x'} \simeq \sigma_{y'} \simeq 0.14$ mrad, the Chromatic Length results $L_C \simeq 4.8$ m. The rms transverse dimension value is strongly affected by a large halo in the tail due to the interaction with the plasma. We performed a transverse cut on the full beam distribution, with radius equal to $1 \cdot 10^{-5}$ m, to avoid a misleading growth of the rms beam transverse dimensions when transporting the full beam through the line.

Focusing again on the methodology to solve the design of TLs, in the next chapter we are going to explain the procedure we have adopted, which gives the TL lattice solution directly from tracking code simulation results. The main actor in our procedure is a genetic algorithm able to generate TLs lattices, drive a tracking code to analyze the goodness of the proposed solutions and then to create better lattices.

Use of GIOTTO to design the TL

As already mentioned, the proposed lines were found with the genetic algorithm owned by our group, GIOTTO.

Our approach to the design of a TL is to start from scratch, i.e. defining a chosen set of switched off quadrupoles (with focusing strengths equal to zero) with arbitrary positions, and change the strengths and the positions gradually, evaluating the fitness value for each solution. Let us compare this problem with a working point optimization problem, in which the main behavior of the line is known and the values of the parameters that identify the solution are in the neighborhood of the values of the starting point of the optimization. In our case the GA need to perform in a bigger area a wide ranging research for the correct parameters, for this reason we treat the problem of drawing the transfer line as a *Wide-Ranging Research Problem* (WRRP). In fact, GA are able to deal very well with this different kind of optimization problems thanks to their ability to move wisely in the space of the solutions. A classical didactic example of application of GA is on the *Traveling Salesmen Problem* (TSP) that requires to start from scratch

and move in a wide solution space [100].

For these reasons we had to further develop GIOTTO to better address the low values of some objective functions (when the solution is close to some target values but far from the others) and to make it able to directly optimize the values of the Twiss functions (whose data, unfortunately, are not available in the output of the tracking code adopted, *ASTRA*).

Table 3.1. Objective values of the parameters that are optimized in the algorithm, a Lorentzian function is assigned to each parameter.

Parameter	Value
α_x	1.48
α_y	-0.65
β_x	5.04 m
β_y	2.11 m
$\varepsilon_{n,x}$	0.42 mm mrad
$\varepsilon_{n,y}$	0.43 mm mrad

The fitness function we used (shown in chapter 3.1) is a sum of objective functions with Lorentzian shape, six in this case, each one centered on the target value of the parameters that we want to optimize at the end of the TL. The final parameters that we needed to control in our optimization are the four values of the transverse Twiss functions (α_x, α_y, β_x, β_y) that must match the values that grant the periodicity condition in the undulator and the values of the transverse normalized emittances of the beam ($\varepsilon_{n,x}$, $\varepsilon_{n,y}$). All these parameters are evaluated at the end of the TL. It is important to check the emittance and keep it constant (or almost constant) avoiding solutions in which the Twiss parameters are correct, but with a much higher emittance value. This variation of emittance, due to highly chromatic beams, is triggered by a strong defocusing of the particles (which accentuates chromatic aberrations).

The exact objective parameters that have been set in GIOTTO are summarized in tab. 3.1.

Procedure and results

Beam preparation. A 40 pC high brightness electron beam has been obtained by simulation using the tracking code ASTRA. The Linac layout simulated was optimized in term of compression, emittance preservation and RF focusing,

with the aim to obtain beam parameters ad hoc for the injection into a plasma wave. The beam is than furthermore focused with a quadrupole triplet and then accelerated up to 1 GeV of energy with a LWFA simulation (with Qfluid [101]).
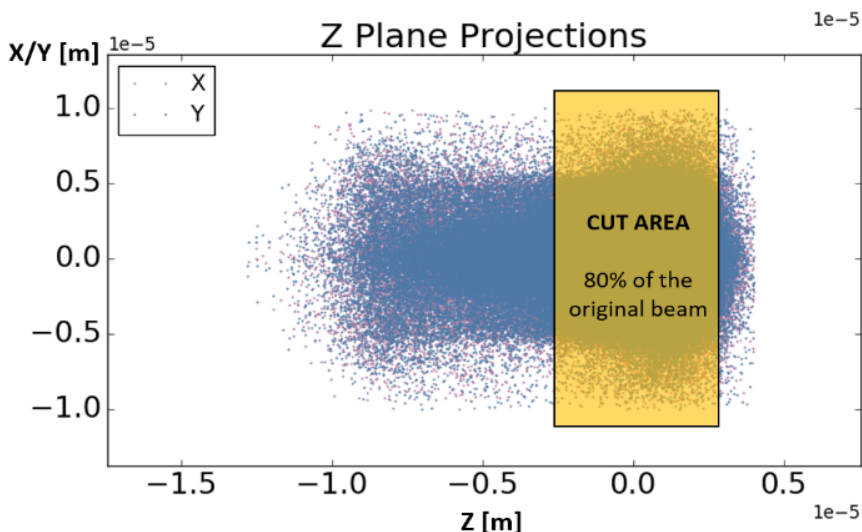
Figure 3.10. Portion of the beam used for the matching, we chose to select the portion with the highest peak current and lowest emittance; in this figure a large beam halo situated in the beam tail has been removed to show better the cut area.

A slice analysis of the bunch at the extraction point of the plasma is performed in order to select the portion of the beam with the best quality, in terms of brightness (highlighted in Fig. 3.10), and match this portion with the TL we are going to design.

A cut of the beam is performed to select the particles that we want to exploit to produce the radiation (Fig. 3.10, Table 3.1) The slice parameters are then used to check the existence of a periodic solution of the Twiss functions associated with this slice inside the undulator. This operation has been performed with GENESIS [102] and the resulting initial values of the Twiss functions are shown in Table 3.2.

TL optimization and results. First, we checked how to reduce the tracking time of the beam in the TL without introducing artifacts in the simulation results. We found that using 10^5 macro-particles to simulate the bunch and disabling the space charge effects is the best compromise. Once the optimization gives us a good solution (i. e. a set of positions and focusing strengths), a tracking with more particles ($2 \cdot 10^6$) and space charge effects taken into account is done to verify the goodness of the line.

With this procedure, we obtained four different possible TLs, they differ in

Table 3.2. Initial parameters of the beam transported in the TL after having cut it.

Parameter	Value
σ_x	2.4 µm
σ_y	2.4 µm
$\varepsilon_{n,x}$	0.42 mm mrad
$\varepsilon_{n,y}$	0.43 mm mrad
Energy	1 GeV ($\gamma \simeq 2000$)
σ_E/E	$3.29 \cdot 10^{-3}$
Total Charge	32 pC

length and quadrupole magnets technology (Fig. 3.11). All the lines make use of Electro-Magnetic Quadrupoles (EMQ), the shorter lines (B, C and D) take advantage also of Permanent Magnet Quadrupoles (PMQ). PMQ can generate much stronger focusing gradients, up to 700 T/m vs 70 T/m of maximum gradient for EMQ.

In Table 3.3 there is a summary of the 4 TLs obtained with the GA, they are all able to match the bunch, the final Fitness values differs from its theoretical maximum by less than 1 ‰, and a summary of the focusing strengths is given in Table 3.4.

Table 3.3. Magnetic elements in the 4 different TLs shown in Fig. 3.11

	Len.	EMQ	EMQ len.	EMQ bore	PMQ	PMQ len.	PMQ bore
A	8 m	9	20 cm	1 cm			
B	5.15 m	4	20 cm	1.5 cm	10	7 cm	1 cm
C	4 m	4	20 cm	1.5 cm	6	7 cm	1 cm
D	3 m	4	20 cm	1.5 cm	6	7 cm	1 cm

In these optimizations, we did not define constraints on quads positions and the number of quads was fixed. An overlap of quadrupoles indicates the need to revise the lattice, this situation has never occurred in these cases. The final positions found are in agreement with a feasible installation and can be deduced on the Fig. 3.11 (in scale). We don't consider here necessary to show all these data, consider this work a proof of principle of the goodness of the method.

Looking at Table 3.4 it's easy to notice that, in some cases, consecutive elements have the same sign of the field, it is due to the number of elements initially chosen, the mechanics of the GA will generate a solution that use all the elements. This condition may suggest the possibility of replacing them with a
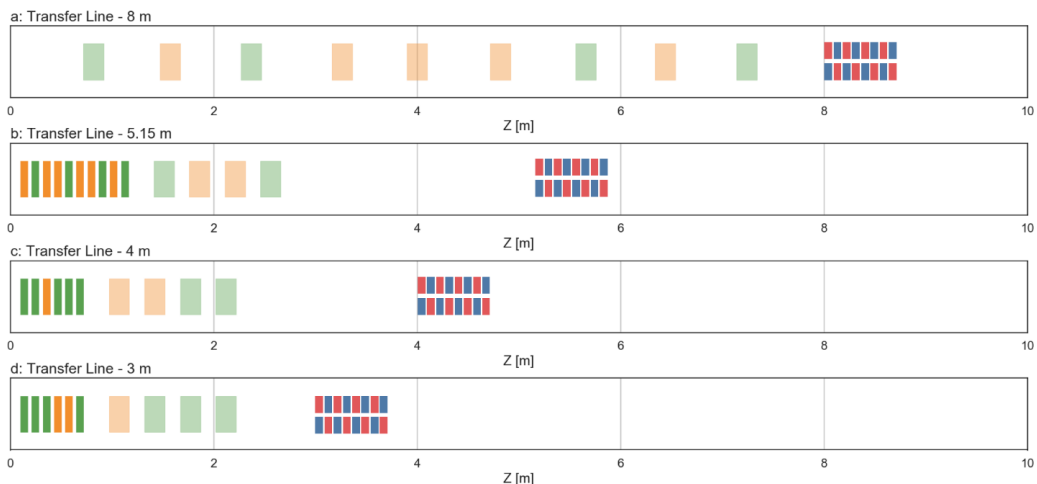
Figure 3.11. Schematic lattice of 4 alternative TLs obtained for different line lengths (from top to bottom: 8 m, 5.15 m, 4 m, 3 m). The orange and the green elements are quadrupoles, with focusing and defocusing effect on the horizontal plane. The transparent style means that they are EMQ, the colourful style mean that they are PMQ. In red and blue the position of the first undulator module is shown (not in scale).

longer equivalent element, this can be done to obtain a simpler line but with fewer knobs that could be used in the future for possible changes of work points. At this point the choice of the strategy to be adopted is linked to one's own needs. In this case, for example, we were looking for a line that could be furthermore optimized in focusing strengths to match to the undulator beams with different energies (see below). We preferred a more complex, but also more flexible, line with a higher number of elements precisely for this reason.

The line C demonstrated to be a good compromise between compactness and reduced growth of the Twiss functions in the PM portion of the line, see Fig. 3.12.

TL flexibility. The C line option has been tested to be able to operate also with beams of significantly different energy. We assumed to use some tunable PMQ that are being developed in these years [103] and repeated the optimization for the same beam but changing its average energy to 500 MeV in the first case and to 2 GeV in the second case and changing the sets of the quads strengths. The gradients were moved inside a range compatible with the state of the art of PMQ/EMQ capabilities. The TL demonstrated to deal very well with this strong changes in the beam parameters. In fact, these quadrupoles positions showed to be able to keep the envelopes dimensions under control preventing beam losses. A visual comparison on the envelopes in the line C for 500 MeV, 1 GeV
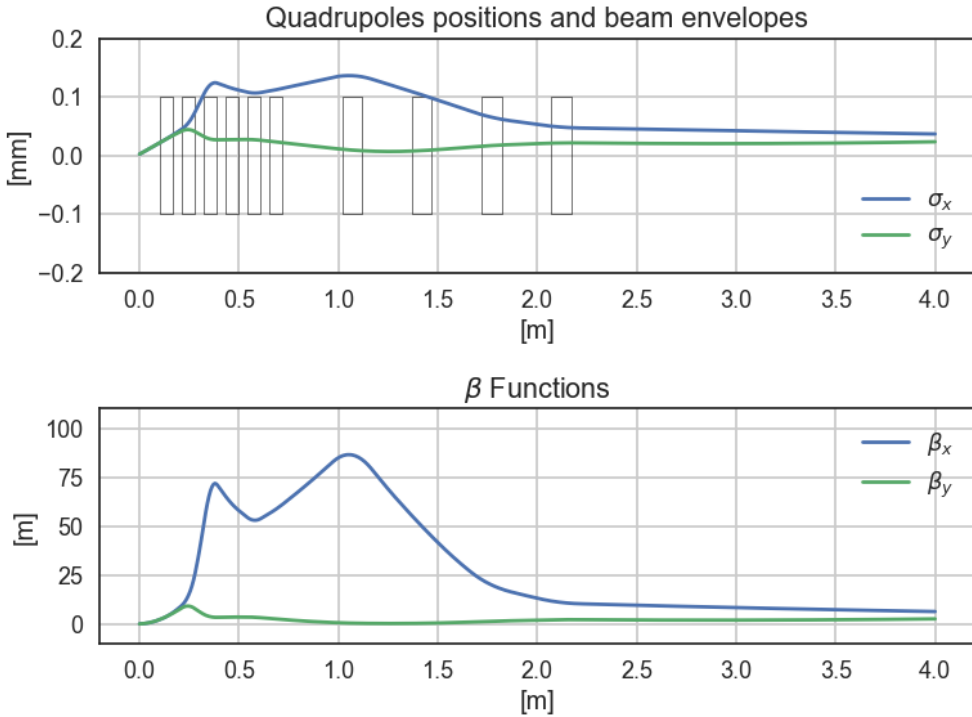
Figure 3.12. A more accurate view of the transverse dynamics in the C line.
Top: the transverse envelopes of the beam are kept small to avoid introducing chromatic aberrations. The positions of the quadrupoles are represented with rectangles. **Bottom:** trend of beta functions during transport. These too have a very low value (the maximum is about 85 m) while preserving the low emittance.

and 2 GeV is provided in Fig. 3.13 and the final focusing strengths values are listed in Table 3.5.

Conclusion

In this work, it has been shown how to apply the code GIOTTO on the TL design problem to perform the matching to the undulator, in particularly when electron beams suffer of strong chromatic effect that quickly degrade the emittance, which is the case of beams coming from plasma accelerators. When the Chromatic Length (eq. 1.14) is many times longer than a TL that has to be designed, the emittance is constant and classical matching approach are successful, differently when L_C is shorter or comparable with the TL path length the problem is much

Table 3.4. Focusing strengths K1 (in m^{-1}) of the four solutions; in bold for PMQ. The values are rounded for sake of compactness; the aim is to give an idea of their magnitude.

	A	B	C	D
Q_1	–14	49	–12	–68
Q_2	10	–134	–120	–21
Q_3	–11	35	100	–61
Q_4	8.7	155	–6	77
Q_5	8.7	–158	–19	18
Q_6	4.3	170	–2	–31
Q_7	–8.2	85	6.7	2.1
Q_8	6.1	–47	0.5	–3.0
Q_9	–8.3	78	–5.2	–3.8
Q_{10}	–	–53	–4.1	–4.0
Q_{11}	–	–5.9	–	–
Q_{12}	–	8.3	–	–
Q_{13}	–	7.1	–	–
Q_{14}	–	–7.0	–	–
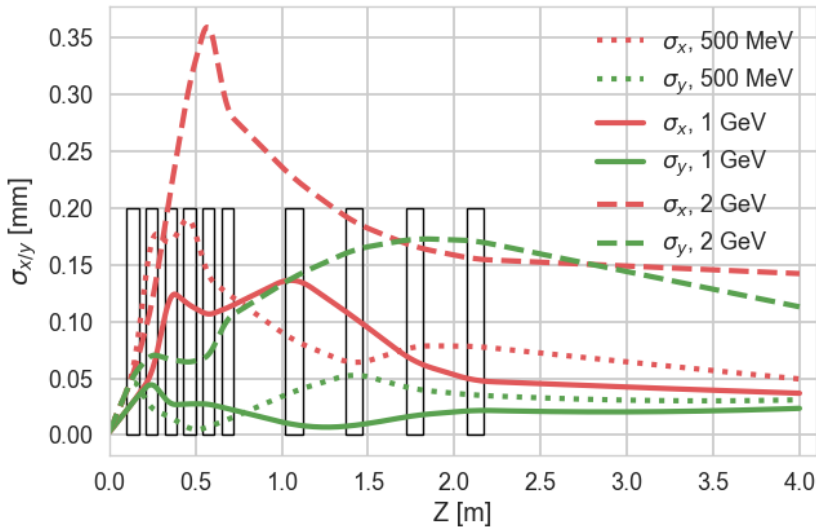
Figure 3.13. Comparison between the beams envelopes for matched bunches of significantly different energies. The position and the dimension of the elements of the line is the same in the three cases (rectangles), only the quads strengths are changed.

more complex and classical methods cannot properly work. The effect of one optic (e.g. a quadrupole) can decrease the L_C accelerating the emittance degradation that in turn correlates with following optics. This results in a non-linear

Table 3.5. Focusing strengths K1 (in m^{-1}) of the line C for different energies; in bold for PMQ. The values are rounded for sake of compactness; the aim is to give an idea of their magnitude.

	Q_1	Q_2	Q_3	Q_4	Q_5	Q_6	Q_7	Q_8	Q_9	Q_{10}
0.5 GeV	−205	**116**	−33	**61**	−40	−1.6	−2.8	−8.5	3.3	0.9
1 GeV	−12	**−120**	100	**−6**	−19	−2	6.7	0.5	−5.2	−4.1
2 GeV	−54	**−46**	51	**15**	54	−31	−0.9	−1.3	−0.9	−0.7

problem that is typically well solved by GA as demonstrated in this study.

GIOTTO has been improved in order to deal with wide-ranging research problems, as the design of a transfer line able to match to the undulator a plasma accelerated beam. The key of this improvement is the adoption of Lorentzian function as part of the fitness function.

We showed 4 alternative lines able to match to undulator the given beam preserving the normalized transverse emittance. In the context of the most interesting line in terms of performance and size (line C), it has been shown that it will be possible to manage large variations in beam energy with the adoption of tunable PM Quads.

The operation of the C line was verified with higher particle statistics and space charge effects.

Ultracold beams production

In chapter 1.3 I explained why using ultracold beams, ie beams characterized by ultralow energy spread, is interesting for the accelerator community.

In 2016, a new collaboration began between the beam physics group of INFN and University of Milan of which I belong and Professor Rodolfo Bonifacio. The aim of the collaboration was the verification of the technological feasibility of a Quantum Free Electron Laser (QFEL) [81]. The collaboration led to the writing of a formulary summarizing the identified work points and the formulas we used but, before that, the possibility of obtaining electron beams with energy spread as low as $\Delta_E/E < 1 \cdot 10^{-5}$ has been verified.

To generate a beam with such extreme characteristics it is necessary to completely or almost completely remove the correlated component of the energy spread. The uncorrelated energy spread that originates in the gun will be the main component that we therefore expect to observe at the end of the optimization. As we have already seen, the 1st and 2nd correlation orders originate in the

accelerating cavities, due to the slippage of the beam on the wave and due to the longitudinal dimension of the beam. These are the orders that we wanted to suppress in this work.

Layout and optimization

To eliminate the first-order correlation we have used a fundamental harmonic accelerating cavity, while the removal of the second-order correlation was carried out by slightly decelerating the beam into a cavity in 4th harmonic like in [80].

As a result, the layout used is rather simple, a scale diagram of the line is shown in the figure 3.14 :

- **A SW S-band photoinjector Gun.** This element must accelerate the bunch as quickly as possible so as to limit the 3rd order correlation. However it is important to work on the longitudinal phase space in a more homogeneous way, which is complicated by the slippage of the beam which is very accentuated here. The photoinjector is coupled with a solenoid for the emittance compensation.

- **Two TW S-band accelerating cavity SLAC type.** The 1st one will be used to accelerate the beam preventing a longitudinal explosion (that would decrease the final beam current and increase the space charge driven energy spread increase), the 2nd one is used to remove the linear correlation that is introduced in the first cavity and in the gun.

- **A TW X-band accelerating cavity.** The purpose of the high harmonic cavity is to remove the remaining quadratic correlation on the beam, it must therefore work in the braking phase (near the belly of the RF).

As we see the function of each element leads it to introduce side effects that must be carefully counterbalanced by the other elements of the beamline. For this reason, a genetic algorithm is very suitable for the optimization of the given working point.

We have chosen to accelerate a low-charge beam (1 pC), simulated with 5000 macro-particles, to limit the 3rd correlation that is introduced by the space-charge forces (which can not be eliminated with this scheme).

Numerous parameters of the line are optimized using GIOTTO:

σ_{clk}, σ_{x_L}. The length and the transverse size of the photocathode laser pulse determine the initial dimensions of the electron bunches and modify the effect of the coulomb forces.
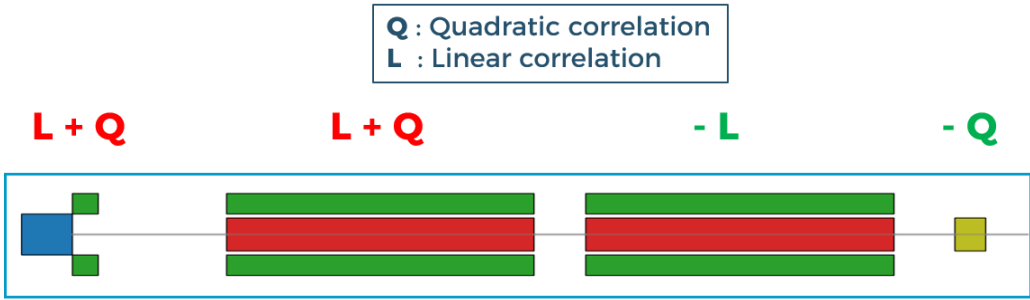
Figure 3.14. A scale diagram of the line, from left to right are represented the gun, two S-band RF-cavities and an X-band cavity. The green rectangles in this scheme are the solenoids of the line. The letters "Q" and "L" indicate the type of correlation that the bunch acquires (if the letter is in red) or loses (if the letter is in green) in the longitudinal phase space.

φ_{gun}, φ_{S_1}, φ_{S_2}, φ_X. The injection phases in the RF wave in the gun in the two S-band cavities and in the X-band are very important and small variations of these parameters change the final energy spread very much.

E_{S_1}, E_{S_2}, E_X. The maximum electric field of RF in the cavities in S and X band (the one in the gun is fixed).

   The objective functions in this case had the objective to minimize the energy spread and the transverse normalized emittance, maintaining the final energy close to 50 MeV. This can be obtained with a fitness function like the following:

$$F = 50 \cdot e^{-\left(\frac{\varepsilon_{n,x}}{1.8}\right)^2} + 50 \cdot e^{-\left(\frac{\frac{\sigma_E}{E}}{3.5 \cdot 10^{-2}}\right)^2} + 50 \cdot e^{-\left(\frac{E_n - 50}{5}\right)^2} \qquad (3.4)$$

Since the beamline retains the cylindrical symmetry of the beam, it is not necessary to optimize the vertical emittance.
   During the first optimized simulations, a strong difficulty was encountered by GIOTTO to reach convergence.
In fact it was impossible to bring the energy spread below a value of 10^{-5}. A more in-depth analysis showed that this limit was introduced by the time step used in the Runge-Kutta integration algorithm. In fact, such a low energy spread is dominated by the effects of numeric noise that are introduced by choosing a time-step like the one normally used in our simulations (500 fs).
   In Fig. 3.15 I show a comparison of the longitudinal phase spaces of two simulated beams with $\Delta_t = 400$ fs and $\Delta_t = 200$ fs, in the left figure it is clear
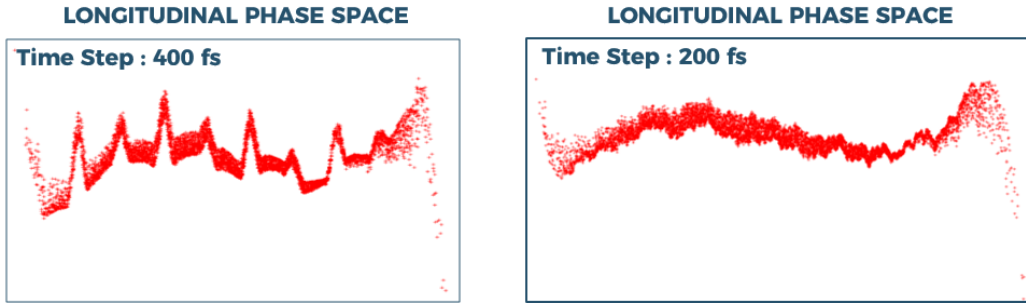
Figure 3.15. To obtain such a low energy spread we need a very small time step for the Runge-Kutta integration to lower numeric noise. In the figure on the left we see an example of limiting the convergence given by the numeric noise, on the right we can see how the noise is eliminated by descending to $\Delta_t = 200$.

how the numeric noise increases the value of the energy spreads limiting the convergence of the genetic algorithm.

Results

In Table 3.6 the parameters that have been found by GIOTTO are shown. These parameters refine the working point from which it started and bring the beam to extremely low energy spread values $\frac{\sigma_E}{E} \simeq 7.3 \cdot 10^{-6}$.

Table 3.6. Final parameters of the beamline found with GIOTTO.

Parameter	Value
σ_{clk}	0.218 ps
σ_{x_L}	13.24 μm
φ_{gun}	4˙
φ_{S_1}	−34˙
φ_{S_2}	105˙
φ_X	177˙
E_{S_1}	32 MV/m
E_{S_2}	18 MV/m
E_X	54 MV/m

Observing the tracking of the bunch (shown in Fig. 3.16) one can observe how the energy spread goes during the transport. It grows very little in the first meter due to the effect of the space charge (which is very well controlled), grows in the first cavity due to the effect of the chirp introduced by the injection phase,

the growth is gradually damped by the increase in energy of the beam. Two sudden decreases of the energy spread are present in the 2nd half of the tracking and are given mostly by the removal of the linear component of the correlation (in the second cavity S band) and by the quadratic one (in the cavity in the X band).

The emittance is preserved very well, at the end of the linac it is $\varepsilon_{n,x-y} = 3.48 \cdot 10^{-2}$ mm mrad.
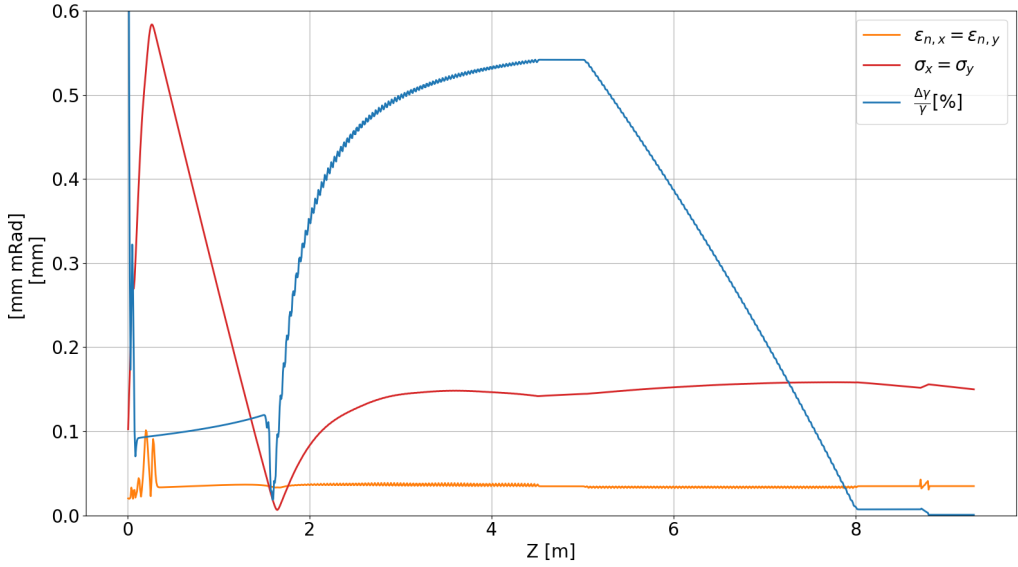

Figure 3.16. Results of the tracking of the ultracold bunch obtained. In this plot the normalized transverse emittance, the transverse envelope and the energy spread are shown.

However, to keep the effects of the space charge low, which are the only correlation effects left (see Fig. 3.17), the beam can not be compressed too much and this limits the current that remains equal to $I \simeq 1$ kA.

Conclusion

1st and 2nd order correlations are eliminated with this scheme, only 3rd order one (from space charge), and uncorrelated component remains evident in the energy spread. This type of manipulation of the longitudinal phase space leads to obtain an ultracold beam with a diffused energy equal to $\frac{\sigma_E}{E} \simeq 7.3 \cdot 10^{-6}$.

I think it would be possible to go further with the relative energy spread by eliminating the 3rd order correlation using an α-magnet downstream of the gun
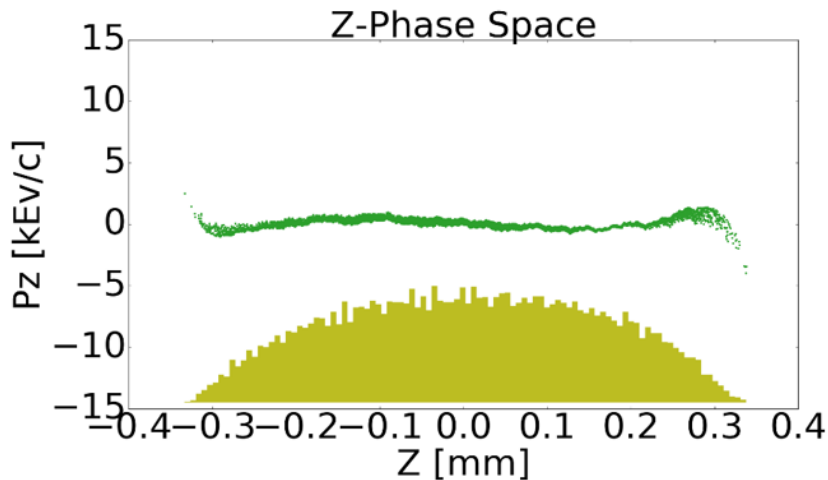
Figure 3.17. The longitudinal phase space of the ultracold beam that we have simulated. The 3rd order correlation is the only component left, it is a very weak component and does not contribute to increasing the uncorrelated energy spread. In olive green a histogram of the macroparticles is shown which reflects a very smooth current distribution.

and accelerating the beam more. We still have to test an updated scheme that takes these observations into account.

The obtained beam necessarily has a low current ($I \simeq 1$ A) because of its final length ($\sigma_z = 152$ µm), to apply this technique in a QFEL experiment it would serve to increase the current at least up to $I = 500$ A. The beam length is kept high to limit the space-charge induced correlation, so the use of the α-magnet could allow us to work with a much shorter beam. Another strategy that we would like to test is the use of *"Laminar Bunching"*, a new technique studied in these years which, as we will see, allows to significantly improve the performance of velocity bunching.

Laminar Bunching

We have already seen in chapter 1 why the ultrashort high-brightness electron beams are essential for FEL, coherent THz transition radiation production, Femtosecond Electron Diffraction and wakefield acceleration experiments.

We also saw many techniques to longitudinally compress electron bunches. Basically all these techniques are based on a linearly correlated energy spread (linear chirp) given along the distribution and accordingly on the velocity differences of the particles which return in to the compression effect. The compression

is performed along a drift in terms of time of flight (ballistic bunching) or along a dispersive line, in terms of different paths length (magnetic compressors). An alternative compression technique, named Velocity Bunching (VB), occurs inside a traveling wave (TW) accelerating cavity, where the beam is accelerated and chirped at the same time. The VB technique operates at low energies, typically electron guns exit energies which are lower than 7 MeV. It is necessary to preserve the laminarity of the beam, which allows to damp the oscillations of the emittance during the compression, in order to prevent the degradation of the emittance. This condition of laminarity of the beam is verified by propagating the beam as close as possible to an equilibrium invariant envelope. This situation represents an exact solution of the envelope equation and is obtained thanks to the following conditions:

- injection into the compressor must take place in a point with laminar envelope waist ($\sigma' = 0$).

- a compression factor that scale linearly with the acceleration $I = \frac{\gamma}{\gamma_0} I_0$ where I stands for the current, γ for the relativistic factor and the index 0 for values before the compression.

Since the technique that I will show in this section completely preserves the cylindrical symmetry of the beam, I will still refer to the transverse quantities of the beam without indicating the reference axis (indeed, $\sigma \equiv \sigma_x = \sigma_y$) and I will use the subscript "z" to indicate the longitudinal quantities (for example σ_z).

VB is a technique used or tested worldwide in various laboratories and is nowadays a reference technique for compressing low-energy electron beams. The typical VB performances, easily achieved, are the peak currents of the beam that approach, or exceed, 1 kA and emittance values lower than 1 mm mrad per group charge of a few hundred pico-coulombs and final energies of $80-100$ MeV. These high brightness bunches generated by VB show the common characteristic of having a peak current on the head of the bunch, where most of the charge is stacked, and a long low charge tail.

The quality of the beam's tail is usually poor, shows a very high energy spread, which is a peculiarity of the VB itself in which the compression is obtained at the expense of the energy spread, and then damped by the acceleration.

This section presents a new compression technique, studied using GIOTTO, that allows compressing a bunch of electrons in an almost uniform way and almost completely compensating the energy spread of the bunch.

This method takes advantage from a space-charge dominated regime and because most of the compression happens along a drift, where the bunch is

laminar, under the effect of its only field, it has been named *Laminar Bunching* (LB). I will present an ideal machine layout to perform the LB and discuss the dynamics of the beam, considering the longitudinal and transverse envelope equations. Finally, a comparison between the VB and the LB is presented from the point of view of the simulations. This comparison is not made to demonstrate which of the two techniques is the best one, but to show how the two techniques, which are united by the ability to compress a bunch without exploiting dispersive paths, present a different way of managing the current distribution in the bunch and which consequences this has on performance.

Beam dynamics

The LB machine layout presented in this work is as follows (Fig. 3.18):

- 1.6 cells S-band photoinjector coupled to a solenoid for the emittance compensation.

- A drift of about 1.3 meters.

- A X-band TW 9 cells accelerating cavity, which is used in decelerating mode.

- A S-band 3 m long, SLAC type, accelerating cavity embedded into a solenoids array.

- A quite long drift, about 3 m long, where the electron bunch enters into the LB.

- A couple of equal TW C-band accelerating cavities, 114 cells, 2 meters long, that boost the beam.

For sake of a better LB beam dynamics understanding let us start analyzing transverse and longitudinal envelope equation, respectively equations 3.5 and 3.6:

$$\sigma'' + \frac{\gamma'}{\gamma}\sigma' + \left(\frac{k}{\gamma}\right)^2 \sigma = \frac{Qc}{2I_A\gamma^3\sigma_z\sigma} + \frac{\varepsilon_n^2}{\gamma^2\sigma} \tag{3.5}$$

where σ is the rms beam envelope, γ the Lorentz factor, $\gamma' \simeq 2E_{acc}$, E_{acc} [MV/m] being the accelerating field, $k = \frac{eB_{sol}}{mc}$ the solenoid focusing strength, considering negligible the RF ponderomotive focusing force, B_{sol} the field intensity of the solenoids around S-band TW structure, $I_A \simeq 17$ kA the Alfvén current and ε_n the normalized rms transverse emittance.
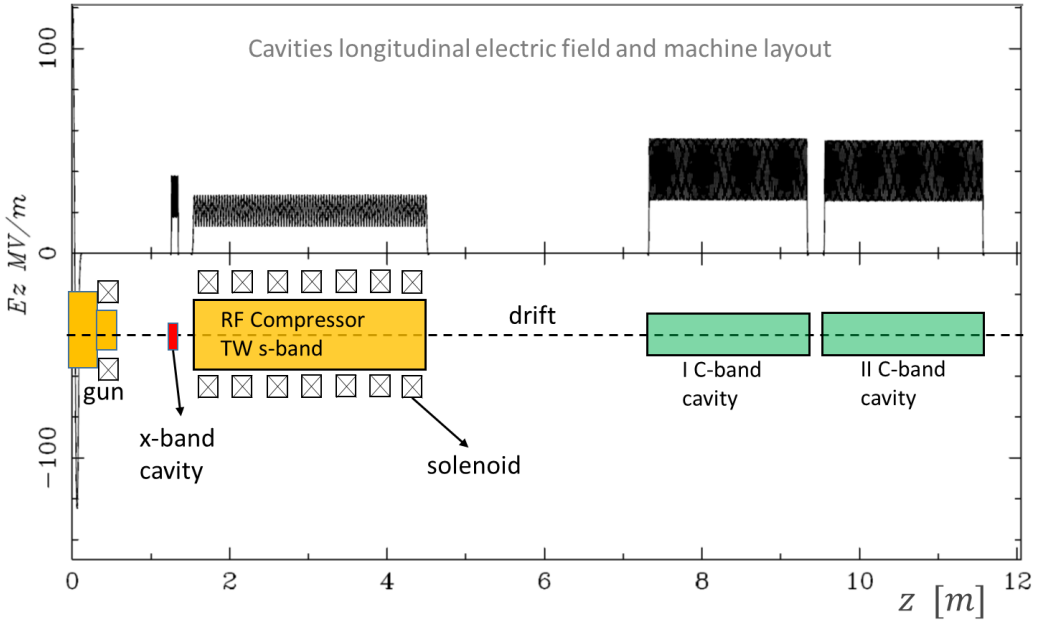
Figure 3.18. The machine layout used for the laminar bunching simulations and the longitudinal fields intensity of the different cavity involved in the new compression method. The gun is a standing wave accelerating cavity, the other cavities work in traveling wave.

The longitudinal envelope equation can be written as follows:

$$\sigma_z'' + \frac{\gamma'}{\beta^2\gamma}\sigma_z' + K_z\sigma_z = \frac{I}{I_A\beta^2\gamma^4\sigma} + \frac{\varepsilon_{n,z}^2}{\beta^2\gamma^6\sigma_z^3} \tag{3.6}$$

with σ_z the rms bunch length, $\beta = \frac{v_e}{c}$ the normalized velocity of the electrons, $\varepsilon_{n,z}$ the normalized rms longitudinal emittance, σ the rms bunch transversal dimension (which couples the two envelope equations 3.5 and 3.6), $\gamma_0' = \frac{eE_{acc}}{mc^2}$ the normalized acceleration gradient and K_z the RF longitudinal strength:

$$K_z = \frac{4\pi\gamma_0'\sin|\varphi_0(z)|}{\lambda_{RF}(\beta\gamma)^3} \tag{3.7}$$

where $\varphi_0(z) = \frac{z}{c}\left(1 - \frac{\gamma}{\sqrt{\gamma^2-1}}\right)$ is the maximum acceleration at $\varphi_0 = 0$.

The 2nd term on the left of Eq. 3.6 is a velocity damping term, always in contrast with focusing or defocusing. The last two terms, on the right hand of the same equation, represent internal forces and are respectively the space charge and the longitudinal emittance pressure, from which is possible to define the longitudinal laminar parameter ρ_z:

$$\rho_z = \frac{Qc(\gamma\sigma_z)^2}{I_0\sigma\varepsilon_{n,z}^2} \tag{3.8}$$

This parameter provides a value of the bunch laminarity and also of its stiffness with respect to the compression. The laminarity is guarantee for values greater the one ($\rho_z > 1$), which is a typical condition during compressions at low energy (VB or LB), differently for over-compression regimes, where the laminarity is lost (Fig. 3.22). The stiffness of the bunch versus the compression decreased for ρ_z approaching the unity, favoring a more effective compression process.

A description of the LB beam dynamics, following the Fig. 3.18 layout and showing in advance some results of the simulations paragraph, is as follows:

- The bunch exiting from the gun, with an energy of 5.9 MeV, under the effect of the gun's solenoid and being space charge dominated, undergoes the emittance compensation process along a drift [104]. So far the dynamics is known, equal to many other low emittance injectors.

- Downstream the drift the bunch enters into a short, high frequency (X-band) accelerating cavity, that decelerate the bunch of 2.3 MeV. This deceleration that bring the bunch at the low energy of 3.6 MeV has many important effects:

    1. it strengthens the long. space charge effects, also if the long. laminarity decreases (Fig.3.22), favoring a faster compression

    2. moves the bunch spike current on the bunch tail pre-compensating the symmetric VB effects (Fig. 3.19 and 3.20), resulting in a much more uniform charge distribution at the compression end

    3. provides a pre-compression

    4. it enlarges the envelope relaxing transversal space charge effects

    5. applies a pre-correction of the radio rf curvature (Fig. 3.20, upper plot)

    6. the energy decreasing results in an larger bunch vs. RF phase slippage, a key effect for the VB technique.

- After the high harmonic cavity, the bunch is injected into a typical cavity for the VB where it is chirped (in the longitudinal phase space), compressed and accelerated.
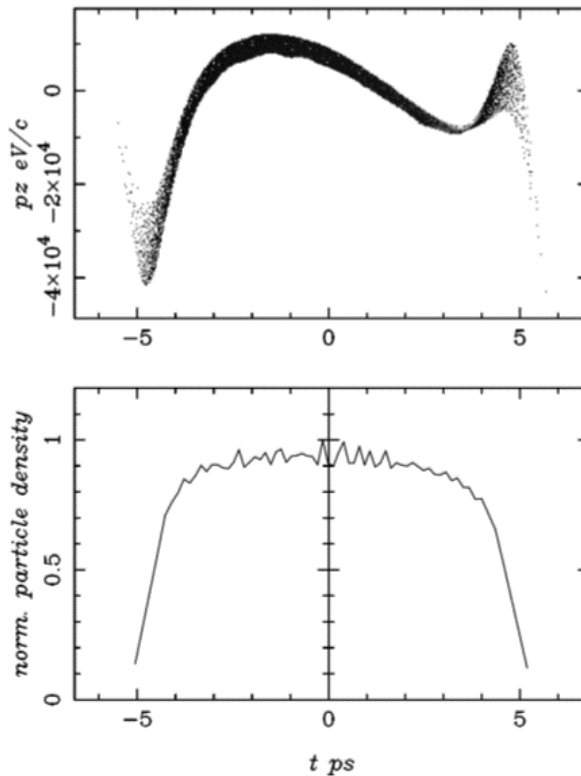
Figure 3.19. The upper plot is the beam Longitudinal phase space, at 1 m from the cathode, i.e. before entering in the high harmonic cavity. It is visible the RF curvature inherited from the gun. The lower image is the particle density along the bunch.

- Downstream the VB cavity there is a long drift where the bunch enters at about 20 MeV and the full effectiveness of the LB takes place, region highlighted in Fig. 3.21. Here the beam propagates under the effects of its own fields and of the momentum distribution at the VB cavity exit. The resulting beam dynamics is peculiar: an envelope that grows linearly (in first approximation) and a bunch length σ_z that decreases following a hyperbolic trend (Fig. 3.21, zoomed box). This behavior shows to be in balance and the compression can be pushed at very high values, at the expense of the envelope enlargement. The peculiar equilibrium of the LB, compression versus enlargement, going forward in the drift at some point is lost. The beam parameters to check are the energy spread σ_E and the transverse normalized emittance ε_n, the first is wonderfully damped by the longitudinal space charge effect (Fig. 3.21, lower plot), while the second ends a long chromatic oscillation, closing the bow tie distribution of the
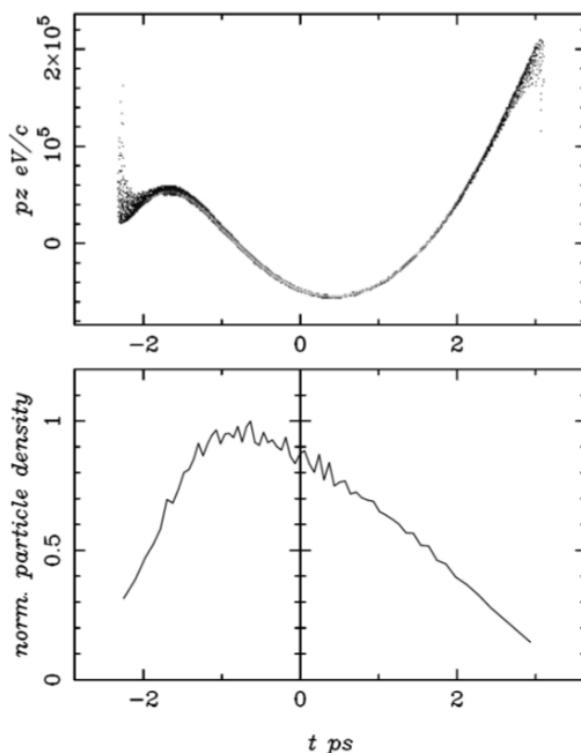
Figure 3.20. The upper plot is the beam Longitudinal phase space, at 2 m from the cathode, i.e. after the high harmonic cavity. It is visible the RF curvature correction (and pre-correction). The lower image is the particle density along the bunch; It is well shown the effect of the decelerating X-band cavity, which pre-correct the current distribution by moving charge on the bunch tail.

transverse phase space (Fig. 3.21, lower plot). The bunching can be frozen by boosting the beam, when the emittance and energy spread are fully damped. The final result is impressive as reported in Fig. 3.24, where it is shown a longitudinal phase space of a bunch almost homogeneous in charge, with a spike current close to the central position and with an energy spread comparable to the one at the gun exit (below 100 keV for the whole bunch, below 20 keV for the spike current). The energy spread, initially responsible of the compression, is quasi completely canceled by the space charge effect. Furthermore, the space charge dominated regime heats the uncorrelated energy spread, which can be an important advantage for applications needed laser heater devices (typically FEL).

Simulations

In this paragraph is presented a comparison between two different compression methods, the VB and the LB. Both where optimized on the brightness of the bunch using the genetic algorithm GIOTTO and the particles tracking have been done using the code ASTRA. The goal is to outline the peculiarities of the LB (a new technique proposed here), compared to a known technique, which like the VB, bunches linearly and works in the same range of energy. Indeed, the two methods are relatives, but their final results are quite different.

When pushed at high compression values the VB favors a single spike compression on the bunch head, differently, the LB works almost on all the bunch charge. Therefore, even if the spikes of current for both VB and LB can be equal (or very similar) at maximum compression (compare Fig. 3.23 with Fig. 3.24) the rms dimensions can be very different, e.g. see the comparison between the compression factors ($C = \frac{\sigma_{z,i}}{\sigma_{z,f}}$ into Fig. 3.22.)
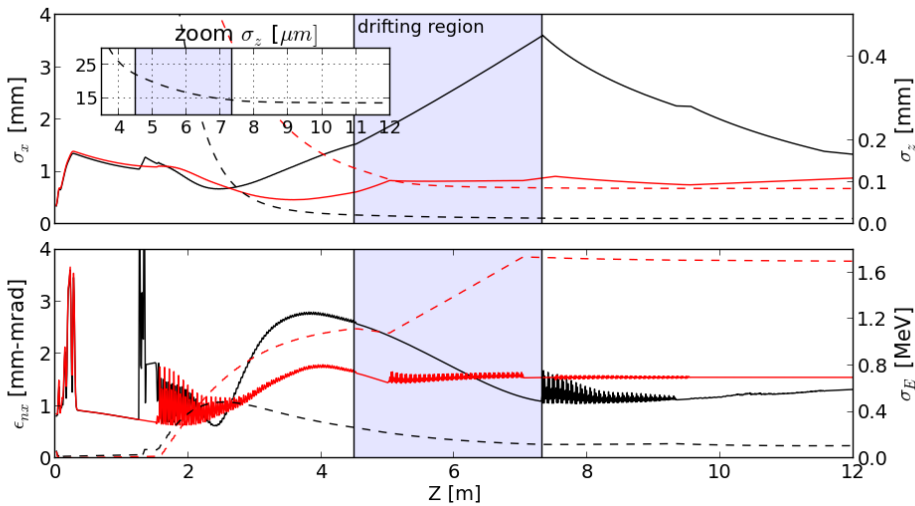
Figure 3.21. VB and LB comparison for simulations that aim to maximize the bunch brightness. In red are reported the VB results, in black the LB ones. The upper plot reports the envelopes (solid lines) and the bunch lengths (dashed lines), in the box is zoomed the bunch length for the LB case, to highlight the hyperbolic trend along the drift. The lower plot reports the emittances (solid lines) and the bunch energy spreads (dashed lines).

The layout used for the LB is shown in Fig. 3.18 and described in the previous paragraph. The VB layout is very close to the LB layout, but with the following differences: the X-band cavity is missing, the long drift is missing and, after the

S-band cavity, the bunch is frozen earlier in terms of compression and emission compensation (there is a C-band booster instead of the LB drift).
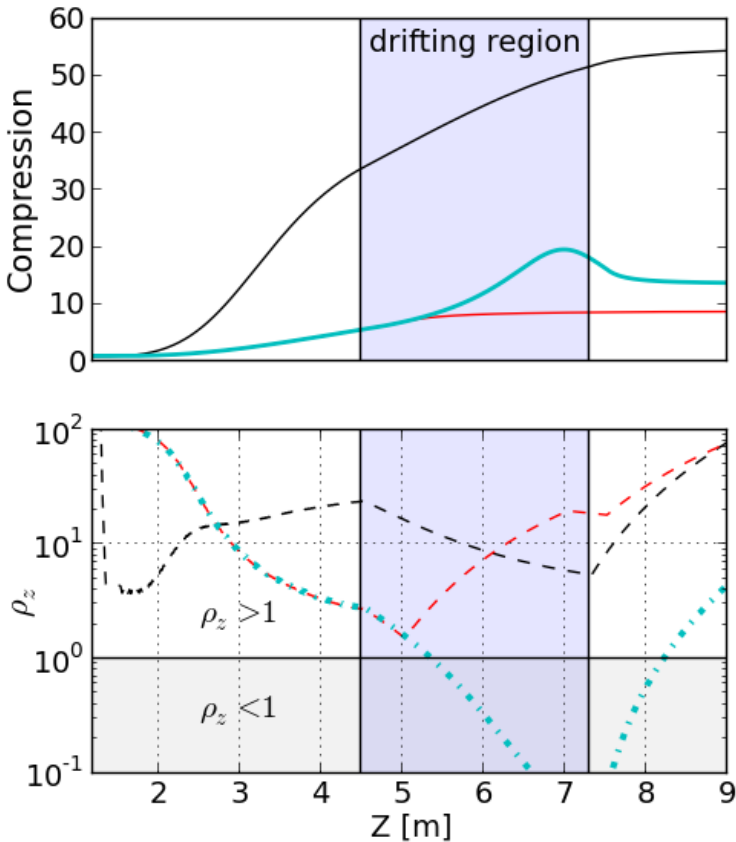

Figure 3.22. The upper plot reports the compression factor for the LB case (in black), the VB case in red and a VB test case (in cyan) where, after the S-band cavity, the bunch travels a drift, rather than being boosted. The lower plot reports the relative laminar parameters (Eq. 3.8).

Figure 3.21, in the upper plot, reports the invariant envelopes (red curve) typical of the VB technique. For sake of completeness the Fig. 3.22 reports also a VB case where, after the S-band cavity, the booster is removed and the bunch enters into a LB drift like. Along this drift the bunch goes straight into the over compression regime (Fig. 3.22 upper plot, cyan curve), and the emittance compensation is completely lost. It is interesting to look at the ρ_z parameter that, because the VB beam conditions are different than for the LB case, the laminarity is lost (Fig. 3.21, lower plot, cyan curve: $\rho_z < 1$), giving the over compression and beam qualities degradation. The parameter ρ_z is also an indicator of the beam response to the compression, in the lower graph of the Fig. 3.21 the black

curve shows the beneficial effect of the high harmonic cavity, which lowers the beam laminarity. In this way, $\rho_z > 1$ is maintained favoring the compression and, at the same time, compensating for the energy spread and preventing the overlapping of bunch slices.

Figure 3.23. Bunch longitudinal phase space (upper plot) and slices beam current (lower plot) at the end of the linac optimized by the VB technique.

Figures 3.23 and 3.24 show the longitudinal phase spaces and the slices bunch currents, respectively for the VB and LB simulations.

Longitudinal Phase−Space

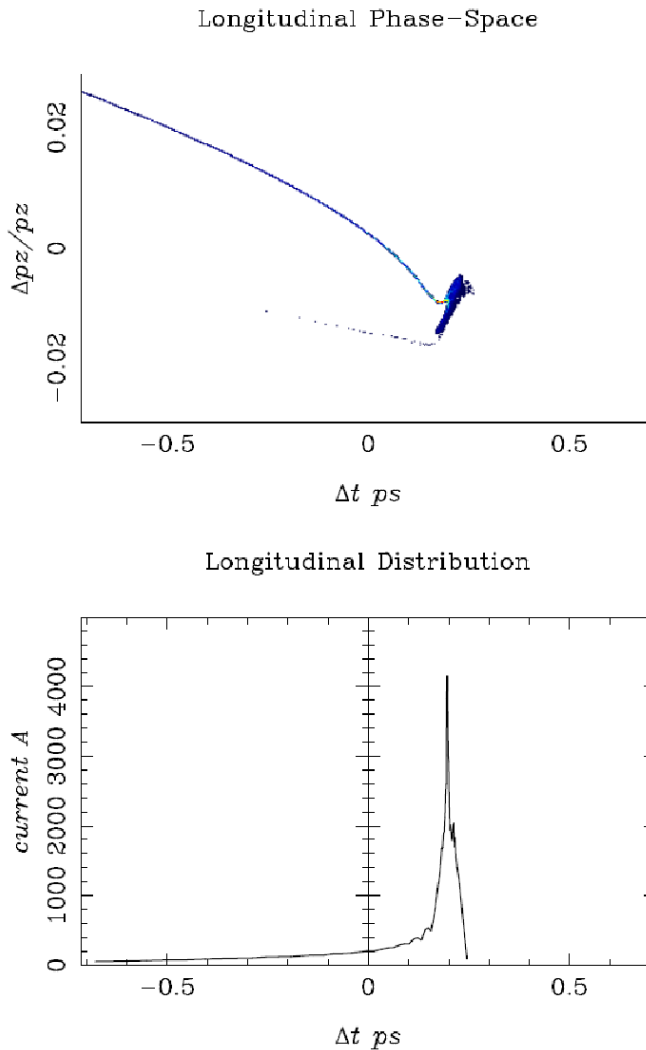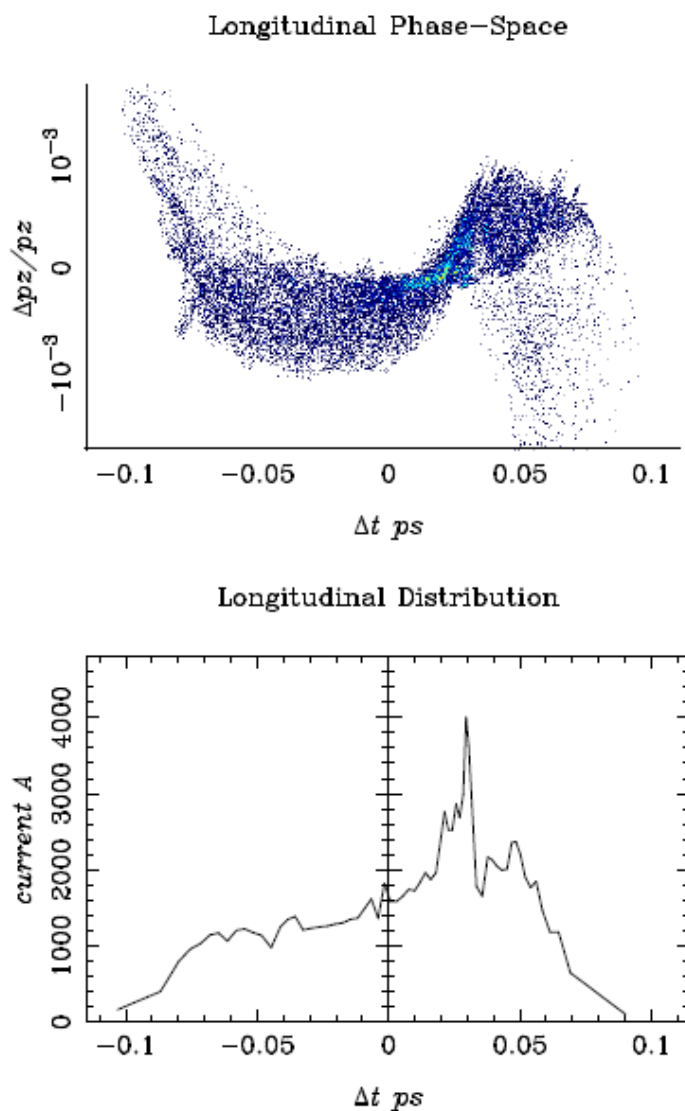## Longitudinal Distribution

Figure 3.24. Bunch longitudinal phase space (upper plot) and slices beam current (lower plot) at the end of the linac optimized by the LB technique.

The longitudinal phase space obtained by using the VB shows a long tail and a very high bunch density on the head, which represents the typical charge distribution of bunches obtained with this technique. The bunch head shows

a space charge dominated portion that reshapes the head distribution but the final effect is not under control.

The VB final performances, considering the bunch spike, are very good: a slice emittance of 2.5 mm mrad, a slice current of 4 kA and a slice spread of 350 keV.

What is new and peculiar in the LB is the capability to work with a much more uniform bunch distribution, which is clearly shown by the current binning of the Fig. 3.24. In this case, the capability to control the space charge effects to quasi completely compensate the energy spread give as result a very cold bunch, with the following slice performances:

- slice emittance below 1 mm mrad

- maximum current of 4 kA

- a really low energy spread of only 20 keV.

RF System

The RF power for the system in Fig. 3.18 will be provided high-power klystrons driven by solid-state modulators. The 1.6 cell S-Band RF photoinjector is fed by about 10 MW of RF power.

The C-band and X-band represent the most crucial components in the pro-posed LB scheme, therefore particular designs will be carried. Such ad-hoc structures will be powered by two different high-power klystrons at 5.712 GHz and 11.424 GHz, respectively.

In our simulations, we employed a TW-type "decelerating" X-band structure but the standing wave (SW) option will be also considered, as well as a C-band short cavity, more details are reported into the Ref [105].

The booster first C-band accelerating structure will be optimized in future studies in order to maximize also the beam focusing. We foresee, for example, the use of cells with modular lengths and fed by separate RF power sources for maximum beam matching.

Conclusion

The LB represents another electron beam manipulation method that takes advan-tage form the space charge nonlinear effects tuning, which is already used for the gun emittance correction. Its performances, as discussed in the paper, are really

impressive. LB can be considered the only method that besides compressing and preserving the emittance, makes it possible to quasi fully correct the energy spread, opening the horizon to a new type of electron beams: extremely high average current, ultracold beams.

3.3   Final considerations on GIOTTO improvements

GIOTTO, the tool on which I worked during the first two years of PhD, is a genetic algorithm designed by the group I worked with and I had the chance to improve it to extend its capabilities.

It was thus possible to apply GIOTTO to 4 major works based on simulations:

1. The dual development of a beam based method for the search of the golden orbit in the linacs and, after having set it, for the correction of the misalignments of solenoids, quadrupoles and cavities. This method allows to increase the brightness of the electron beams produced by the linac improving its setting. Furthermore, this methodology is particularly suitable for test facilities which are by their nature designed to run with different working energies as it allows to guarantee the stability of the trajectory when the energy changes.

2. The flexible dimensioning of transfer lines dedicated to the transport and matching of FELs plasma driven beams. In these particular conditions often happens to work with extremely low chromatic length beams and the emittance of the transported bunches tends to grow spontaneously, even in drift spaces. GIOTTO is able to find the correct positioning and the correct gradient of quadrupoles set (with permanent or electromagnetic magnets) that allows to transport the beam and match it correctly to the undulator.

   Thanks to the changes made to GIOTTO to allow it to work with these wide-ranging research problems, it proves to be an excellent candidate for the study of flexible lines to change the energy of the beam and, more in general, as a tool to perform matching based on tracking of bunches taking into account the space-charge forces.

3. The study of an innovative laminar longitudinal acceleration and compression technique that exploits RF bunching and ballistic bunching in the first place.

This technique takes advantage of the qualities of Velocity Bunching by proposing a softer way to offset the energy spread of the bunch. In fact, the ballistic compression makes it possible to compensate the longitudinal energy spread in a softer way than the pure Coulomb repulsion. As a result this technique allows to reach very high compressions but also extremely low energy spread values. Today it is the only beam manipulation technique capable of producing ultracold high-brightness beams.

4. Finally, GIOTTO was used to optimize the correction of the higher order correlations in the bunches obtained with an high brightness linac to obtain ultracold beams. Beams of this kind are in great demand in electron microscopy and electron diffraction experiments as the measurement noise decreases. In our case they were requested by Professor Rodolfo Bonifacio as bunches to be used in simulations of a quantum FEL.

GIOTTO has proven to be a fundamental tool in seeking and optimizing new extreme working points for linear machines thanks to its ability to simultaneously optimize different beam parameters and the ability to explore vast spaces of solutions. In the future I would like to continue its development by implementing a non-dominated solution research mode as typically done in MOGA-like optimizations (*Multi-Objective Genetic Algorithm*) [106], although GIOTTO is already able to handle multi-object optimizations. The aim is to implement the search for Pareto optimal solutions set in wide-ranging research problems that would thus allow to identify, with a single in-depth research, all the different working points that satisfy the requests.

This new modality could be compared with a new alternative way of performing parallel optimization based on "islands" with different types of optimizations and migration of optimal solutions (*Coarse-Grained Parallel Genetic Algorithm with migration*) [107].

Design of an Arc Compressor

Contents

4.1   MariX project

The name of *"MariX Project"* identifies an important linac based facility planned in the future Scientific Campus of the University of Milan, currently designed for the Milan Expo area, whose development is expected over the next 5–6 years. It is a femtosecond-class combined radiation source that provides X-ray coherent, with ultrahigh flux. The energy of these photons varies in a wide range, extending from 300 eV up to 180 keV. This structure will allow fundamental and applied research with non-receding photon beam performance.

This ambitious project aims to propose a new paradigm for X-ray sources, showing typical characteristics of synchrotron light sources (the continuous flux) and those of the modern *Free Electron Lasers* (source coherence, high flux).

These performances are guaranteed by the choice to operate in *continuous wave mode* (CW) with high repetition rate ranging from 1 MHz up to 100 MHz.

This combined source exploits two different (but related) X-ray production mechanisms:

- An *Inverse Compton Source* (ICS) that uses electron beams of high average current (tens of mA) and high power lasers (in the MW). The portion of the machine dedicated to this source takes the name of *"BriXS"*.

- A GeV-class FEL based on electron beams with ultrahigh brightness. This FEL, which takes the name of *"MariX"* from the whole project, shares with the BriXS the injector and the first cryomodule that brings the electrons to the energy of 100 MeV.

It will thus be possible to produce soft X-rays from 0.3 keV to 10 keV thanks to the FEL and hard X-rays from 20 keV up to 180 keV of energy with the ICS.

The main fields of research that can be explored by MariX are: imaging of proteins and nano-objects with nano-metric resolution, linear time-resolved femtosecond spectroscopy, new radiotherapy techniques that harness monochromatic hard X-rays, advanced multi-color X-ray based imaging.
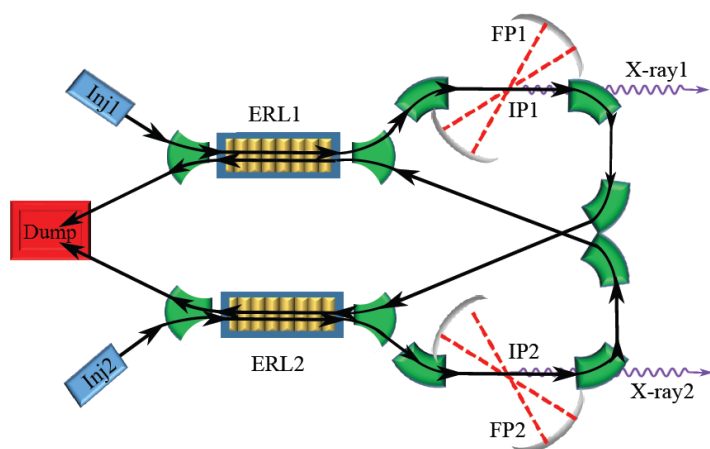

Figure 4.1. Pictorial view of the BriXS layout: From left: Inj1 and Inj2: photocathodes. ERL1 and ERL2: Superconducting linacs. FP1 and FP2: Fabri-Pérot cavities. IP1 and IP2: interaction points. X-ray1 and X-ray2: X rays beams, going towards Compton users. The long side of this machine has a length of about 40 m.
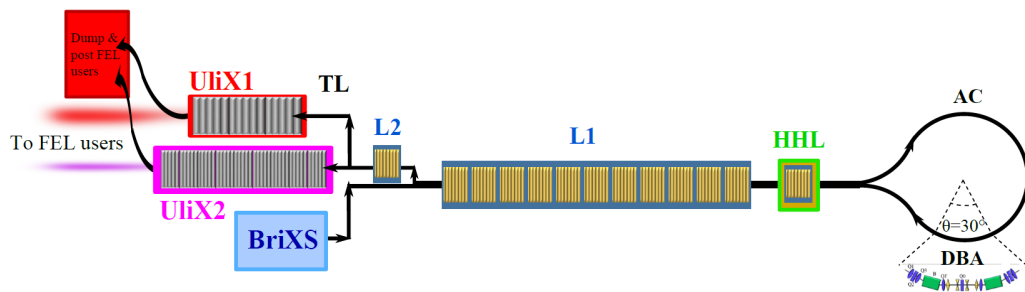
Figure 4.2. Scheme of the layout of MariX. BirXS works as injector, L1 is the long superconducting booster and L2 is a separate single cryomodule. HHL is the high harmonic cavity, AC the arc compressor composed by 14 double bend achromat (DBA). TL are the transfer lines the take the beam to the undulators: UliX1 and UliX2.

BriXS introduces technological challenges related to the high repetition rate (100 MHz) applied to energy recovery mechanisms, and the need to provide two beams of different characteristics and with different repetition rates for the two sources. Even MariX, which is the largest of the two sources introduces a very interesting challenge: to achieve competitive FEL performance with those of the main operating machines and in the design phase (LCLS-II, EuXFEL) undergoing the alleys of dimensions that the site that will host the machine imposes.

During the last year of my PhD I dedicated myself to study the beam dynamics inside the Bubble Arc of MariX which, as we shall see, represents the solution to this last problem.

4.2   A bubble arc for MariX

The MariX FEL is characterized by a high flow. As we have seen in section 1.3, this requires to a high accelerated average current electron beam in superconducting cavities operating in CW.

The MariX beamline operates in CW by transporting 50 pC bunches with a repetition rate of 1 MHz from the common line with BriXS (consisting of an injector and a single cryomodule) up to the UliX1-UliX2 undulators, as shown in Fig. 4.2.

The electron bunches must be taken from the operating energy of BriXS, 100 MeV, up to the operational energy of the 3.2 GeV FEL, maintaining a low normalized emittance ($\varepsilon_{n,x-y} = 0.4$–$0.5$ mm mrad) and showing high peak current $I_{peak} = 1.6$ kA.

The beamline dedicated to the main acceleration of the bunch is a booster composed of 11 cryomodules containing 8 Tesla-like SW superconducting cavities (9–cell, 1.3 GHz) each. Thanks to the SW operation it is possible to accelerate electron bunches with an appropriate injection from left to right but also vice versa without having to modify the cavity feed. Then the beam, after being accelerated in the booster, is injected in some Tesla cavities in high harmonic (3.9 GHz) and is passed in a dispersive path with the task of applying a complete inversion of direction to the beam that thus traces back the booster doubling the energy gain. Thanks to this peculiar scheme, the total dimension of the booster is virtually doubled making it possible to accelerate the beam from 100 MeV up to 3.2 GeV with a short booster long less than 140 m and the bunch, as explained below, is strongly compressed without the use of magnetic chicanes.

To bring back the beam at the linac exit with opposite propagation direction we need to bend it by a total of $420°$, $60°$ in one direction, $300°$ in the opposite one and again $60°$ in the initial one (see Fig. 4.2). The Arc used in the turnaround, called *Arc Compressor* (AC), is composed by a series of achromatic cells and it is able to deflect the beam by large angles performing a bunch length compression without spoiling the beam quality [108].

In our case, such a device can be used to take a beam in a precise point of the line, deviate its path of $420°$ and bring it back to the starting point with inverted propagation direction. The shape of the arc reminds that of a soap bubble before detaching from the straw that generates it, for this reason it is also called *Bubble Arc* (BA).

Lattice simulation

The arc compressors are used in FELs with the aim to raise the peak current of the electron bunches, compressing them, as they pass through dispersive paths characterized by the presence of numerous bending magnets. When a bunch of high current passes through a bending magnet it emits Coherent Synchrotron Radiation (CSR) a collective radiation emission phenomena by neighboring particles responsible for the degradation of transverse emittance of the beam. And it is precisely to take into account the effect of the CSR issue that `elegant` [90] was chosen as a tracking code to study the beam dynamics in the BA.

The BA of MariX is based on the arc described in Ref. [108] which uses the arc cells of the Elettra storage ring at Sincrotrone Trieste [10], in fact the modeling of its lattice started right from there. Elettra storage ring consists of 12 achromatic

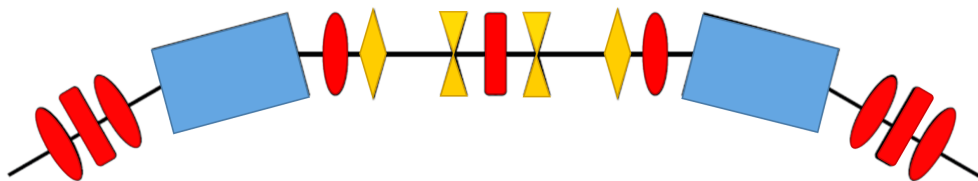cells repeated in series, these cells are called *Double Bend Achromat* (DBA).

Figure 4.3. The DBA scheme or "Chasman-Green lattice", is composed of 2 bending magnets (in blue) 9 quadrupoles (in red) and 4 sextupoles (in yellow).

The DBA scheme was first studied in the 1975 by R. Chasman and G. K. Green [109], in fact, it is often referred to as "Chasman-Green lattice". The DBA cell used in the BA (shown in Fig. 4.3) bends the beam by $30°$ and is composed as follows:

2 Bending Magnets. Those devices deviate the beam of 15° each and are responsible for opening and closing the dispersion in the line.

9 Quadrupole Magnets. They are used to control the transverse dimensions of the beam. The first and last triplets are used to match the beam to the cell, the three central quadrupoles are in the open dispersion area and are used to reverse the dispersion trend and to allow it to close in the second bending magnet.

4 Sextupole Magnets. These magnets are used to compensate for the chromatic aberrations introduced by the quadrupoles due to the energy spread of the beam (which we will see is essential for the compressor to operate).

Figure 4.4 shows how DBA are used in the Elettra storage ring and in MariX.
Since we need two types of cells with opposite bending angles, I have modified the cell changing the bending field.

The reverse magnetic field that is generated opens the dispersion in the opposite direction (same trend but with opposite sign), so the less energetic particle will always be curved with a greater angle but this time to the left.

So we try to think of the electron bunch in the dispersed area of the DBA as a cloud that opens up like a fan on the horizontal axis, only the centroid of the beam, which we assume to have energy equal to the average energy of the

beam, will be deviated at the right angle and will remain on the propagation axis.

The quadrupoles must apply to the particles a restoring force towards the propagation trajectory of the centroid of the beam, they must therefore be fed as in the original DBA and focus on the horizontal axis.

Sextupoles, on the other hand, apply a dipolar kick which grows symmetrically as you move (keeping us in the horizontal plane) from the propagation axis and must have an inverted field with respect to the original DBA to apply the correct return force on the halo of the beam.

In Table 4.1 the main parameters of the used DBA are shown.
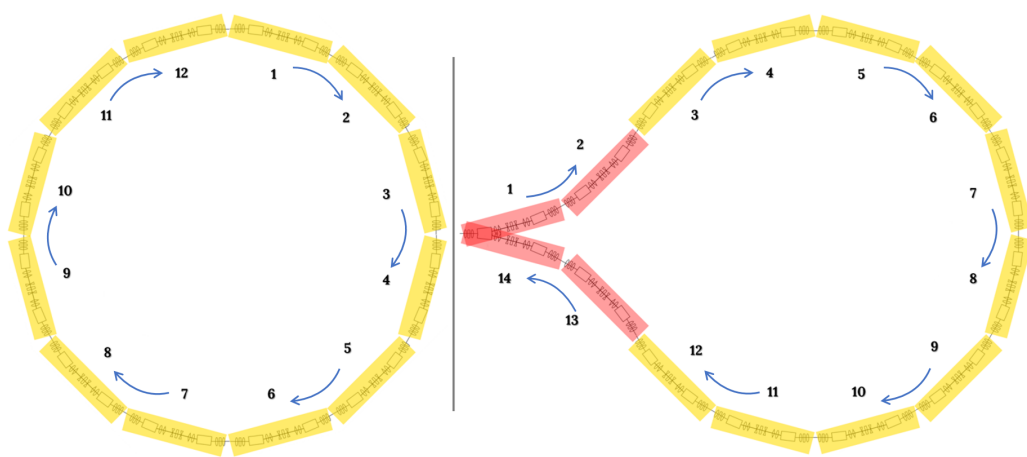
Figure 4.4. Left: The Elettra storage ring is shown, it consists of 12 DBAs that fold the beam to the right.
Right: is the layout of the BA of MariX. It is composed (in order of number) by 2 DBAs that fold the beam to the left, 10 DBAs that bend to the right and finally 2 DBAs that bend it left again bringing it back to the starting point.

An ideal beam in the BA

A series of simulations of the DBA cell were carried out in the initial phase to verify its operating mechanism and, more generally, to construct the lattice composing the arc.

During this phase it was sufficient to work with a so-called "ideal beam", that is a bunch of electrons that reflected the correct nominal characteristics expected (average energy, rms size, energy spread, emittance, charge, ...) without simulating the tracking from the gun to the arc. This can be done by generating it

Table 4.1. A summary of the main parameters of the DBA cells and of the BA is shown.

Parameter	Value
Cell length	$\simeq 21.8$ m
Dipole bending angle	$15°$
Dipole length	1.4 m
R_{56} per DBA cell	35 mm
# of dipoles per DBA	2
# of quadrupoles per DBA	9
# of sextupoles per DBA	4
# of DBA cells in the BA	14
Total R_{56} in the BA	490 mm

directly in `elegant` by specifying the beam parameters (shown in Table 4.2) that you want to propagate in the specified lattice.

Table 4.2. The table shows the parameters used to generate the ideal beam that we used to test the arc.

Parameter	Value
σ_s	150 μm
σ_x	31.5 μm
σ_y	17.8 μm
$\varepsilon_{n,x}$	0.39 mm mrad
$\varepsilon_{n,y}$	0.39 mm mrad
γ	3200 (E $\simeq 1.6$ GeV)
Q_{tot}	50 pC
# macroparticles	1×10^4

Beam Matching

The propagation in the arc compressors has some similarities with that in an FEL's undulators. They are both periodic structures in which the beam must maintain its transverse characteristics. For this reason the beam matching must be done in a similar way to the one described for the FEL in the chapter 3.2. I then found the initial values of the Twiss transverse functions (α and β) that guarantee the periodicity of the function in the DBA ($\alpha_{x_i} = \alpha_{x_f}$, $\beta_{x_i} = \beta_{x_f}$, ...).

Table 4.3. The parameters in the table guarantee the matching of the beam to the cell. That is to guarantee equal values in input and output from the DBA (and therefore allow the serialization of these cells). They concern the horizontal and vertical Twiss functions and the value of the dispersion and its derivative respect to the longitudinal coordinate.

Parameter	Value
α_x	$\simeq 0$
α_y	$\simeq 0$
β_x	8.109 m
β_y	2.608 m
η_x	$\simeq 0$
η_x'	$\simeq 0$

In our specific case, we grant the periodicity of the envelope forcing it to be in a focal point on both transverse planes at the cells borders, this means having $\alpha_x = \alpha_y = 0$ and both β_x and β_y in a local minimum. To check the correct functioning of the lattice I also checked that the initial and final dispersion was closed $\eta_x = \eta_y = 0$.

To have periodicity of the envelope it is necessary that the beam is in a focal point on both transverse planes, this means having $\alpha_x = \alpha_y = 0$ and both β_x and β_y in a local minimum. To check the correct functioning of the lattice I also checked that the initial and final dispersion was closed $\eta_x = \eta_y = 0$.

After finding the correct initial Twiss parameters (shown in Table 4.3) with `elegant`, I did the first tracking in the single DBA and then in the whole BA.

The matching parameters are the same for the inverted DBA.

Tracking results

Figure 4.5 shows how the β functions evolve in the DBA from information about the beam size and the η_x dispersion.

The beta functions contain information on the size of the beam in relation to the emittance ($\beta_x = \frac{\sigma_x}{\varepsilon_{n,x}}\langle\gamma\rangle$, same for the y coordinate), we see very well that the periodicity of the line is respected.

The trend of the parameter η_x, that represents the dispersion, must be very well seen its opening and closing in the dipoles (long and low rectangles on the field profile) and how the three quadrupoles in the dispersed area act on its progress controlling it and guaranteeing its closing in the second dipole.
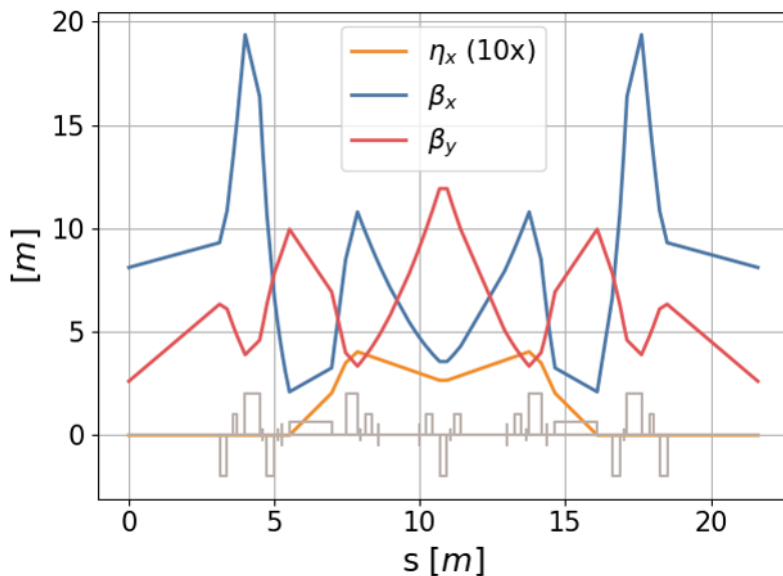
Figure 4.5. The evolution of some key parameters (dispersion and beta functions) of a properly matched beam in the DBA. The gray rectangles show the magnetic profile of the elements that line.

The bunch matched to the cell keeps its initial emittance at the output as shown in Fig. 4.6 on the left. Still in the same figure on the right I show the trend of the rms dimensions of the beam, on the transverse these are maintained with precision as we expected, on the longitudinal instead we see the compressive effect of the DBA.
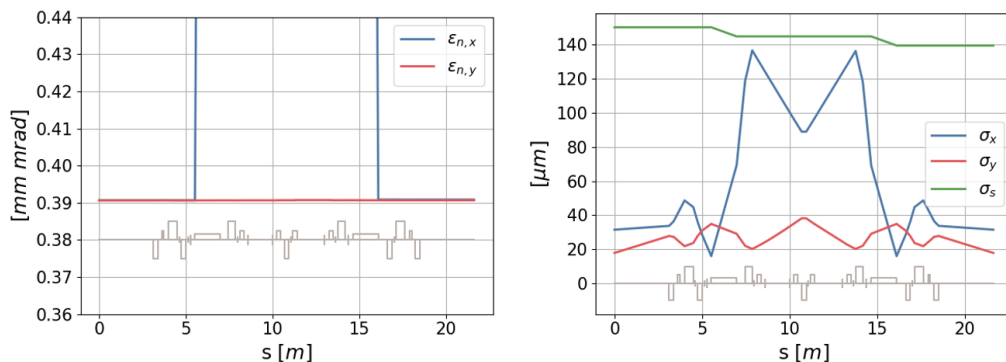

Figure 4.6. On the **left** I show the trend of the bunch emittance in the DBA after matching the optical functions, on the **right** instead I show the trend of its rms dimensions, the green line indicates the length of the beam which decreases due to the magnetic compression.

The compression of the arc

The dispersive stretch of the DBA in fact behaves on the beam just like that of the chicane-style compressors described in the chapter 1.3: smaller energy particles are deviated to larger angles and travel a longer path arriving at the second bending later compared to the more energetic ones. Therefore, with a proper chirp of the bunch, it is possible to exploit the arc also as a magnetic compressor (hence the name arc compressor).

The chirp must therefore be chosen so as to compress the bunch as much as possible and extract it from the arc at the point where it has the shortest length. A chirp too high, in fact, would lead to over-compression the beam, in practice the tail of the beam would go over his head returning to lengthen the beam.
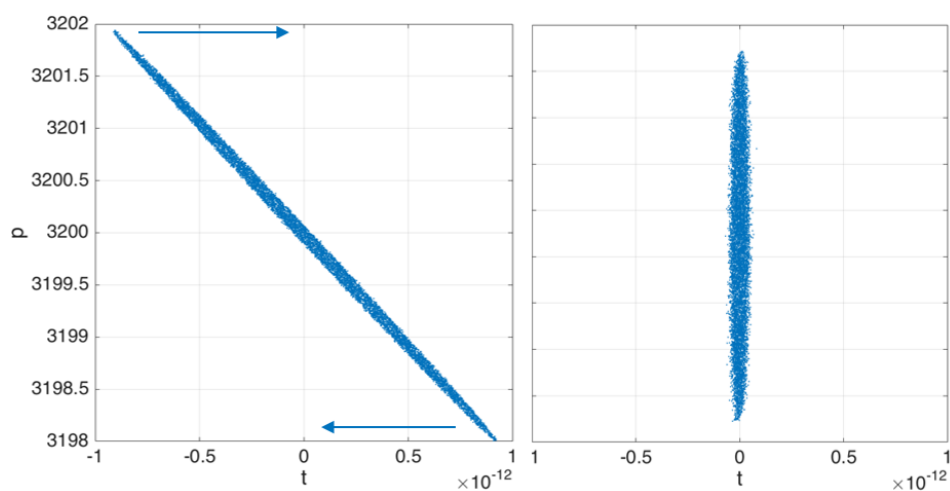

Figure 4.7. The figure shows the phase spaces before and after the compression. As can be seen, the minimum final length (at maximum compression) is linked to the uncorrelated energy spread of the beam.

The dynamics of compression is well shown in figure 4.7, where the phase space of the chirped beam at the entrance and at the exit of the arc is shown. As can be seen, the minimum final length (at maximum compression) is linked to the uncorrelated energy spread of the beam. This anticipates the fact that, to maximize beam peak current, it will be important to accumulate less uncorrelated and correlated energy spread as well as being able to impress the correct chirp.

The connection between uncorrelated energy spread and final bunch length at maximum compression is very well shown in Fig. 4.8. Here 3 different values of uncorrelated energy spread are considered in order to see the effects on the final beam length, they are properly chirped to grant the extraction close to

the point of maximum compression. We considered 2 realistic values of energy spread, an an extremely bad case. The first case is represented by the green line and is the energy spread that we expect to see once all the correlated energy spread is removed by the realistic beam. The yellow case considers the total energy spread that we expect the beam to accumulate in the booster linac L1 of MariX without linearization. The worst case is wanted to be extremely bad to show the difference, this is represented by the red line.

Table 4.4 resumes the uncorrelated energy spread of every bunch, their final dimensions and the corresponding compression factor, defined as $C_f \equiv \frac{\sigma_{s_i}}{\sigma_{s_f}}$, remember that $\sigma_{s_i} = 150$ µm.
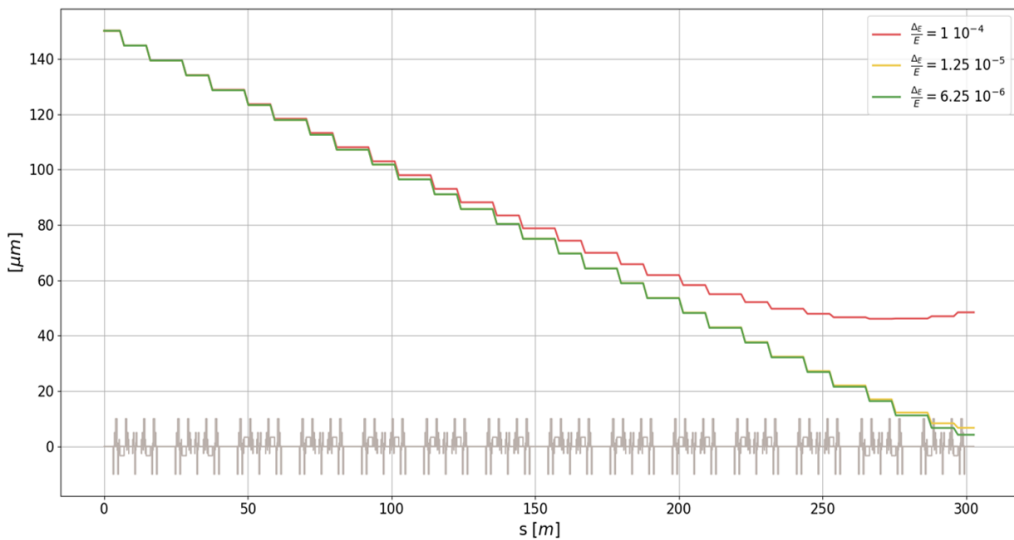

Figure 4.8. Beam length during the tracking in the BA for 3 different values of the initial uncorrelated energy spread. The bunches are properly chirped in order to be extracted close to the maximum compression point.
The green line represents the best possible scenario, the final dimension is $\sigma_s \simeq 4.22$ µm corresponding to a compression factor $C_f \simeq 35.5$. The yellow case shows a final length $\sigma_s \simeq 6.72$ µm, $C_f \simeq 22$. The red case is an extreme case, in this situation $\sigma_s \simeq 48.4$ µm, $C_f \simeq 3.6$.

The Fig. 4.9 shows the growth of the normalized emittance on the two transversal planes as the arc is traversed by the beam with a minimum energy spread. The two cases differ only on the initial value of the normalized emittance $\varepsilon_{n,x} \simeq 0.3$ mm mrad for the case on the left and $\varepsilon_{n,x} \simeq 0.4$ mm mrad for the one on the right.

In both cases the growth for the horizontal emittance is less than 5 ‰, that is completely negligible. The vertical normalized emittance, as expected, is

Table 4.4. Summary of the results obtained in the experiments of maximum compression of ideal bunches. The table shows the color of the line used in Fig. 4.8, the initial uncorrelated energy spread, the final rms length at the extraction point and the corresponding compression factor (considering that the initial length of the beam is 150 μm).

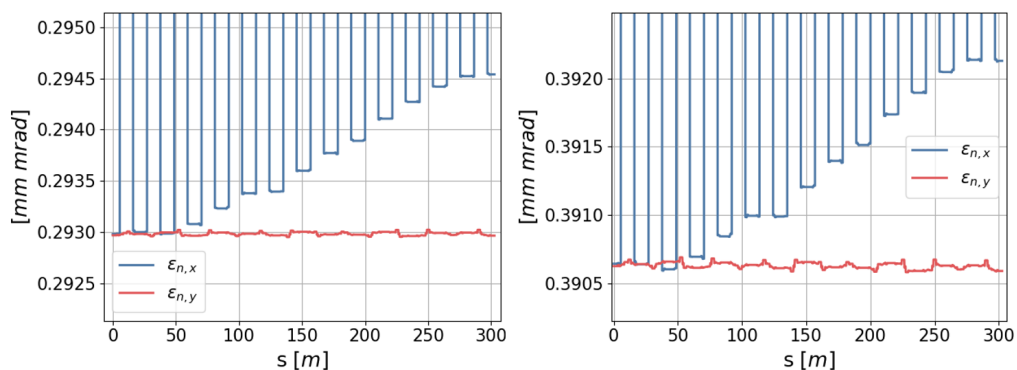| Color	$\frac{\Delta_E}{E}$	σ_{s_f}	C_f
Red	1×10^{-4}	48.4 μm	3.6
Yellow	1.25×10^{-5}	6.72 μm	22
Green	6.25×10^{-6}	4.22 μm	35.5

completely stable.

Figure 4.9. Two different cases, differing in the value of the initial emittance, of tracking of matched beams in the BA, the trend of the normalized trasverse emittances is shown.

A realistic beam in the BA

At this point we decided to move to simulations of a more realistic beam to which we refer, calling it "real beam". The latter was transported with the Astra tracking code up to the entrance of the BA in order to verify that the arc was able to achieve good compression performance even with beams having the typical irregularities given by the space charge (halos and residual correlations). To simulate this bunch, 5000 macro-particles were used.

To accelerate the simulations in the arc, about 17% of the beam has been cut, this is the head and tail particles present in the areas with a lower charge density.

First, the particle distribution obtained with Astra and cut was appropriately converted in the `elegant` format. At this point a series of specific manipulations of

the beam have been carried out which have allowed optimization of compression and transport in the BA:

Acceleration The beam arrives from the accelerating cavity booster to 1.6 GeV of energy, during the acceleration a modulation in energy is given to the beam given by the curvature of the electric field of the radiofrequency. This modulation can be eliminated by using a high harmonic cavity used in the decelerating phase [80]. For this reason it is necessary to supply additional energy, which eventually turned out to be 200 MeV, to the beam that will be removed in the decelerating phase from the linearizer. So beam is injected into an ideal , that means dimensionless, cavity that instantly imparts the effect of the simulated field. The cavity is works in L-band at 1.3 GHz and the beam is injected in pure accelerating phase (into the wave crest).

Linearization The bunch, then, is fed into an ideal cavity that works with the 3rd harmonic of the fundamental frequency that corresponds to $3.9 GHz$ while the injection phase is completely decelerating. The beam is linearized by losing the 200 MeV that was supplied to it by the previous cavity returning to 1.6 GeV.

Chirp Once the energy has been corrected it is necessary to chirp the beam, ie to impart the correct linear correlation between position and energy of the particles so that the arc behaves as a compressor. This can also be done with an ideal cavity in fundamental harmonic, it is sufficient to inject into the zero crossing point and to give the peak field necessary to maximize the compression.

Match At this point the bunch is ready to be matched to the arc, this was done with an ideal element that applies a manipulation of the beam that keeps constant the emittance on the various planes. In this way, the effect of a dedicated matching line like the one designed in chapter 3.2 (which must be considered in the future in the actual lattice) is realistically simulated. The matching parameters are those illustrated in the Table 4.3.

At this point the beam is ready for injection into the arc, with a bit of testing on the parameters of the cavities it was possible to set the correct extraction point (setting the chirper) and minimize the size of the beam at the exit (removing correctly the quadratic correlation in the energy of the bunch with the linearizer). The optimal values for cavity feeding are summarized in Table 4.5 and the results of the tracking in the arc thus obtained are shown in Fig. 4.10.

Table 4.5. This table shows the supply parameters of the ideal cavities that were used to prepare the beam for injection in the BA and achieve the maximum compression.

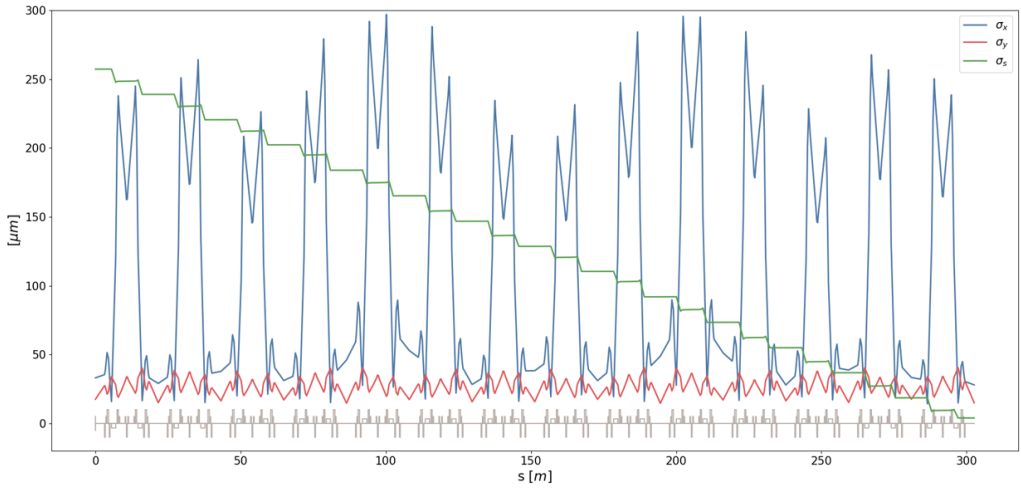| Cavity	Injection Phase	Cavity frequency	Peak voltage
Accelerator	90°	1.3×10^9 Hz	11×10^7 V
Linearizer	268.5°	3.9×10^9 Hz	11×10^7 V
Chirper	180°	1.3×10^9 Hz	30.4×10^7 V

Figure 4.10. Trend of the rms dimensions of the realistic beam in the BA in the case of maximum compression.

The realistic bunch at the injection point in the BA has a rms length of about 270 μm, while at the point of extraction its size is 3.96 μm for a compression factor $C_f \simeq 64.9$. Care must be taken to interpret this last value because, although the final dimensions are comparable to those of the ideal case, the compression factor appears considerably higher. This simply happens because we are starting with a longer beam, while the minimum final dimensions are somehow fixed by the uncorrelated energy spread inside the beam.

As we can see the transverse dimensions have a periodic behavior with a different period compared to a single cell (as we should expect). This is due to the non-ideality of the beam which has areas in which the halos generated by the previous simulation with space charge alter the local parameters of the bunch and un-match it slightly.

Fig. 4.11 shows the final longitudinal phase space of the bunch. As we can see, this is vertical, but we note the presence of a local quadratic correlation

located in the most energetic part of the bunch. This correlation is inherited from a residual local correlation present in a portion of the tail of the beam injected into the BA, this component can not be eliminated, in any case does not involve a marked lengthening of the beam.
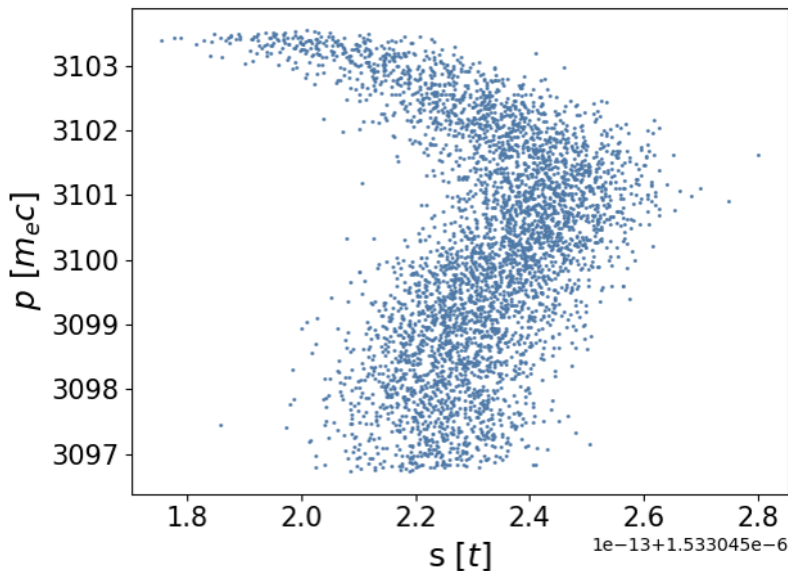

Figure 4.11. The longitudinal phase space of the realistic bunch at BA exit.
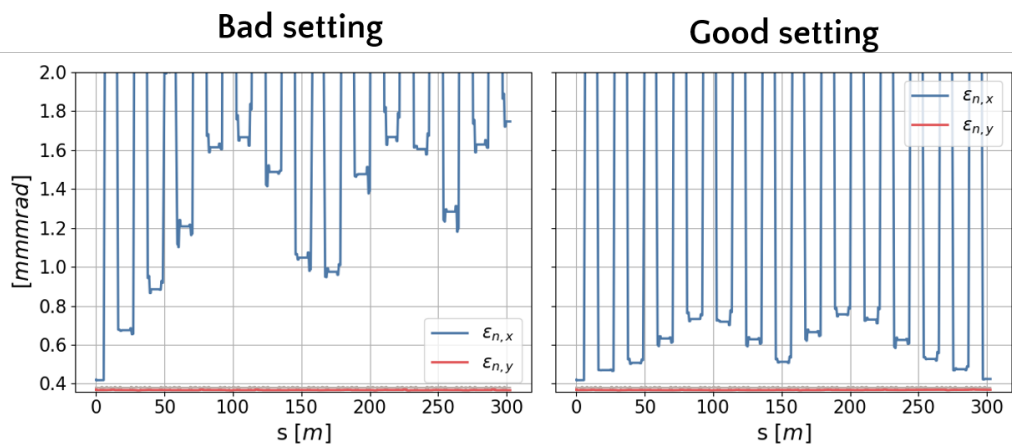

Figure 4.12. The effects on the compensation of the transverse normalized emittance of the sextuples.
Left: trend of the emittance with the wrong setting. **Right:** we observe the beneficial effect of the sextupoles that control the fluctuations of emittance.

Initially, the sextupoles of the line have not been set, this makes the oscillations of the normalized horizontal emittance uncontrollable as the cells are traversed by the bunch Fig. 4.12 on the left. In this specific case, the final value of emittances was more than quadrupled.

The effect is due to the chromatic aberrations that are gradually introduced by the quadrupoles on the different portions of the bunch and can be corrected by optimizing the current values set in the sextupoles. The figure on the right shows that the fluctuations of emittance can be controlled very well thanks to these magnetic elements.

Evaluation of the CSR effects

The synchrotron radiation is emitted from the bunches of electrons when they pass through a bending magnet. When the wavelength of the emitted radiation is comparable with the length of the bunch, *Coherent Synchrotron Radiation* (CSR) is emitted. This last type of radiation represents a big problem for high energy bunches, in fact the power loss due to the emitted radiation can be significant as it is proportional to the square in the number of emitters. In linacs and circular machines for a Gaussian bunch in free space, the total coherent power radiated is:

$$P[W] = 2.42 \times 10^{-20} \frac{N^2}{\sqrt[3]{\rho^2[m]\ \sigma_z^4[m]}} \tag{4.1}$$

where N is the number of emitters, ρ the bending radius and σ_z is the rms bunch length. As we see shorter the bunch of electrons, and therefore higher the peak current, and the greater the power emitted.

In the case of MariX, power losses were evaluated to be negligible, but the problem to be analyzed is the influence of the radiation emitted by the tail of the bunch on the particles of the head. In fact, the radiation travels at a speed of c, and for a given period remains superimposed on the distribution of particles, influencing it with its own electric field and introducing *microbunching instability* (μbi).

This leads to an inevitable rise in the energy spread which is then translated into an increase in transverse emittance in subsequent bending magnets. Moreover, in the case of compressor arches, the CSR can limit the compression factor by deforming the longitudinal phase space of the bunch due to non-uniform local energy losses, thereby ruining the chirp of the essential package for compression.

Both effects can be detrimental to the performance of the FEL so it is important to correctly simulate the effects of the CSR and understand how to minimize them.

Bunch preparation for CSR evaluation

The loss of energy by radiation emission and the effect of the CSR field on the bunch are calculated during the tracking of `elegant` by dividing the distribution of particles into longitudinal bins. This procedure is actually very delicate because the bunch must be divided into a high number of bins, but at the same time the bins must be well populated in order not to overestimate the effects of the CSR due to numerical errors.

These observations therefore suggest adopting a high number of bins and a high number of macroparticles that simulate the package while maintaining a correct relationship between these two values. The increase of these two parameters leads to a considerable slowdown of the simulations, especially considering that the line is more than 300 m long.

The approach adopted was therefore to gradually increase the number of bins until convergence is reached, which means to arrive at observing that the increase in the parameter does not involve any more variation of the final values of $\varepsilon_{n,x}$ or $\frac{\Delta_E}{E}$ of the beam, then increase the number of particles of the beam up to convergence and continue the operation iteratively. In this way we guarantee an accurate simulation that is as fast as possible.

Another very important point to keep in mind is that any fictitious periodicity in the spatial distribution of the particles stimulated the emission of frequencies that then resonate with the distribution itself amplifying the phenomenon. This is a problem similar to the FEL simulations under the SASE regime.

Periodic distributions of this type can be introduced from various sources:

- From the integration step of Runge-Kutta of Astra (similar to what we saw in Fig. 3.15 in the chapter 3.2) which must therefore be very short.

- From the program that performs the conversion of the particles from the Astra format to that of `elegant`, for this it is necessary to use the maximum precision available in the representation of numbers.

- Finally, from the program used to oversample the bunch of electrons during the convergence research process with the number of bins and particles. In fact transporting with Astra beams so much populated (in the order of 10^7 macro particles) would be excessively time consuming, for this we

resort to a specific `elegant` tool called *SmoothDist6s*. This tool increases the number of particles in a particle distribution taken as input. At the same time, smooths the distribution and adds optional energy and density modulation. It is intended to increase the number of particles produced by photoinjector simulations to improve the stability of CSR simulations.

Bins, macroparticles and uniform distribution test

The very first CSR simulations carried out were made directly with a bunch filled with a low number of macroparticles $N_{MP} = 12000$ and the CSR evaluation was made choosing an initial bins number $N_B = 500$. That bunch was simulated from the cathode to the Arc entrance with ASTRA, part of the long tails (approximately 17% of the total charge) was cut and than the particle distribution have been converted in `elegant` format.

The number of bins turned out to be much higher than expected and showed us the typical situation in which the effects of CSR are overestimated because of the amplification of numerical sampling noise. Furthermore, the cut performed on the charge distribution introduces some very intense fictitious sources of radiation. In fact, the system used by elegant to simulate the amount of radiation emitted looses the one-dimensional model developed by Saldin-Schneidmiller-Yurkov [110, 111] that depends on the first derivative of the current profile and, in case of cuts in regions where the slice current is high, it can generate large amounts of fictitious radiation.

In this situation the longitudinal phase space of the beam is filamentated due to the strongly amplified microbunching instability, this is comparable to a local increase in the uncorrelated energy spread of a beam portion and, together with the compression dynamics of the BA, leads to lengthening the bunch at the end of the arc. The effect is that of masking the real distribution of the particles under a very amplified numerical noise, it is therefore impossible to optimize the compression in this situation.

It is possible to reduce the numerical error due to the sampling of the bunch by drastically reducing the number of bins, however in this way the CSR effects can not be well simulated as the statistical errors introduced when the beam histogram is filled are amplified.

In Fig. 4.13 I show a comparison of the phase spaces that are obtained by sampling the bunch with histograms from $N_B = 500$ and $N_B = 100$.

The strong numerical noise that can be seen in the figure on the left is due to the low number of particles in the bin, the effect is that of obtaining a beam at
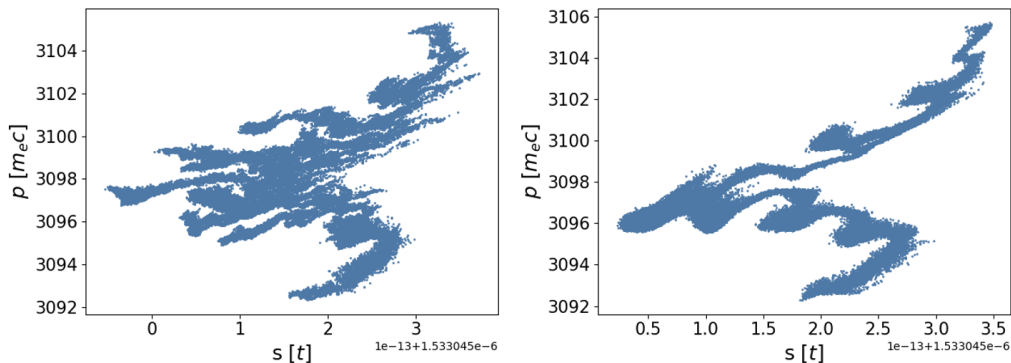
Figure 4.13. Two different final phase spaces obtained with CSR simulations of the transport in the BA of the same bunch consisting of $N_{MP} = 12000$. On the left there is a case in which the numerical sampling noise is greatly amplified by the high number of bins $N_B = 500$, on the right the noise is reduced by choosing $N_B = 100$ and repeating the simulation.

the output of the BA whose longitudinal phase space presents a layered shape, called "pancake shape". A histogram on particle energy would reveal a very irregular structure (compare Fig. 4.14 - 4.18). For this reason from now on I will show the longitudinal phase spaces in the form of 2D histograms also showing the histogram projections on the axes in order to better show the density fluctuations of the particles.

At this point we started working on a 50 pC ideal beam, 270 µm long (rms), generated with elegant with gaussian transverse particle distribution and uniform longitudinal distribution. This approach makes it easier to study the effect of the choice of the number of macroparticles and the number of bins on the dynamics in the arc, while the elegant internal generator uses special measures to generate distributions that do not introduce numerical noise in CSR simulations.

We have significantly increased the number of particles transposed in the arc up to several millions by varying the number of bins, after few tries a good initial compromise was found at $N_{MP} = 2 \times 10^6$, $N_B = 200$ (Fig. 4.15).

This particular set of parameters almost completely eliminates the filamentation of the longitudinal phase space (as well shown by the vertical histogram on particle energy distribution). In these conditions I have been able to re-optimize on the phases and the gradients of the ideal cavities that prepare the bunch to the injection in the arc to compensate the effects of the CSR thus maximizing the height of the current peak improving the compression performance.

The distribution is very compact and has a long tail with little charge enclosed inside (as shown by the histogram on the time of the particles). 3 After several

Figure 4.14. 2D Histogram of the longitudinal phase space of a bunch with $N_{MP} = 1 \times 10^6$, $N_B = 600$. These parameters greatly accentuate the numerical noise due to the sampling of the histogram. The result is these filamentations of phase space generating this "pancake shape" feature (whose layers are clearly visible in the energy histogram) that masks the real shape of the bunch.

Figure 4.15. 2D Histogram of the longitudinal phase space of a bunch with $N_{MP} = 2 \times 10^6$, $N_B = 200$. With this new set of parameters, the numerical errors were almost completely eliminated, so the final phase space could be straightened by changing the setting of the linearizer and of the chirper before the BA.
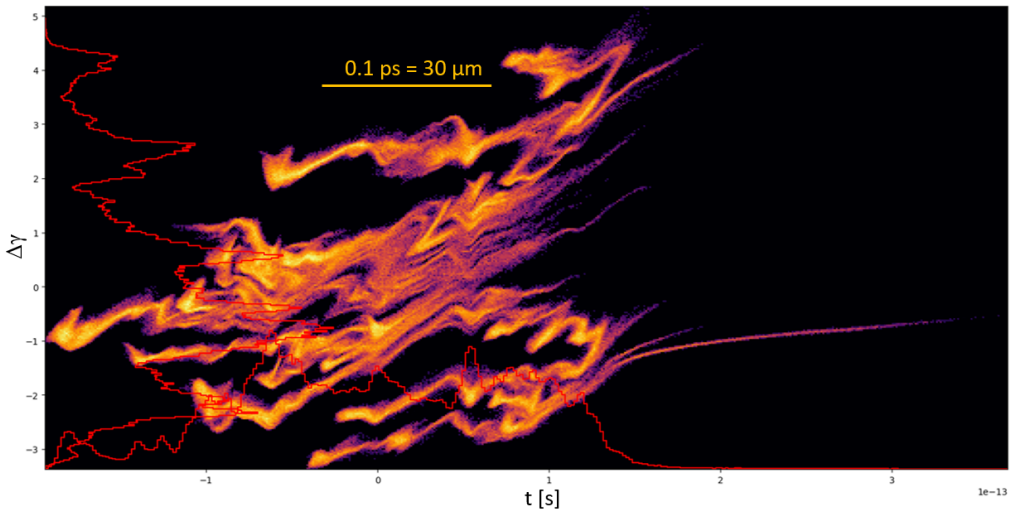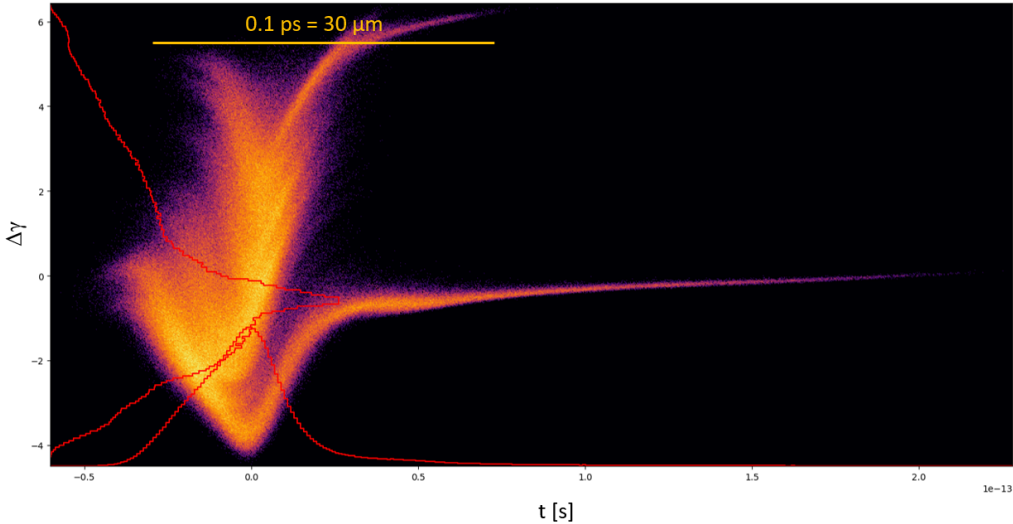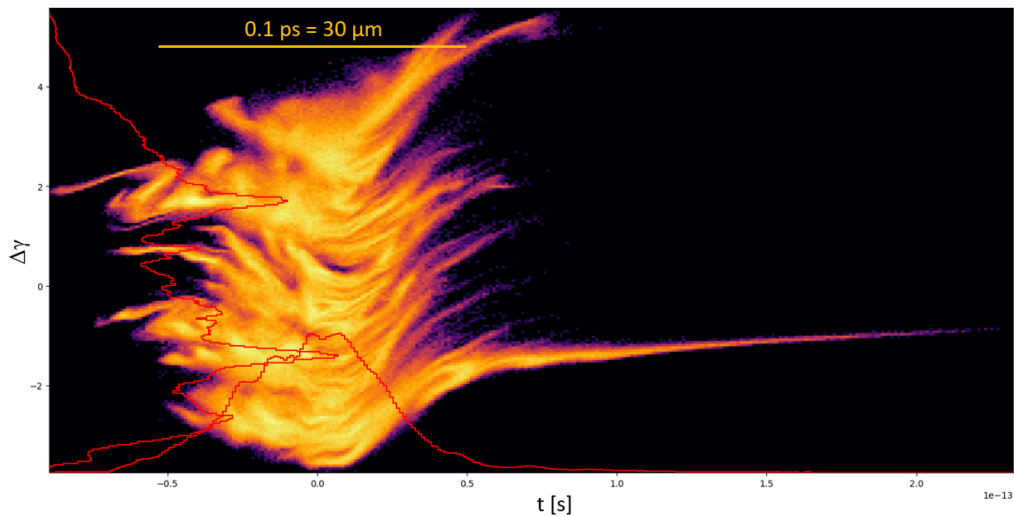
Figure 4.16. 2D Histogram of the longitudinal phase space of a bunch with $N_{MP} = 2 \times 10^6$, $N_B = 800$. The same number of macro particles and the setting of the cavities that praparate the beam at the injection of Fig. 4.15 has been maintained, but the number of bins has quadrupled. As you can see the filamentation reappears but the beam dynamics remain the same (the backbone of the beam maintains the same geometry).

attempts, some of which are shown below, I found a good numerical noise reduction at $N_{MP} = 2 \times 10^7$, $N_B = 500$. The result obtained is similar to that observed with $N_{MP} = 2 \times 10^6$, $N_B = 200$ even if you require a much higher simulation time. This therefore confirms the possibility of using the previous parameters for the simulation of the tracking in the BA.

The setting of the cavities used has a very interesting result: the CSR has an effect similar to that of the linearizer on the beam and introduces a very marked curvature of the phase space (this was visible even in the presence of high noise, for example in Fig. 4.14) In fact, the phase of the linearizer that allowed to maximize the current is in accelerating crest (90°), whereas before it was exactly in counterphase. So the effect of the CSR alone corrects the curvature introduced by the RF in the booster, rather it requires to further amplify it with the linearizer to completely cancel the effect. In this situation it was no longer necessary to use the ideal accelerating cavity but only the linearizer and the chirper, voltage and injection phase (whose operating parameters can be consulted in Table 4.6).

All this interesting study allowed us to become familiar with the effects introduced by the numerical errors given by the low number of bins and the low number of particles per bin. Surprisingly, it also indicated that the high harmonic cavities can be used to pre-compensate the effect of CSR and linearize the final
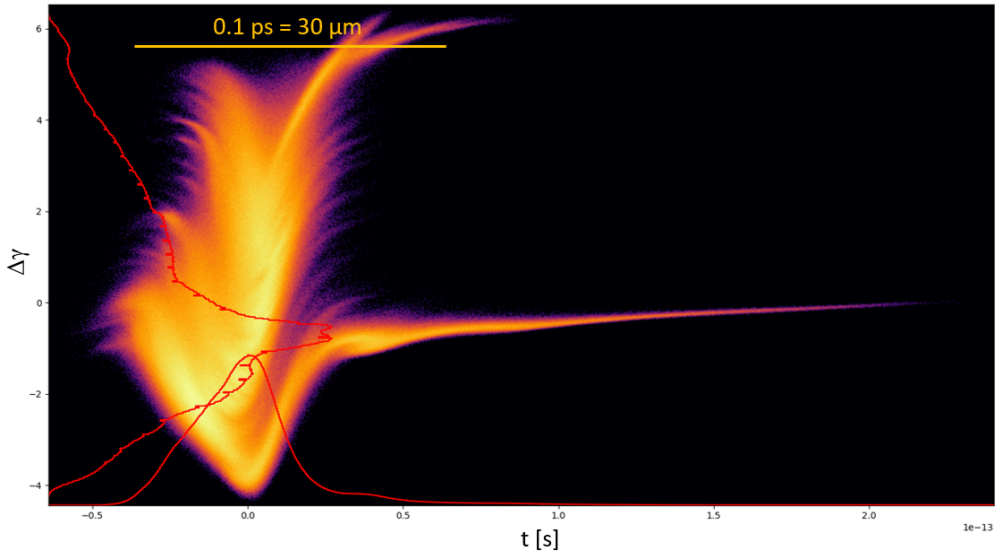
Figure 4.17. 2D Histogram of the longitudinal phase space of a bunch with $N_{MP} = 2 \times 10^7$, $N_B = 500$. A result very similar to that obtained in Fig. 4.15 the simulation parameters of the CSR are considerably greater (and so is the time of computation). Output bunch parameters are compatible with the faster simulation ones and confirm its reliability.

Table 4.6. This table shows the supply parameters of the virtual cavities that were used to prepare the ideal beam for injection in the BA in presence of CSR and achieve the maximum compression.

Cavity	Injection Phase	Cavity frequency	Peak voltage
Linearizer	90°	3.9×10^9 Hz	10.7275×10^7 V
Chirper	180°	1.3×10^9 Hz	313.75×10^6 V

phase space.

However, the simulations carried out with this uniform charge distribution have proved not to be accurate as the charge discontinuities in the head and in the tail proved to be important sources of fictitious radiation. The radiation produced by the tail of the bunch propagates on the distribution of particles gradually altering the space of the longitudinal phases and increasing the emittance of the beam.

The last step of this study of the effects of CSR in the BA of MariX, is to simulate a realistic beam, that is transported from the cathode up to the arc in the real beamline, exploiting the knowledge acquired on the setting of the bins,
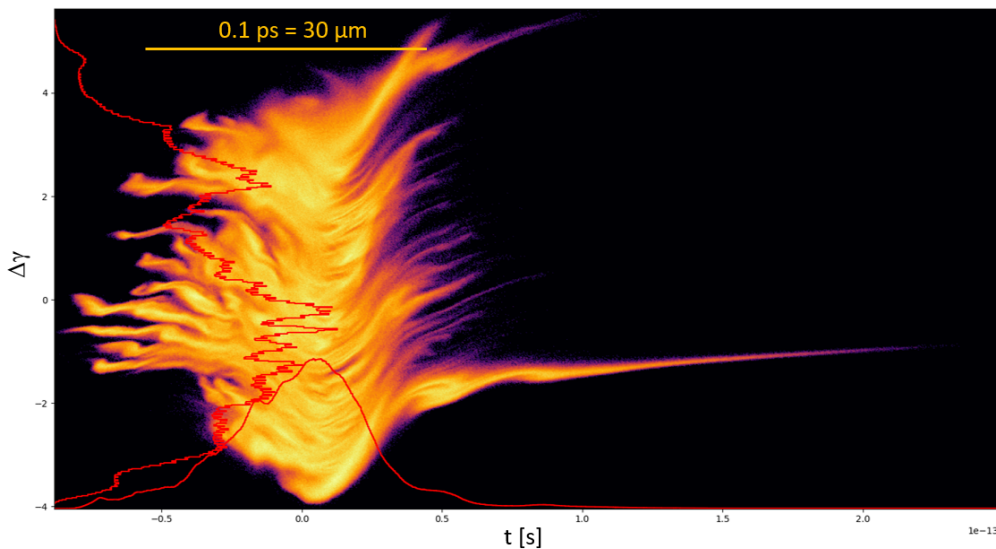
Figure 4.18. 2D Histogram of the longitudinal phase space of a bunch with $N_{MP} = 2 \times 10^7$, $N_B = 3000$. Another situation where the number of bins is too high and the numeric noise widens the particle distribution, this time with the maximum number of simulated particles.

the number of macroparticles and of the current distribution.

CSR compensation with a realistic beam

During the period of study of the numerical effects introduced by the parameters with which the CSR is simulated, as described in the previous subsection, an optimization of the injector was performed. This optimization (done with GIOTTO, the tool described in Subsection 2.2 and Chapter 3) was performed to improve the original working point by reducing the longitudinal emittance of the bunches transported up to the arc. This condition allows to have a lower correlation of orders higher than the 1st in the bunch keeping its length under control. The bunch obtained has parameters much better than the previous one summarized in Table 4.7: a lower transverse emittance and a current distribution similar to an isosceles triangle that shows smaller values in the prime derivative of the current distribution respect to a gaussian shaped one (as can be seen by observing the green distribution in Fig. 4.19).

After a quick study it was decided to use 10^5 macroparticles and 70 bins for the simulation of CSR in the arc. These values have proved, in the case of

Table 4.7. The table shows the parameters of the Realistic beam, transported with ASTRA up to the BA entrance, that we used in the final simulation of the CSR in the arc.

Parameter	Value
σ_s	365 µm
σ_x	83.3 µm
σ_y	83.6 µm
$\varepsilon_{n,x}$	0.20 mm mrad
$\varepsilon_{n,y}$	0.20 mm mrad
γ	3053.2 (E $\simeq$ 1.56 GeV)
Q_{tot}	50 pC
# macroparticles	1×10^5
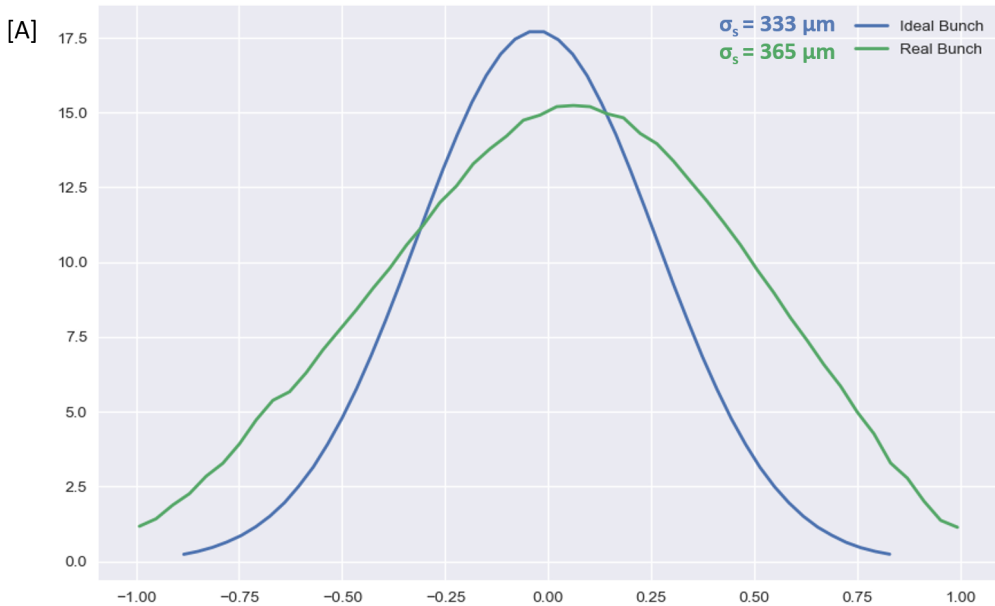
Figure 4.19. Comparison of the realistic beam current distribution (the green line), similar to an isosceles triangle, used for the final study of CSR in the BA and a slightly tighter ideal Gaussian distribution with a 3σ cutoff (the blue line).

the available bunch, a good compromise between an accurate simulation and a sufficiently fast one to guarantee an optimization of the beamline parameters.

Since in `elegant` it is not possible to optimize directly on the bunch peak current, the optimization phase of the result was divided into two parts:

Bunch compression. This phase was aimed at minimizing the product $\varepsilon_{n,x} \cdot \sigma_s$ in

order to keep under control the emittance growth. The variables available to the optimizer were the fields applied to the chirper cavity and to the linearizer (set in acceleration phase to compensate the curvature induced by the CSR in the longitudinal phase space) and the field applied to all the sextupoles of the arc in order to linearize at best the phase space and control the fluctuations of emittance induced by chromatic aberrations. The result of this simulation can be observed in Fig. 4.20.

Peak current maximization. In this case the optimization was carried out manually by further increasing the electric field of the high harmonic cavity so as to concentrate the majority of the bunch charge in the same current spike. The distribution thus obtained at the exit of the arc is shown in Fig. 4.21.
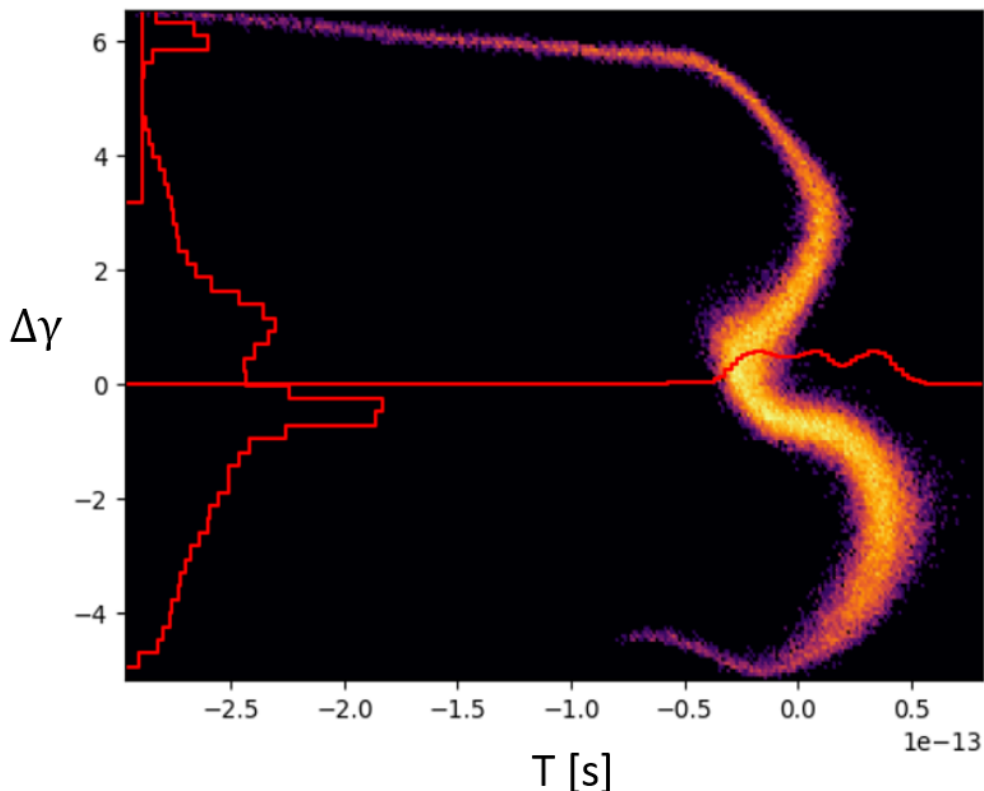

Figure 4.20. The phase space obtained at the output of the arc compressor optimizing only on the fields of the sextupoles of the arc, of the linerizer and of the chirper. The goal was to minimize the product $\varepsilon_{n,x} \cdot \sigma_s$, as you can see this instruction is not sufficient to maximize the peak beam current and for this reason it is necessary to proceed manually.
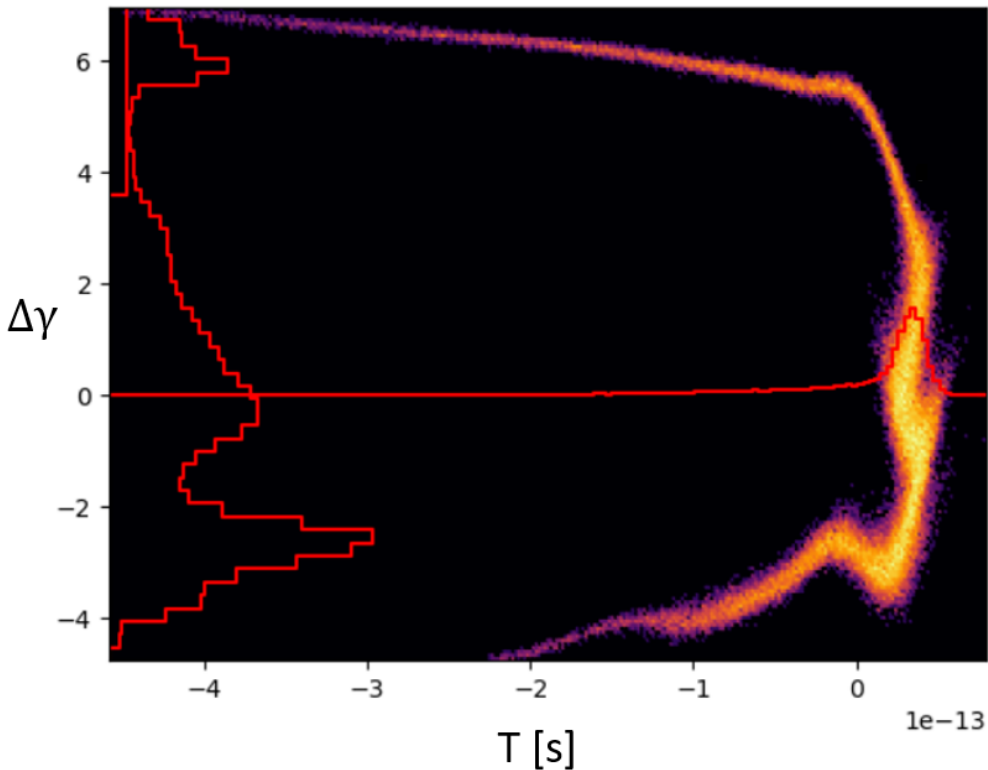
Figure 4.21. The phase space obtained at the output of the arc compressor optimizing manually on the field applied to the linarizer, in fact, by increasing the intensity of the electric field and injecting in pure accelerating phase it is possible to correct the "hump" introduced by the CSR which is observed in Fig. 4.20.

The final values individuated for voltage and injection phase applied to the linearizer and the chirper can be consulted in Table 4.9. The longitudinal phase space of the obtained bunch does not show great distortions induced by the CSR. The solution found proved stable by adequately increasing the number of macroparticles and bins, in Fig. 4.22 I show the results of a run with 10^6 macroparticles and 100 bins, the form remains the same and some sources of CSR are slightly amplified. More than 70% of the bunch charge is enclosed in the high current spike which reaches a peak of $\simeq 1.6$ kA in a spike long $\simeq 5$ μm (FWHM).

As can be seen in Table 4.8, the bunch presents a considerable increase in the normalized projected horizontal emittance that takes place in the last bending magnet of the arc, where the beam has maximum peak current and the effect of CSR is greater (as you can see in Fig. 4.23). This increase is due to the transverse

Table 4.8. Realistic beam parameters at Bubble Arc exit. The high value of total horizontal normalized emittance is physiological due to the large variation of transverse moments between the tails and the spike at the back of the bunch. Slice values on the brighter spike, on the other hand, are very good.

Parameter	Value
σ_s	20.6 μm
σ_x	52.0 μm
σ_y	13.2 μm
$\varepsilon_{n,x}$	1.01 mm mrad
$\varepsilon_{n,y}$	0.20 mm mrad
γ	3050.6 (E $\simeq$ 1.56 GeV)
Q_{tot}	50 pC
I_{peak}	1580 kA
$\frac{\Delta_E}{E}$	1.01×10^{-3}
# bins	70
# macroparticles	1×10^6
Slice $\varepsilon_{n,x}$	< 0.4 mm mrad
Slice $\varepsilon_{n,y}$	< 0.2 mm mrad
Slice $\frac{\Delta_E}{E}$	2.68×10^{-4}

Table 4.9. This table shows the supply parameters of the virtual cavities that were used to prepare the realistic beam for injection in the BA in presence of CSR and achieve the maximum peak current amplification.

Cavity	Injection Phase	Cavity frequency	Peak voltage
Linearizer	90°	3.9×10^9 Hz	80.0×10^6 V
Chirper	180°	1.3×10^9 Hz	410.0×10^6 V

kick imparted by the intense emission of CSR to the high current region, which increases the local value of $\langle x \rangle$ and $\langle x' \rangle$ (as shown in Fig. 4.24), where $x' = \frac{p_x}{p_z}$ is the horizontal slope of the trajectory of the single particle, greatly increasing the standard deviations of the quantities x and x' of the total bunch. However, the effect of this kick induced by the emission of CSR is very uniform on the particles in the spike and does not alter the local values of the slice emittance (as can be seen in Fig. 4.25).

To summarize, I have studied how to simulate the effects of CSR on a bunch transported from the cathode up to the injection of the bubble arc. Once a realistic and noise-free simulation was obtained, I optimized the beam dynamics
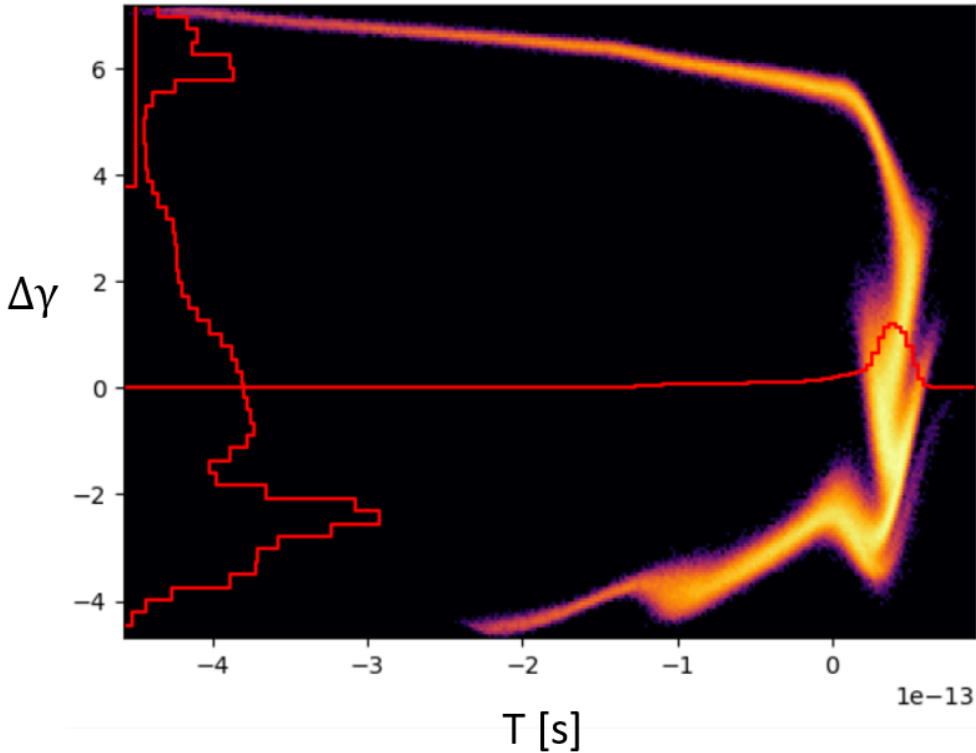
Figure 4.22. I show the results of a run with 10^6 macroparticles and 100 bins, the shape shown in 4.21 remains the same and some sources of CSR are slightly amplified.

in the arc to maximize compression and peak current. The result obtained with the beam from $N_{MP} = 1 \times 10^5$ and using $N_B = 70$, which proved to be substantially the same as that obtained with an order of magnitude more than macroparticles, is for now the reference one.

The final length of the bunch is $\sigma_s \simeq 20.6$ µm with a compression factor $C_f \simeq 18$ and a current amplification factor of $\simeq 105$. Surely the long tail of the bunch contributes to lengthen the rms value of the bunch, while the high current core, which represents the portion of the beam that will work in the FEL, is even more compact ($\simeq 5$ µm FWHM).

The final relative energy spread is $\frac{\Delta_E}{E} \simeq 1.01 \times 10^{-3}$ and will be further halved following the second acceleration in the booster which will double the average beam energy. The slice relative energy spread at the height of the spike is considerably lower $\frac{\Delta_E}{E} \simeq 2.68 \times 10^{-4}$ that have still to be halved by the energy doubling due to the second pass in the main booster. The absolute energy
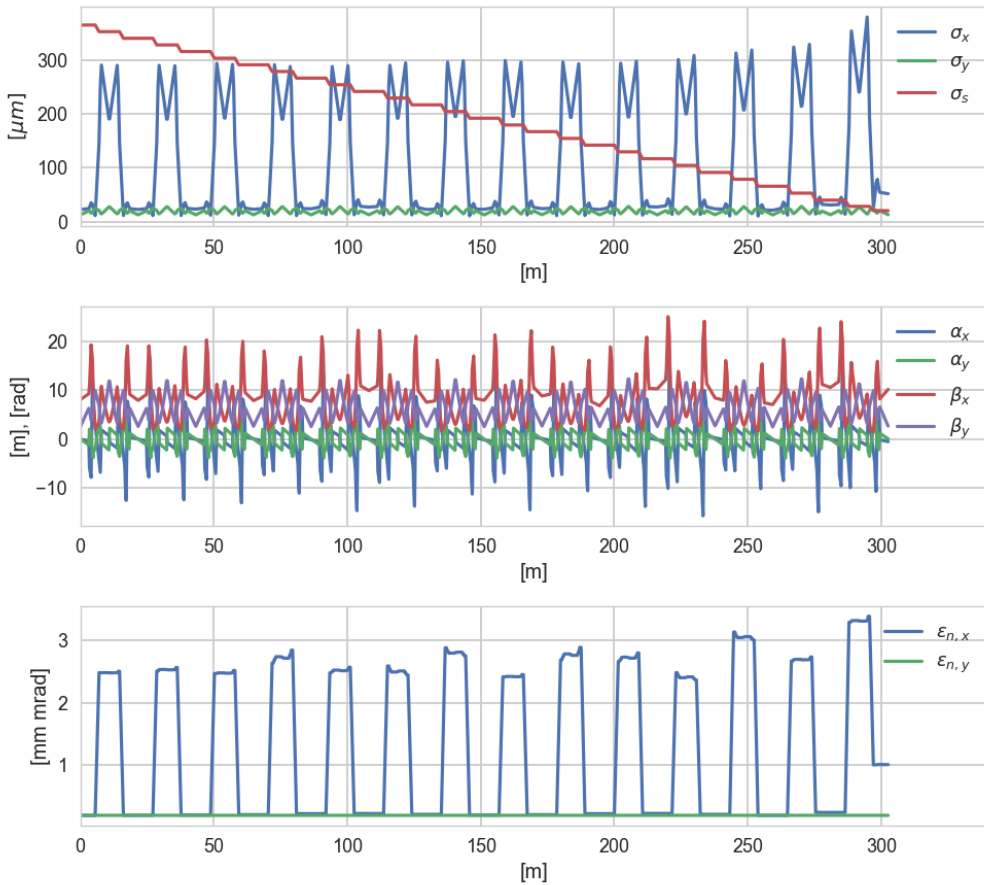
Figure 4.23. Main parameters of the bunch in the simulation of the Bubble Arc in presence of CSR effects.
Top: longitudinal and transverse beam envelopes.
Middle: main Twiss parameters.
Bottom: transverse normalized total beam emittances.

spread is due to the product between the initial length of the bunch and the chirp that is impressed on the beam, which is a fixed value for the moment, linked to the R_{56} of the arc.

The average current is $\langle I \rangle \simeq 154$ A while the peak current is instead equal to $I_{peak} \simeq 1.58$ kA leading to a very high peak normalized brightness $B_n = 5.85 \times 10^{16}$ A/$(\pi$ m rad$)^2$.
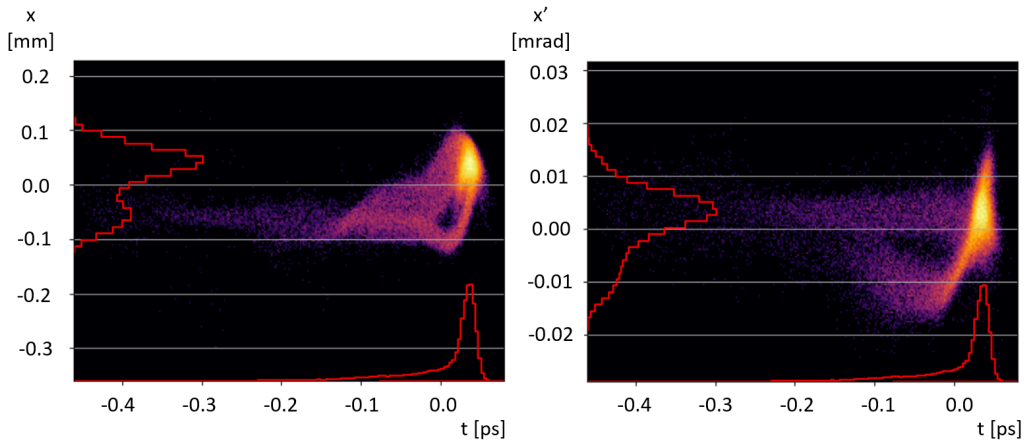
Figure 4.24. The effects of the CSR kick on the bunch responsible for the increase of projected horizontal emittance.
Left: horizontal position of the particles as function of the time coordinate. The densest (yellow) part, corresponding to the spike particles, is slightly offset from the axis ($x = 0$), the average displacement is about 50 μm.
Right: horizontal slope of the particles as function of the time coordinate. Also in this case it is noticed that the particles in the spike have a non-zero mean slope, estimated around 5 μrad.

4.3   Conclusion

The innovative scheme that allows to build compact superconducting SW linacs that, in fact, double the energy supply to the beam have been tested. To make this scheme work, a special arc compressor is required, called *Bubble Arc*, which must make a complete U-turn to the beam, compressing the bunches at the same time. In this way the bunches peak current is raised by a factor of the order of 10^2 approaching their parameters to those required for injection into the FEL. In this thesis work I tested the feasibility of this new type of scheme, verifying that the effects introduced by the CSR, in particular the increase of beam emittance, energy spread and the distortion of the particles distribution of the longitudinal phase space, have not turned out to be a showstopper.

   Some measures have shown great effectiveness in compensating for the effects induced by CSR. In particular, adopting a symmetrical current distribution similar to an isosceles triangle at the entrance of the arc seems to soften the effect of distortion of the phase space effected by the radiation. Moreover, in this particular condition the use of a high harmonic cavity, injecting the bunch in accelerating phase, to pre-compensate the distortion effect introduced by the
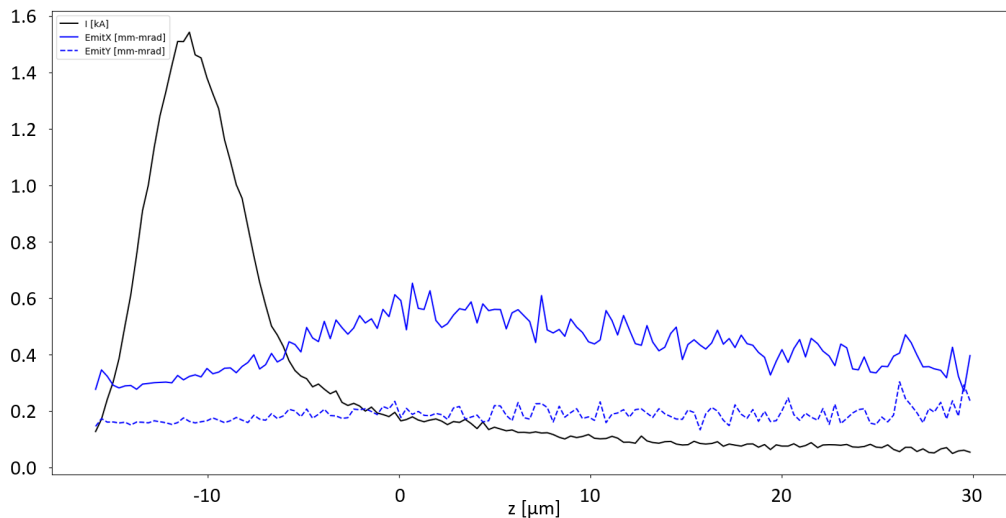
Figure 4.25. Slice analysis of the bunch at the exit of the Arc Compressor, the normalized transverse emittances (blue lines) and the slice current (black line) are calculated by dividing the bunch into 150 slices. The beam is represented with respect to the spatial coordinate z, consequently it appears overturned with respect to the images of the phase spaces represented with respect to time. The emittances within the spike remain below 0.4 mm mrad.

CSR in the last bendings of the arc and linearize the compression at best, has proved to be very effective.

Using `elegant` I simulated the effects of CSR emission in the arc's bending magnets and drifts and the effect that this radiation gives propagating on the bunch. These simulations have revealed that the bunch can be transported without ruining its slice quality, also allowing to compress the bunches considerably.

These preliminary tests set the stages for future studies with the aim of achieving a compact acceleration and compression scheme of this kind.

Further preliminary tests on the energy tolerance of the arc have yet to be completed.

Conclusion and Perspectives

In the first two years of my PhD, I carried out 4 different activities related to the production of extreme electron beams by using linear accelerators optimized with a code named GIOTTO. This code is based on a genetic algorithm and is capable of interfacing with a tracking code, Astra, to deal with beam dynamics problems in presence of space charge an high chromaticity of the beam. In particular, I have developed new features in GIOTTO making it able to deal with new kind of beam dynamics problems reaching the reported results:

1. The dual development of a beam based method for the search of the golden orbit in the linacs and, after having set it, for the correction of the misalignments of solenoids, quadrupoles and cavities. This method allows to increase the brightness of the electron beams produced by the linac improving its setting. Furthermore, this methodology is particularly suitable for test facilities which are by their nature designed to run with different working energies as it allows to guarantee the stability of the trajectory when the energy changes. I presented the results at the International Particle Accelerator Conference which was held in Busan, in south Korea in May 2016 and published in [2].

2. The flexible dimensioning of transfer lines dedicated to the transport and matching of FELs plasma driven beams. In these particular conditions it is possible to work with extremely low chromatic length beams and the emittance of the beam spontaneously spontaneously also in the drift. GIOTTO is able to find the correct positioning and the correct gradient of quadrupoles set (with permanent or electromagnetic magnets) that allows to transport the beam and match it correctly to the undulator. Thanks to the changes made to GIOTTO to allow it to work with these wide-ranging

research problems, it proves to be an excellent candidate for the study of flexible lines to change the energy of the beam and, more in general, as a tool to perform matching based on tracking of bunches taking into account the space-charge forces.

The transfer line for Eupraxia@SPARC_LAB designed with GIOTTO was presented in the Design study of the machine this year [6]. I presented the preliminary results at the European Advanced Accelerator Concepts which was held on Elba Island in September 2017, and the final results at the International Particle Accelerator Conference which was held in Vancouver, Canada in May 2018 and published in [3, 4].

3. The study of an innovative laminar longitudinal compression and acceleration technique that exploits RF bunching and ballistic bunching in the first place.

   This technique is called laminar bunching and can be considered an evolution of the velocity bunching technique that overcomes its limits. In fact, the ballistic compression makes it possible to compensate the longitudinal energy spread in a softer way than the pure Coulomb repulsion. As a result this technique allows to reach very high compressions but also extremely low energy spread values. The results were presented at the Linear Accelerator Conference held in Beijing in September 2018 and publisher in [5].

4. Finally, GIOTTO was used to optimize the correction of the higher order correlations in the bunches obtained with an high brightness linac to obtain ultracold beams. Beams of this kind are in great demand in electron microscopy and electron diffraction experiments as the measurement noise decreases. In our case they were requested by Professor Rodolfo Bonifacio as bunches to be used in simulations of a quantum FEL.

GIOTTO has proved to be an extremely useful tool in seeking and optimizing new working points for linear machines. In the future I would like to continue its development by implementing a *MOGA* (Multi-Objective Genetic Algorithm) optimization mode [106] to search for Pareto optimal solutions in wide-ranging research problems. In fact, it would allow to identify with a single in-depth research all the different working points that satisfy the requests.

   This new modality could be compared with a new alternative way of performing parallel optimization based on "islands" with different types of optimizations and migration of optimal solutions (Coarse-Grained Parallel Genetic Algorithm with migration) [107].

During the last year of PhD I had the opportunity to participate in the design of an FEL source, named MariX. In the context of this work, a innovative scheme that allows to build compact superconducting standing wave linacs that double the energy supply to the beam have been tested. To make this scheme work, a special arc compressor is required, called *Bubble Arc*, which must make a complete U-turn to the beam, compressing the bunches at the same time. In this way the bunches current is raised approaching their parameters to those required for injection into the FEL. In this thesis it is showed how I have tested the feasibility of this new type of scheme, verifying that the effects of CSR on the beam in the arc did not turn out to be a showstopper.

Using `elegant` I simulated the effects of CSR emission in the arc's bending magnets and drifts and the effect that this radiation gives propagating on the bunch. These simulations revealed that the bunch can be transported in the arc, allowing to compress the bunches considerably and increase the peak current by a factor greater than 100, keeping the slice normalized emittance and the energy spread low in the higher current area.

These preliminary tests set the stages for future studies with the aim of achieving a compact acceleration and compression scheme of this kind. We expect the MariX Bubble Arc to be the key to build a compact 1 MHz FEL capable of producing radiation up to 1.5 Å and we hope that the scheme can also be applied to other machines of this kind. The study of this scheme will be an integral part of the MariX Conceptual Design Report which will be presented soon.

Introduction to Genetic Algorithms

The *Genetic Algorithms* (GA) are a family of stochastic optimization methods inspired by the evolutionary theory of Charles Darwin. This calculation logic, initially theorized by John Holland in 1975, is now applied in many fields, such as artificial intelligences, economics, engineering and physics. In the physical field, GAs, thanks to their nature as global optimizers, are particularly suitable for solving the complex problems of electromagnetism, where they are often used to design and solve inverse problems [92].

Within a program based on an algorithm of this type an initial population of data evolves according to the rules of natural selection, generating, finally, a good solution to the problem that is being addressed. First you must choose the function called *fitness function*. This gives us an evaluation of the validity of the solution taken into consideration by simulating the system's response and must be maximized or minimized according to the case.

The proposed solution is presented in the form of *chromosome* (in jargon). Each chromosome consists of *genes*, ie the individual data that make up the set representing the solution.

As can be understood, the size of the chromosomes, N_{genes}, and the type of information contained in the genes are dependent on the problem addressed. A great strength of GAs is the ability to simultaneously optimize whole *populations* of configurations. The population size (N_{pop}) is another value whose choice is free.

To do this, a GA programmer uses operators (*subroutines* and *functions* in our program) that produce a succession of populations whose members return better fitness values.

For a program of this kind to work properly, it is essential to assign the parameters as correct as possible. These must not only define the dimensions

of the chromosomes or the population but must also give the probabilities of activation and functioning of the fundamental operators and of the Fitness Function.

Therefore, the first step that an algorithm will have to face will be to evaluate the suitability of each single element of the starting population, if it is not supplied at the start it will be sufficient to generate an initial random set.

After which the genetic operators are applied whose cyclic execution simulates the *evolution*, they are the operators of *selection*, *crossover*, *mutation* and *elitism*.

Once the most suitable solution belonging to the population proves to be sufficiently accurate, the evolutionary cycle is interrupted by providing the values relative to the best chromosome.

Now I will go more into the details of the process.

The genetic manipulation of the population is based on the idea of changing the set of starting solutions, creating a new set of solutions and canceling the previous one. This process begins with the selection of the best chromosomes based on the fitness values provided by the Fitness Function. The selection operator produces a new population composed of the same number of chromosomes. The purpose of this passage is to eliminate solutions that are less "suitable for the environment" to use a Darwinian term. The most used selection methods are: the *roulette wheel*, the *ranking* and the *stochastic binary tournament*.

The *roulette wheel* generates the new population by selecting the elements of the old one with a probability proportional to their suitability, in practice the most suitable individuals will have more chances to be selected.

The *ranking* in its most popular version puts n copies of the best N_{pop}/n chromosomes that make up the initial generation, with N_{pop} equal to the number of items and n a divisor, while the *stochastic binary tournament* iteratively chooses pairs of chromosomes and puts the best in the new population up to fill it.

The selection operators are responsible for the convergence of the algorithm and are the only ones that take into account fitness values.

After selection, the crossover is used, which is used to mix the configurations traits, creating a new population of N_{pop}, just as in the case of genetic reproduction in biology (Fig. A.2).

The crossover operator is activated with a probability P_{cross} for each single pair. Once in use randomly chooses a chromosome from our set, after which it assigns the couple partner paying attention not to choose the same, now mixes the genetic material of the two chromosomes.

As in the case of selection, there are different algorithms that guarantee a good crossover. In the case of the *single-point crossover* you choose random

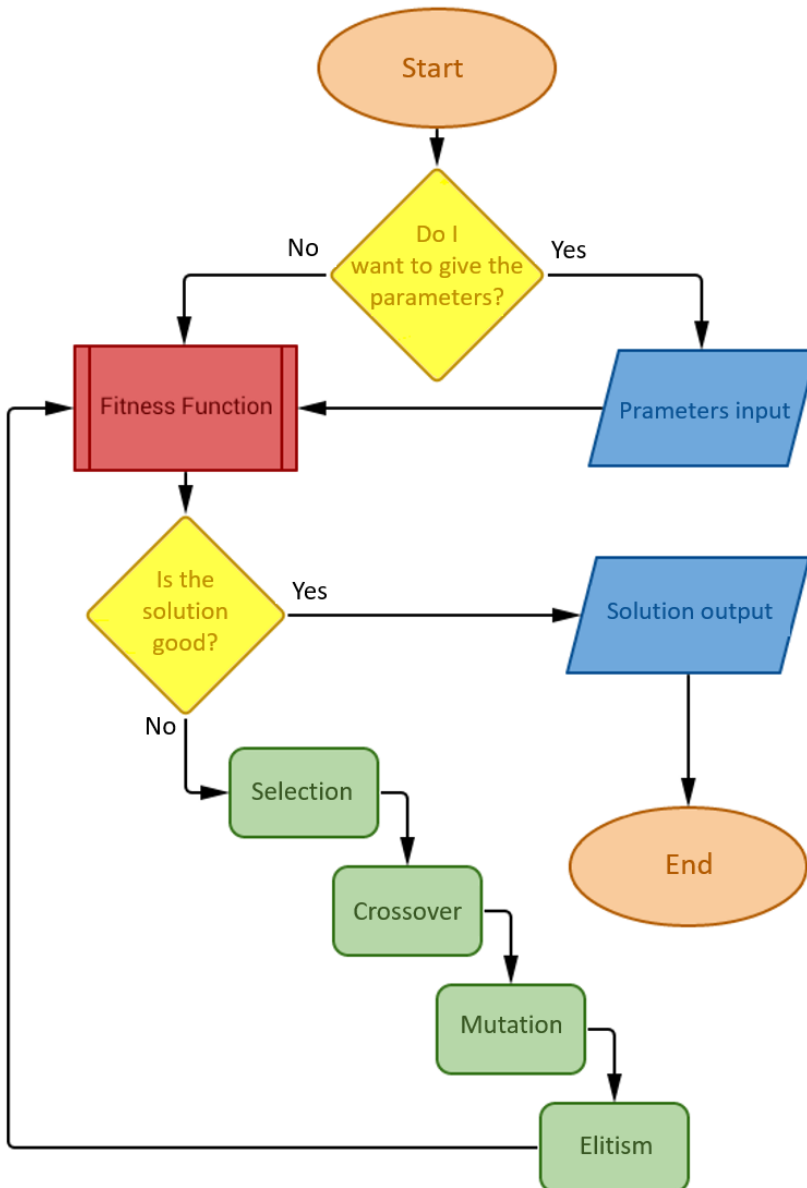**Figure A.1.** A flowchart that schematizes the general functioning of a Genetic Algorithm.

the crossover point $k < N$ genes (clearly k must be an integer) after which all the genes of the first chromosome are beyond the position k are exchanged with the genes of the second occupying the same position (Fig. A.2); alternatively a *double-point crossing* can be adopted (the chromosome is divided into three

parts and the exchange occurs on the central one) or a *uniform crossover* (each of the parents' genes is exchanged with a given possibility).
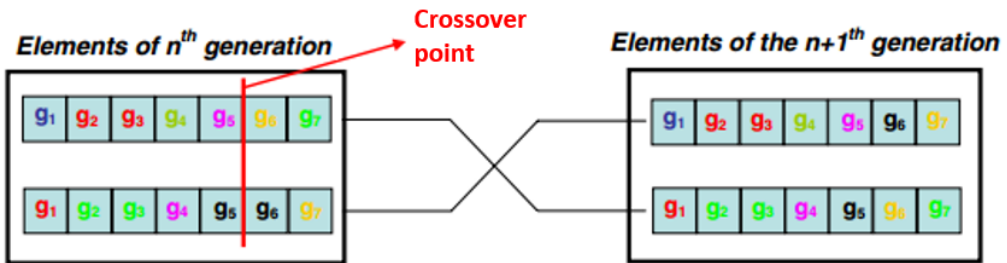

Figure A.2. An example of a single-point crossover.

After the mutation operators change, with a typical P_{mut} probability, one last time the population perturbates it in a variety of ways. The mutation is useful to renew the population in order to prevent a premature convergence of the algorithm in some local minimum.

Finally, the *elitism* operator is responsible for ensuring the presence in the final solution set of the chromosome that possessed the maximum eligibility before selection (this is because mutations and crossovers can destroy it).

The process will be traced to the point where no further improvement can be achieved, the hypothesized result is achieved or the expected number of generations has been exhausted.

Despite the success of the GAs and their easy implementation, the theory that concerns them remains mostly enigmatic [112]. We still do not have a general theory available that ensures the convergence of a given population to the optimal solution and there is not even a classification of the problems for which the GAs are most appropriate. In fact, the behavior of these algorithms is extremely chaotic, even slightly varying an internal parameter can change a lot and in a non-predictable performance. These GAs can be coded to handle binary chromosomes (we speak of GA *binary-coded*), whose genes are sets of 0 and 1, or real chromosomes (*real-coded*), whose genes they are real numbers. Only studies on GA *binary-coded* have led to the definition of mathematical theories that could help the GA programmer, but most of the physical problems are *real-coded* because the solution we are looking for it is often a set of real numbers.

Much of the knowledge on GAs is based on experience, over time some

commonly used indications have been defined:

- In the case of *binary-coded* GAs the most common probabilities of *mutation* and *crossover* are in the ranges $0.6 \leqslant P_{cross} \leqslant 0.9$ and $0.001 \leqslant P_{mut} \leqslant 0.01$; typically P_{mut} corresponds to the mutation of one or two genes per chromosome, we speak of a few chromosomes per population.

- In *real-coded* GAs the mutation frequency must be increased but there is no default range.

- Problems with real numbers should be addressed with *real-coded* GAs even if a binary translation of parameters is possible.

- The introduction of a global optimizer can be extremely useful for accelerating convergence to the solution. This operator must take care of:

  1. Generating the starting population.
  2. Optimizing intermediate populations (every N_{step} steps).
  3. Retouch the final results.

- The selection with the *binary tournament* method works faster than the *roulette rule* and prevents any convergence problems.

- When the stagnation algorithm, typical behavior of the achievement of a local stationary point of the *fitness function*, but the suitability parameter is not satisfactory it is useful to increase P_{mut} in order to force a wider exploration of the solution space.

Candidate publications and proceedings

[1] **M. Rossetti Conti** and A. Bacci. Beam Based Alignment Methods for Cavities and Solenoids in Photo-Injectors. In *Proceedings, 7th International Particle Accelerator Conference (IPAC 2016): Busan, Korea*, page THPMB011, 2016.

[2] A. Bacci, **M. Rossetti Conti**, and V. Petrillo. GIOTTO: A Genetic Code for Demanding Beam-dynamics Optimizations. In *Proceedings, 7th International Particle Accelerator Conference (IPAC 2016): Busan, Korea, May 8-13, 2016*, pages 3073–3076, 2016.

[3] A. Bacci et al. Status of the STAR Project. In *Proceedings, 7th International Particle Accelerator Conference (IPAC 2016): Busan, Korea, May 8-13, 2016*, page TUPOW004, 2016.

[4] E. Chiadroni A. Cianchi C. Curatolo I. Drebot A. Giribono A. Mostacci V. Petrillo **M. Rossetti Conti** A. Rossi, A. Bacci. Quadrupole scan emittance measurements for the eli-np compton gamma source. In *Proceedings, 7th International Particle Accelerator Conference (IPAC 2016): Busan, Korea, May 8-13, 2016*, page MOPMB019, 2016.

[5] D. Micieli, I. Drebot, A. Bacci, E. Milotti, V. Petrillo, **M. Rossetti Conti**, A. R. Rossi, E. Tassi, and L. Serafini. Compton sources for the observation of elastic photon-photon scattering events. *Phys. Rev. Accel. Beams*, 19(9):093401, 2016.

[6] A. Bacci et al. Photoinjector Emittance Measurement at STAR. In *Proceedings, 8th International Particle Accelerator Conference (IPAC 2017): Copenhagen, Denmark, May 14-19, 2017*, page MOPAB064, 2017.

[7] I. Drebot, A. Bacci, D. Micieli, E. Milotti, V. Petrillo, **M. Rossetti Conti**, A.R. Rossi, E. Tassi, and L. Serafini. Study of photon–photon scattering events. *Nucl. Instrum. Methods Phys. Res. A*, 865:9 – 12, 2017.

[8] **M. Rossetti Conti**, A. Bacci, A. Giribono, V. Petrillo, A.R. Rossi, L. Serafini, and C. Vaccarezza. Electron beam transfer line design for plasma driven free electron lasers. *Nucl. Instrum. Methods Phys. Res. A*, 2018.

[9] M. Ferrario et al. Eupraxia@sparc_lab design study towards a compact fel

facility at lnf. *Nucl. Instrum. Methods Phys. Res. A*, 2018.

[10] C. Vaccarezza, D. Alesini, A. Bacci, A. Cianchi, E. Chiadroni, M. Croia, M. Diomede, M. Ferrario, A. Gallo, A. Giribono, A. Latina, A. Marocchino, V. Petrillo, R. Pompili, S. Romeo, **M. Rossetti Conti**, A.R. Rossi, L. Serafini, and B. Spataro. Eupraxia@sparc_lab: Beam dynamics studies for the x-band linac. *Nucl. Instrum. Methods Phys. Res. A*, 2018.

[11] A.R. Rossi, V. Petrillo, A. Bacci, E. Chiadroni, A. Cianchi, M. Ferrario, A. Giribono, A. Marocchino, **M. Rossetti Conti**, L. Serafini, and C. Vaccarezza. Plasma boosted electron beams for driving free electron lasers. *Nucl. Instrum. Methods Phys. Res. A*, 2018.

[12] A. Giribono, A. Bacci, E. Chiadroni, A. Cianchi, M. Croia, M. Ferrario, A. Marocchino, V. Petrillo, R. Pompili, S. Romeo, **M. Rossetti Conti**, A.R. Rossi, and C. Vaccarezza. Eupraxia@sparc_lab: The high-brightness rf photo-injector layout proposal. *Nucl. Instrum. Methods Phys. Res. A*, 2018.

[13] A. Giribono, A. Bacci, E. Chiadroni, A. Cianchi, M. Croia, M. Ferrario, A. Marocchino, V. Petrillo, R. Pompili, S. Romeo, **M. Rossetti Conti**, A.R. Rossi, and C. Vaccarezza. Rf injector design studies for the trailing witness bunch for a plasma-based user facility. *Nucl. Instrum. Methods Phys. Res. A*, 2018.

[14] V. Petrillo, A. Bacci, E. Chiadroni, G. Dattoli, M. Ferrario, A. Giribono, A. Marocchino, A. Petralia, **M. Rossetti Conti**, A.R. Rossi, L. Serafini, C. Vaccarezza, and F. Villa. Free electron laser in the water window with plasma driven electron beams. *Nucl. Instrum. Methods Phys. Res. A*, 2018.

[15] L. Serafini, I. Drebot, A. Bacci, F. Broggi, C. Curatolo, A. Marocchino, N. Panzeri, V. Petrillo, A.R. Rossi, and **M. Rossetti Conti**. A muon source based on plasma accelerators. *Nucl. Instrum. Methods Phys. Res. A*, 2018.

[16] **M. Rossetti Conti**, A. Bacci, A. Giribono, A. Rossi, and C. Vaccarezza. Wide-Ranging Genetic Research of Matching Line Design for Plasma Accelerated Beams with GIOTTO. In *Proceedings, 9th International Particle Accelerator Conference (IPAC 2018): Vancouver, BC Canada*, page THPAK136, 2018.

[17] L. Serafini et al. The marix source (multidisciplinary advanced research infrastructure with x-rays). In *IPAC2018. Proceedings of the 9th International Particle Accelerator Conference*, pages 4199–4202. JACoW Publishing, 2018.

[18] I. Drebot et al. Optimisation Study of the Fabry-Pérot Optical Cavity for the MARIX/BRIXS Compton X-Ray Source. In *Proceedings, 9th International Particle Accelerator Conference (IPAC 2018): Vancouver, BC Canada*, page THPMF056, 2018.

[19] A. Bacci, L. Faillace, and **M. Rossetti Conti**. Extreme High Brightness Electron Beam Generation in a Space Charge Regime. In *Proceedings, 29th Linear Accelerator Conference (LINAC 2018): Beijing, China*, page TU1P01, 2018.

Bibliography

[1]   A. Bacci. "GIOTTO: A Genetic Code for Demanding Beam-dynamics Optimizations". In *Proceedings, 7th International Particle Accelerator Conference (IPAC 2016): Busan, Korea, May 8-13, 2016*, pages 3073–3076, 2016.

[2]   M. Rossetti Conti and A. Bacci. "Beam Based Alignment Methods for Cavities and Solenoids in Photo-Injectors". In *Proceedings, 7th International Particle Accelerator Conference (IPAC 2016): Busan, Korea*, page THPMB011, 2016.

[3]   M. Rossetti Conti et al. "Electron beam transfer line design for plasma driven Free Electron Lasers". *Nucl. Instrum. Methods Phys. Res. A*, 2018.

[4]   M. Rossetti Conti et al. "Wide-Ranging Genetic Research of Matching Line Design for Plasma Accelerated Beams with GIOTTO". In *Proceedings, 9th International Particle Accelerator Conference (IPAC 2018): Vancouver, BC Canada*, page THPAK136, 2018.

[5]   A. Bacci et al. "Extreme High Brightness Electron Beam Generation in a Space Charge Regime". In *Proceedings, 29th Linear Accelerator Conference (LINAC 2018): Beijing, China*, page TU1P01, 2018.

[6]   M. Ferrario et al. "EuPRAXIA@SPARC_LAB Design study towards a compact FEL facility at LNF". *Nucl. Instrum. Methods Phys. Res. A*, 2018.

[7]   FLASH. "Desy". `https://flash.desy.de/`.

[8]   LCLS. "Slac". `https://lcls.slac.stanford.edu/`.

[9]   SACLA. "SPring 8". `http://xfel.riken.jp/eng/`.

[10]   FERMI. "Elettra". `https://www.elettra.trieste.it/lightsources/fermi`.

[11]   M. Ferrario et al. "SPARC_LAB present and future". *Nucl. Instrum. Methods Phys. Res. B*, 309:183 – 188, 2013.

[12]   SWISSFEL. "PSI". `https://www.psi.ch/swissfel/`.

[13]   XFEL. "DESY". `https://www.xfel.eu/`.

[14]   C. Pellegrini et al. "The history of X-ray free-electron lasers". *Eur. Phys. J.*

H, 659(37):659 – 708, 2012.

[15] R. Bonifacio et al. "Collective instabilities and high-gain regime in a free electron laser". *Opt. Comm.*, 50(6):373 – 378, 1984.

[16] K. Kwang-Je. "An analysis of self-amplified spontaneous emission". *Nucl. Instrum. Methods Phys. Res. A*, 250(1):396 – 403, 1986.

[17] G. Dattoli et al. "Progress in the Hamiltonian picture of the free-electron laser". *IEEE Journal of Quantum Electronics*, 17(8):1371–1387, Aug 1981.

[18] M. Xie. "Design optimization for an X-ray free electron laser driven by SLAC linac". In *Proceedings of Particle Accelerator Conference*, volume 1, pages 183–185, May 1995.

[19] F. Ciocci et al. "The variable gap permanent magnet linear undulator for the ENEA-FEL experiment". *Nucl. Instrum. Methods Phys. Res. A*, 250(1):134 – 137, 1986.

[20] L. Giannessi et al. "Self-amplified spontaneous emission for a single pass free-electron laser". *Phys. Rev. ST Accel. Beams*, 14:060712, Jun 2011.

[21] R. Bonifacio et al. "Spectrum, temporal structure, and fluctuations in a high-gain free-electron laser starting from noise". *Phys. Rev. Lett.*, 73:70–73, Jul 1994.

[22] L.H. Yu et al. "High-Gain Harmonic-Generation Free-Electron Laser". *Science*, 289(5481):932–934, 2000.

[23] L. H. Yu et al. "First Ultraviolet High-Gain Harmonic-Generation Free-Electron Laser". *Phys. Rev. Lett.*, 91:074801, Aug 2003.

[24] L. Giannessi et al. "High-Order-Harmonic Generation and Superradiance in a Seeded Free-Electron Laser". *Phys. Rev. Lett.*, 108:164801, Apr 2012.

[25] M. Labat et al. "High-Gain Harmonic-Generation Free-Electron Laser Seeded by Harmonics Generated in Gas". *Phys. Rev. Lett.*, 107:224801, Nov 2011.

[26] L. Giannessi et al. "Superradiant Cascade in a Seeded Free-Electron Laser". *Phys. Rev. Lett.*, 110:044801, Jan 2013.

[27] G. Geloni et al. "A novel self-seeding scheme for hard X-ray FELs". *J. Mod. Opt.*, 58(16):1391–1403, 2011.

[28] D. Xiang et al. "Echo-enabled harmonic generation free electron laser". *Phys. Rev. ST Accel. Beams*, 12:030702, Mar 2009.

[29] M.D. Alaimo et al. "Mapping the transverse coherence of the self amplified spontaneous emission of a free-electron laser with the heterodyne speckle method". *Opt. Express*, 22(24):30013–30023, Dec 2014.

[30] J.B. Rosenzweig et al. "Generation of ultra-short, high brightness electron beams for single-spike SASE FEL operation". *Nucl. Instrum. Methods Phys.*

Res. A, 593(1):39 – 44, 2008. FEL Frontiers 2007.

[31] F. Villa et al. "Generation and characterization of ultra-short electron beams for single spike infrared FEL radiation at SPARC_LAB". *Nucl. Instrum. Methods Phys. Res. A*, 865:43 – 46, 2017. Physics and Applications of High Brightness Beams 2016.

[32] L. Giannessi et al. "Self-Amplified Spontaneous Emission Free-Electron Laser with an Energy-Chirped Electron Beam and Undulator Tapering". *Phys. Rev. Lett.*, 106:144801, Apr 2011.

[33] L. Young et al. "Roadmap of ultrafast x-ray atomic and molecular physics". *J. Phys. B At. Mol. Opt. Phys.*, 51(3):032003, 2018.

[34] Martin Reiser. "Theory and design of charged particles beams". *Particle Accelerators*, 49(2):143, 1995.

[35] G. Wormser et al. *The White Book of ELI Nuclear Physics Bucharest-Magurele, Romania*. 12 2010.

[36] I.V. Pogorelsky et al. "Demonstration of 8×10^{18} photons/second peaked at 1.8 Åin a relativistic Thomson scattering experiment". *Phys. Rev. ST Accel. Beams*, 3(9):090702, 2000.

[37] W.J. Brown et al. "Experimental characterization of an ultrafast Thomson scattering x-ray source with three-dimensional time and frequency-domain analysis". *Phys. Rev. ST Accel. Beams*, 7(6):060702, 2004.

[38] M. Babzien et al. "Observation of the second harmonic in Thomson scattering from relativistic electrons". *Phys. Rev. Lett.*, 96(5):054802, 2006.

[39] Martin Bech, Oliver Bunk, Christian David, Ronald Ruth, Jeff Rifkin, Rod Loewen, Robert Feidenhans'l, and Franz Pfeiffer. "Hard X-ray phase-contrast imaging with the Compact Light Source based on inverse Compton X-rays". *J. Sync. Rad.*, 16(1):43–47, 2009.

[40] R. Kuroda et al. "Quasi-monochromatic hard X-ray source via laser Compton scattering and its application". *Nucl. Instrum. Methods Phys. Res. A*, 637(1):S183–S186, 2011.

[41] T. Akagi et al. "Narrow-band photon beam via laser Compton scattering in an energy recovery linac". *Phys. Rev. Accel. Beams*, 19(11):114701, 2016.

[42] Y. Du et al. "Generation of first hard X-ray pulse at Tsinghua Thomson Scattering X-ray Source". *Rev. Sci. Inst.*, 84(5):053301, 2013.

[43] C. Vaccarezza et al. "The SPARC_LAB Thomson source". *Nucl. Instrum. Methods Phys. Res. A*, 829:237–242, 2016.

[44] E. Eggl et al. "X-ray phase-contrast tomosynthesis of a human ex vivo breast slice with an inverse Compton x-ray source". *EPL (Europhys. Lett.)*, 116(6):68003, 2017.

[45] A. Jochmann et al. "High resolution energy-angle correlation measurement of hard x rays from laser-Thomson backscattering". *Phys. Rev. Lett.*, 111(11):114803, 2013.

[46] Y. Sakai et al. "Single shot, double differential spectral measurements of inverse Compton scattering in the nonlinear regime". *Phys. Rev. Accel. Beams*, 20(6):060701, 2017.

[47] K. Achterhold et al. "Monochromatic computed tomography with a compact laser-driven X-ray source". *Sci. Rep.*, 3:1313, 2013.

[48] H. Ikeura-Sekiguchi et al. "In-line phase-contrast imaging of a biological specimen using a compact laser-Compton scattering-based x-ray source". *Applied Physics Letters*, 92(13):131107, 2008.

[49] Felix G. Meinel et al. "Diagnosing and mapping pulmonary emphysema on X-ray projection images: incremental value of grating-based X-ray dark-field imaging". *PloS one*, 8(3):e59526, 2013.

[50] F. Schwab et al. "Comparison of contrast-to-noise ratios of transmission and dark-field signal in grating-based X-ray imaging for healthy murine lung tissue". *Zeitschrift für Medizinische Physik*, 23(3):236–242, 2013.

[51] X. Wang et al. "Quasi-monoenergetic laser-plasma acceleration of electrons to 2 GeV".

[52] T. Tajima and J. M. Dawson. "Laser Electron Accelerator". *Phys. Rev. Lett.*, 43:267–270, Jul 1979.

[53] P. Antici et al. "Laser-driven electron beamlines generated by coupling laser-plasma sources with conventional transport systems". 112, 08 2012.

[54] M. Migliorati et al. "Intrinsic normalized emittance growth in laser-driven electron accelerators". *Phys. Rev. ST Accel. Beams*, 16:011302, Jan 2013.

[55] G. Sciaini and R. J. Dwayne Miller. "Femtosecond electron diffraction: heralding the era of atomically resolved dynamics". *Rep. Prog. Phys.*, 74(9):096101, 2011.

[56] R. J. Dwayne Miller. "Femtosecond Crystallography with Ultrabright Electrons and X-rays: Capturing Chemistry in Action". *Science*, 343(6175):1108–1116, 2014.

[57] R.J. Dwayne Miller. "Mapping Atomic Motions with Ultrabright Electrons: The Chemists' Gedanken Experiment Enters the Lab Frame". *Ann. Rev. Phys. Chem.*, 65(1):583–604, 2014.

[58] B. J. Siwick et al. "An Atomic-Level View of Melting Using Femtosecond Electron Diffraction". *Science*, 302(5649):1382–1385, 2003.

[59] K. S. Novoselov et al. "Electric Field Effect in Atomically Thin Carbon Films". *Science*, 306(5696):666–669, 2004.

[60] DESY. "Regae". `https://regae.desy.de/`.

[61] S. Manz et al. "Mapping atomic motions with ultrabright electrons: towards fundamental limits in space-time resolution". *Faraday Discuss.*, 177:467–491, 2015.

[62] V. L. Ginzburg and I. M. Frank. "Radiation of a uniformly moving electron due to its transition from one medium into another". *J. Phys.(USSR)*, 9:353–362, 1945.

[63] R. B. Fiorito et al. "Interference of diffraction and transition radiation and its application as a beam divergence diagnostic". *Phys. Rev. ST Accel. Beams*, 9:052802, May 2006.

[64] R. B. Fiorito and Donald W. Rule. "Optical transition radiation beam emittance diagnostics". *AIP Conference Proceedings*, 319(1):21–37, 1994.

[65] L. Yun-Shik. *Principles of Terahertz Science and Technology*. 01 2009.

[66] B. Zhu et al. "Terahertz science and technology and applications". 2:1139–1143, 01 2009.

[67] M. Ferrario et al. "Laser comb with velocity bunching: Preliminary results at SPARC". 637, 05 2011.

[68] E. Chiadroni et al. "The SPARC linear accelerator based terahertz source". 102:094101, 03 2013.

[69] F. Giorgianni et al. "Tailoring of Highly Intense THz Radiation Through High Brightness Electron Beams Longitudinal Manipulation". 6:56, 02 2016.

[70] M. Gensch et al. "New infrared undulator beamline at FLASH". *Infrared Phys. Technol.*, 51(5):423 – 425, 2008. 4th International Workshop on Infrared Microscopy and Spectroscopy with Accelerator-Based Sources.

[71] M. A. Cook et al. "Observation of Narrow-Band Terahertz Coherent Cherenkov Radiation from a Cylindrical Dielectric-Lined Waveguide". 103:095003, 08 2009.

[72] H. N. Chapman et al. "Diffraction before destruction". 369(1647), 2014.

[73] M. Ferrario et al. "Experimental Demonstration of Emittance Compensation with Velocity Bunching". *Phys. Rev. Lett.*, 104:054801, Feb 2010.

[74] LCLS. "LCLS Parameters (Update Dec. 2017)". `https://portal.slac.stanford.edu/sites/lclscore_public/Accelerator_Physics_Published_Documents/LCLS-parameters-3-22-17.pdf`.

[75] M. Altarelli et al., editors. *XFEL: The European X-Ray Free-Electron Laser. Technical design report.* 2006.

[76] A. R. Rossi et al.

[77] Y. Ding et al. "Measurements and Simulations of Ultralow Emittance and Ultrashort Electron Beams in the Linac Coherent Light Source". *Phys. Rev.*

Lett., 102:254801, Jun 2009.

[78] E. Schneidmiller and M. Yurkov. "Baseline Parameters of the European XFEL". In *Proceedings, 38th International Free Electron Laser Conference, FEL2017*, page MOP033, 2018.

[79] T. Hara et al. "High peak current operation of x-ray free-electron laser multiple beam lines by suppressing coherent synchrotron radiation effects". *Phys. Rev. Accel. Beams*, 21:040701, Apr 2018.

[80] B. Zeitler et al. "Linearization of the longitudinal phase space without higher harmonic field". *Phys. Rev. ST Accel. Beams*, 18:120102, Dec 2015.

[81] "The quantum free-electron laser". *Nucl. Instrum. Methods Phys. Res. A*, 593(1):69 – 74.

[82] J. G. Power et al. "Wakefield excitation in multimode structures by a train of electron bunches". *Phys. Rev. E*, 60:6061–6067, Nov 1999.

[83] P. Piot et al. "Generation and Characterization of Electron Bunches with Ramped Current Profiles in a Dual-Frequency Superconducting Linear Accelerator". *Phys. Rev. Lett.*, 108:034801, Jan 2012.

[84] F. Lemery and P. Piot. "Tailored electron bunches with smooth current profiles for enhanced transformer ratios in beam-driven acceleration". *Phys. Rev. ST Accel. Beams*, 18:081301, Aug 2015.

[85] Q. Gao et al. "Observation of High Transformer Ratio of Shaped Bunch Generated by an Emittance-Exchange Beam Line". *Phys. Rev. Lett.*, 120:114801, Mar 2018.

[86] G. Ha et al. "Precision Control of the Electron Longitudinal Bunch Shape Using an Emittance-Exchange Beam Line". *Phys. Rev. Lett.*, 118:104801, Mar 2017.

[87] I. V. Bazarov et al. "Initial beam results from the Cornell high-current ERL injector prototype". 9, 01 2009.

[88] L. Serafini et al. "The MariX source (Multidisciplinary Advanced Research Infrastructure with X-rays)". In *IPAC2018. Proceedings of the 9th International Particle Accelerator Conference*, pages 4199–4202. JACoW Publishing, 2018.

[89] K. Floettmann. ""ASTRA, A Space-charge TRacking Algorithm", Version 3.2, March 2017". `http://www.desy.de/~mpyflo/`.

[90] M. Borland. "elegant: A Flexible SDDS-Compliant Code for Accelerator Simulation". In *6th International Computational Accelerator Physics Conference (ICAP 2000) Darmstadt, Germany, September 11-14, 2000*, 2000.

[91] S. Reiche et al. "Start-to-end simulation for the LCLS X-ray FEL". In

PACS2001. Proceedings of the 2001 Particle Accelerator Conference (Cat. No.01CH37268), pages 2751–2753. IEEE, 2001.

[92] D. S. Weile and E. Michielssen. "Genetic algorithm optimization applied to electromagnetics: A review". *IEEE Transactions on Antennas and Propagation*, 45(3):343–353, 1997.

[93] G. van Rossum. "Python tutorial". Technical Report CS-R9526, Centrum voor Wiskunde en Informatica (CWI), Amsterdam, May 1995.

[94] A. Bacci and Others. "Maximizing the brightness of an electron beam by means of a genetic algorithm". *Nucl. Instrum. Methods Phys. Res. B*, 263(2):488 – 496, 2007.

[95] A. Bacci and Others. "Optimization of the beam line characteristics by means of a genetic algorithm". In *2007 IEEE Particle Accelerator Conference (PAC)*, 2007.

[96] V. Kumar. "Understanding the focusing of charged particle beams in a solenoid magnetic field". *Am. J. Phys.*, 77(8):737–741, 2009.

[97] M. Quattromini et al. "Focusing properties of linear undulators". *Phys. Rev. ST Accel. Beams*, 15:080704, Aug 2012.

[98] S. Y. Lee. *Accelerator Physics | 3rd Edition*, chapter 2.2.2. World Scientific Publishing, Oxford, 2012.

[99] Karl L. Brown. "A First and Second Order Matrix Theory for the Design of Beam Transport Systems and Charged Particle Spectrometers". *Adv. Part. Phys.*, 1:71–134, 1968.

[100] P. Larrañaga et al. "Genetic Algorithms for the Travelling Salesman Problem: A Review of Representations and Operators". *Artificial Intelligence Review*, 13(2):129–170, Apr 1999.

[101] P. Tomassini and A. Rossi. "Matching strategies for a plasma booster". *Plas. Phys. Cont. Fus.*, 58:034001, 03 2016.

[102] S. Reiche. "GENESIS 1.3: a fully 3D time-dependent FEL simulation code". *Nucl. Instrum. Methods Phys. Res. A*, 429(1):243 – 248, 1999.

[103] A. Ghaith et al. "Tunable high gradient quadrupoles for a laser plasma acceleration based FEL". *Nucl. Instrum. Methods Phys. Res. A*, 2018.

[104] M. Ferrario et al. "Direct Measurement of the Double Emittance Minimum in the Beam Dynamics of the Sparc High-Brightness Photoinjector". *Phys. Rev. Lett.*, 99:234801, Dec 2007.

[105] D. Alesini et al. "Study of a C-band harmonic RF system to optimize the RF bunch compression process of the SPARC beam". In *Proceedings, 6th International Particle Accelerator Conference (IPAC 2015): Richmond, Virginia, USA, May 3-8, 2015*, page TUPWA058, 2015.

[106] T. Murata and H. Ishibuchi. "MOGA: multi-objective genetic algorithms". In *Proceedings of 1995 IEEE International Conference on Evolutionary Computation*, volume 1, pages 289–, Nov 1995.

[107] S. Yussof et al. "A Coarse-Grained Parallel Genetic Algorithm with Migration for Shortest Path Routing Problem". In *2009 11th IEEE International Conference on High Performance Computing and Communications*, pages 615–621, June 2009.

[108] S. Di Mitri and M. Cornacchia. "Transverse emittance-preserving arc compressor for high-brightness electron beam-based light sources and colliders". *EPL*, 109(6):62002, 2015.

[109] R. Chasman, G. K. Green, and E. M. Rowe. "Preliminary Design of a Dedicated Synchrotron Radiation Facility". *IEEE Trans. on Nucl. Sci.*, 22(3):1765–1767, June 1975.

[110] E.L. Saldin, E.A. Schneidmiller, and M.V. Yurkov. "On the coherent radiation of an electron bunch moving in an arc of a circle". *Nucl. Instrum. Methods Phys. Res. A*, 398:373–394, 10 1997.

[111] M. Borland. "Simple method for particle tracking with coherent synchrotron radiation". *Phys. Rev. ST Accel. Beams*, 4, 07 2001.

[112] D. Whitley. "A Genetic Algorithm Tutorial". A tutorial from Computer Science Department, Colorado State University, 1993.

Acknowledgments

I would like to extend thanks to the many people who so generously contributed to the work presented in this thesis. Especially I would like to say thank you to **Cristina Vaccarezza** and **Simone Di Mitri** for their valuable advices, to **Susanna Guiducci** and **Christelle Bruni**, reviewers of this document, for the feedbacks on the thesis they gave me and to **Mauro Gambaccini**, **Ezio Puppin** and **Simone Cialdi**, who accepted to co-examinate this thesis, for the time they will devote to this.

Special mention goes to my enthusiastic supervisors, **Vittoria Petrillo** and **Alberto Bacci**. My PhD was an important and educational experience both from a scientific and a human point of view. I thank you for all the suggestions given, for listening to me and, when necessary, having changed my mind.

I absolutely have to thank my group leader, **Luca Serafini**, for being a model of inspiration, but also for giving me many wonderful opportunities. Not many PhDs travel 4 continents to learn, meet new colleagues and show off their work.

I would like to say thank you to **Illya Drebot** for suggestions on how best to perform my PhD (even this thesis would be different, without the editor you suggested me) and to **Camilla Curatolo** for the chats at the bar and in the office when I was looking for comfort or a working heater.

If it was not for the morning coffee ritual with **Andrea Renato Rossi**, the days of work would not have started laughing, thanks for this and all the valuable advice you gave us.

Furthermore, I would like to thank again **Vittoria**, **Alberto** and **Illya** for the time shared together drinking tea, talking about physics, culture and personal anecdotes.

I sincerely wish to thank my girlfriend **Cristina** for enduring me in the sad days and giving me so many precious advices. Without you I would not have come this far and I would not smile when I get home.

I thank the friends of PhD **Giacomo**, **Marco**, **Silvia**, **Simone**, and **Lorenzo** (even if he is PostDoc) for having partly lightened and partly weighed down every day that required it with our wonderful lunches. Thanks for the advice on how to overcome the obstacles, especially bureaucratic but not only, that fate has disseminated on our way.

To **my closest friends**, now scattered around the world, thanks for every pleasant moment spent together swimming, drinking and talking, you are the lifeblood that makes every day work.

Finally, but only for reverted order of importance, I thank **my mother**, **my father** and my brother **Claudio** for believing in me, and having supported me, your contribution is often not seen but is always the greatest.